AD-766 796

ANNUAL RESEARCH REPORT, 1 JULY 1971-30 JUNE 1972

Armed Forces Radiobiology Research Institute

Prepared for:

Defense Nuclear Agency

30 June 1972

ARR-6

ARMED FORCES RADIOBIOLOGY RESEARCH INSTITUTE

ANNUAL RESEARCH REPORT

1 JULY 1971 – 30 JUNE 1972

Defense Nuclear Agency, Bethesda, Maryland

Approved for public release; distribution unlimited

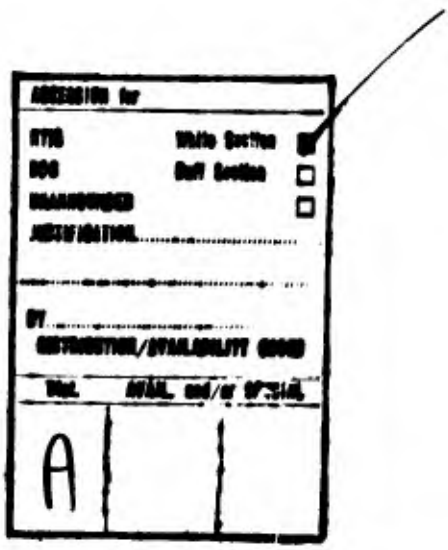

Research was conducted according to the principles enunciated in the "Guide for Laboratory Animal Facilities and Care," prepared by the National Academy of Sciences - National Research Council.

UNCLASSIFIED

Security Classification

DOCUMENT CONTROL DATA - R & D

(Security classification of title, body of abstract and indexing annotation must be entered when the overall report is classified)

1 ORIGINATING ACTIVITY *(Corporate author)*

Armed Forces Radiobiology Research Institute
Defense Nuclear Agency
Bethesda, Maryland 20014

2a. REPORT SECURITY CLASSIFICATION

UNCLASSIFIED

2b. GROUP

N/A

3 REPORT TITLE

ANNUAL RESEARCH REPORT 1 July 1971 -- 30 June 1972

4 DESCRIPTIVE NOTES *(Type of report and inclusive dates)*

5 AUTHOR(S) *(First name, middle initial, last name)*

6 REPORT DATE

7a. TOTAL NO. OF PAGES

~~93~~ 97

7b. NO. OF REFS

8a. CONTRACT OR GRANT NO.

b. PROJECT NO.

c.

d.

9a. ORIGINATOR'S REPORT NUMBER(S)

ARR-6

9b. OTHER REPORT NO(S) *(Any other numbers that may be assigned this report)*

10 DISTRIBUTION STATEMENT

Approved for public release; distribution unlimited

11 SUPPLEMENTARY NOTES

Details of illustrations in this document may be better studied on microfiche.

12. SPONSORING MILITARY ACTIVITY

Director
Defense Nuclear Agency
Washington, D. C. 20305

13 ABSTRACT

This report contains a summary of the research projects of the Armed Forces Radiobiology Research Institute for the period 1 July 1971 to 30 June 1972.

DD FORM 1 NOV 65 1473

UNCLASSIFIED

Security Classification

14 KEY WORDS	LINK A		LINK B		LINK C	
	ROLE	WT	ROLE	WT	ROLE	WT

ARR-6

ANNUAL RESEARCH REPORT
1 JULY 1971 – 30 JUNE 1972

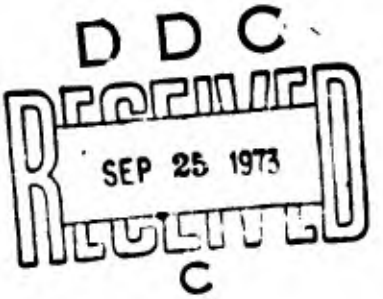

ARMED FORCES RADIOBIOLOGY RESEARCH INSTITUTE
DEFENSE NUCLEAR AGENCY
BETHESDA, MARYLAND 20014

FOREWORD

This report summarizes the research accomplishments of the Armed Forces Radiobiology Research Institute (AFRRI) for the period 1 July 1971 to 30 June 1972.

During this period, the research mission and program of the Institute were broadened in accordance with the provisions of a new charter, issued 11 May 1972. The Board of Governors, made up of the Surgeons General and the Director of the Defense Nuclear Agency (DNA), was reactivated and met twice, October and April.

The overall capabilities and resources of the AFRRI were reviewed by the Surgeons General and the Assistant Secretary of Defense for Health and Environment, and the development of a new research program, including collaborative projects with other medical agencies and activities in the area, was recommended to the Director, DNA. With his approval, a new program was developed, with particular emphasis on Neurobiology and Nuclear Medicine. This program was presented to the Joint Medical Research Committee of the Office of Research and Engineering, DoD, chaired by Dr. C. J. D. Zarafonetis, and was reviewed and approved by the AFRRI Board of Governors. To accomplish the new program, the scientific staff of the Institute was increased by an augmentation of the military positions, and a reorganization of the Institute, with the establishment of a new Department of Neurobiology, was proposed. The reorganization has been approved and is incorporated into the current Joint Table of Distribution for the Institute.

Problems in radiation biology remained a major part of the AFRRI research program during this period, and the results of research done in these areas constitute the majority of this report. The new nuclear medicine and radiopharmaceutical program is reported, in part, and other aspects of the new program will be covered in future annual reports.

Myron I. Varon

MYRON I. VARON
Captain MC USN
Director

TABLE OF CONTENTS

MARROW STEM CELL RELATIONSHIP WITH INDICATORS OF RADIOSENSITIVITY

Principal Investigator: *M. E. Ekstrom*
Collaborators: *A. S. Evans, J. E. West and J. F. Taylor*
Technical Assistance: *D. F. Trainor, P. E. Haynesworth, J. E. Egan, F. A. Quinn and M. H. Gobbett*

The objective of this research was to evaluate the possible relationship between preirradiation levels of serum protein-bound carbohydrates (PBC) measured as neutral hexoses (mannose and galactose) and the relative sensitivity or radioresistance of animals tested (C_3H mice).

Evans et al.[1,2] found that the preirradiation PBC value may be a relative index of radiosensitivity in C_3H mice and beagles, especially at gamma-neutron radiation dosages at or below the median lethal dose.

The experimental animals used in this study were 200 healthy young adult male C_3H mice which had been carefully screened for evidence of parasitism and other pathologic processes during the 2-month conditioning period. After base-line PBC values were determined, the mice were randomly divided into groups of 20 animals and irradiated with ^{60}Co gamma rays at 40 rads/minute over a dosage range of 600 - 1150 rads midline tissue dose (MTD) at 75-rad increments. The calculated $LD_{50/30}$ was 880 rads MTD. The mouse population's mean preirradiation PBC concentration was 151.3 mg/100 ml of serum and the median was 153.2 mg/100 ml of serum. Preliminary data in Table I do not suggest a relationship between the

Table I. Preirradiation Plasma PBC Concentrations for 20 Young Adult Male C_3H Mice which were Exposed to 875 Rads ($LD_{50/30}$ = 880 Rads) ^{60}Co Gamma Radiation at 40 Rads/Minute. For Nonsurvivors and Survivors the Distribution of the Preirradiation PBC's about the Population Median Reveals No Apparent Evidence for Preirradiation PBC Predictability.

PBC (mg/100 mg biuret protein)	PBC distribution (nonsurvivors)	Number of mice	PBC distribution (survivors)	Number of mice
Range of PBC's below median (123.0-153.2)	123.6 134.9 143.3 143.6	4	139.8 141.7 142.5 148.4 151.0	5
Median PBC 153.4				
Range of PBC's median and above (153.4-170.7)	153.4 162.2 162.3 163.2 165.9	5	154.0 155.6 155.7 157.2 159.9 165.1	6

preirradiation PBC and relative radiosensitivity under the present experimental conditions.

REFERENCES

1. Evans, A. S. Effect of ionizing radiations on distribution of plasma protein-bound neutral hexoses in mice and dogs. Radiation Res. 43:152-160, 1970.

2. Evans, A. S., Quinn, F. A., Brown, J. A. and Strike, T. A. Effect of ionizing radiation on total protein-bound neutral hexoses in the plasma of mice. Radiation Res. 36:128-137, 1968.

HEMATOPOIETIC KINETICS DURING RADIATION RECOVERY IN MINIATURE SWINE

Principal Investigators: *J. F. Taylor, J. E. West, M. E. Ekstrom and J. L. Terry, Jr.*
Technical Assistance: *E. L. Barron, F. A. Mitchell, D. F. Trainor, J. E. Egan, N. L. Fleming, M. E. Flynn, P. E. Haynesworth, J. K. Warrenfeltz and W. W. Wolfe*

Unique among the numerous recovery studies with mammalian species following whole-body irradiation is the recovery pattern of domestic swine reported by Nachtwey et al.[1] Using the split-dose technique of measuring residual injury with time following the initial sublethal radiation (conditioning) exposure, Nachtwey et al. showed that swine recover completely from the initial injury by 11 days, reach a stage of "over-recovery" or radioresistance (~ 200 percent recovery) by 20 days and remain in this radioresistant state in excess of 100 days after the initial exposure.

This recovery phenomenon is currently under study at AFRRI using miniature swine. The AFRRI ^{60}Co facility is being used exclusively, with all midline tissue doses (MTD) being delivered at 34 - 35 rads/minute. The $LD_{50/30}$ for miniature swine exposed to ^{60}Co gamma radiation at the above dose rate is 237 rads MTD. The dose response data are presented in Table II.

The split-dose mortality study is nearing completion. The conditioning dose used in our study is 150 rads (63 percent of the LD_{50}) with the second (challenge) dose being delivered on the 28th day following the conditioning dose. Preliminary results indicate that miniature swine respond similarly to domestic swine. These data are summarized in Table III.

Table II. Dose Response and Mortality Data for Miniature Swine Following ^{60}Co Gamma Irradiation

Midline tissue dose (rads)	Mortality Number dead/number exposed	Day of death postirradiation
180	0/5	-
203	0/1	-
220	4/7	16(2)*, 21, 24
240	3/8	14, 15, 18
270	6/8	15, 16(2), 17, 18(2)
330	7/7	11, 13(2), 15, 16, 17(2)
400	1/1	16
$LD_{50/30}$ 237 rads (215-262)*		Mean survival time 16.3 days

* Numbers in parentheses denote number of animals dying at specified time postirradiation when greater than one

* 95 percent confidence limits

Table III. Dose Response for Miniature Swine Following a 150-Rad Conditioning Dose

Challenge dose 28th Day (rads)	Mortality Number dead/number exposed
100	0/3
250	0/4
280	2/3
320	1/7
360	2/3
400	4/6
450	0/7

Having established that miniature swine demonstrate a radioresistance phase after sublethal irradiation, studies are currently underway to determine a physiological basis for this phenomenon. The ^{60}Co gamma dosage range used in this study produces the hematopoietic syndrome. To evaluate the state of hematopoiesis after both the conditioning and challenge doses, bone marrow and peripheral blood were sampled at 48 hours, thence at weekly intervals following both exposures in several irradiated animals.

Necropsies and subsequent histopathological examinations are being carried out to confirm either radiation-induced lethalities or the degree of hematopoietic tissue repair in survivors euthanatized at the end of the 1-month or 2-month observation period for the lethality and split-dose studies, respectively.

Additional measurements of hematopoietic activity, i.e., granulocyte pool size determinations, granulocyte turnover rates, and active hematopoietic tissue distribution before and after irradiation, will be studied. Also, determinations on selected clinical chemistry indices will be made to better define the overall physiological state of the radioresistant animals.

REFERENCE

1. Nachtwey, D. S., Ainsworth, E. J. and Leong, G. F. Recovery from radiation injury in swine as evaluated by the split-dose technique. Radiation Res. 31:353-367, 1967.

RECOVERY AND RESIDUAL INJURY OF THE HEMATOPOIETIC SYSTEM IN IRRADIATED MAMMALS

Principal Investigators: *K. F. McCarthy, W. D. Skidmore and S. J. Baum*

Enhancing granulopoiesis in the postirradiated animal by suppressing erythropoiesis proceeded along two lines of investigation: (a) blocking the humorally affected erythropoietic pathway through the use of actinomycin D and (b) examining the effect of microenvironment on stem cell differentiation and/or proliferation by use of Ficoll density gradients.

Humoral suppression. It was found that daily subcutaneous injections of .2 mg/gm body weight (b.w.) of actinomycin D resulted in complete suppression of circulating reticulocytes and a twofold to threefold increase in circulating granulocytes. The number of circulating lymphocytes remained constant. However, higher doses of actinomycin D reduced the number of lymphocytes and caused death. Doses of actinomycin D lower than .2 mg/gm b.w. did not affect any of the formed blood elements. In the postirradiated (300 R) animal, injections of actinomycin D suppressed reticulocyte formation but had no apparent effect on granulocyte recovery.

Separation of spleen cells in iso-osmotic Ficoll density gradients. The object of this research was to improve existing methods of isopycnic density centrifugation for the purification of viable cell populations from hematopoietic organs. A cell or other particle will move through a density gradient under a centrifugal force until it reaches its own density or isopycnic level. In the past, the rationale for using high molecular weight polymers for the generation of density gradients was that according to the van't Hoff equation dense polymer solutions should generate low osmotic pressure.

However, when the osmotic pressure of polymer solutions was measured directly it was found that the van't Hoff equation cannot be used to calculate the osmotic pressure of polymer solutions at concentrations greater than 5 percent. Therefore, previous methods for the generation of density gradients appear also to have created hyperosmotic gradients. However, since cells maintain their integrity best in an isotonic solution, an iso-osmotic density gradient can be prepared by superimposing a reverse salt gradient on a Ficoll gradient.

Using this method, the density profiles of several cell populations were determined,[1] and the following observations on fractionated C57BL mouse spleen were made: (1) despite the high centrifugal force used (16,000 g for 1 hour) the recovery of biological activity was greater than 75 percent; (2) the density profile of the 19S plaque-forming cells showed this cell population to be extremely heterogeneous and, furthermore, the density profile remained constant during the primary immune response (Figure 1); (3) the

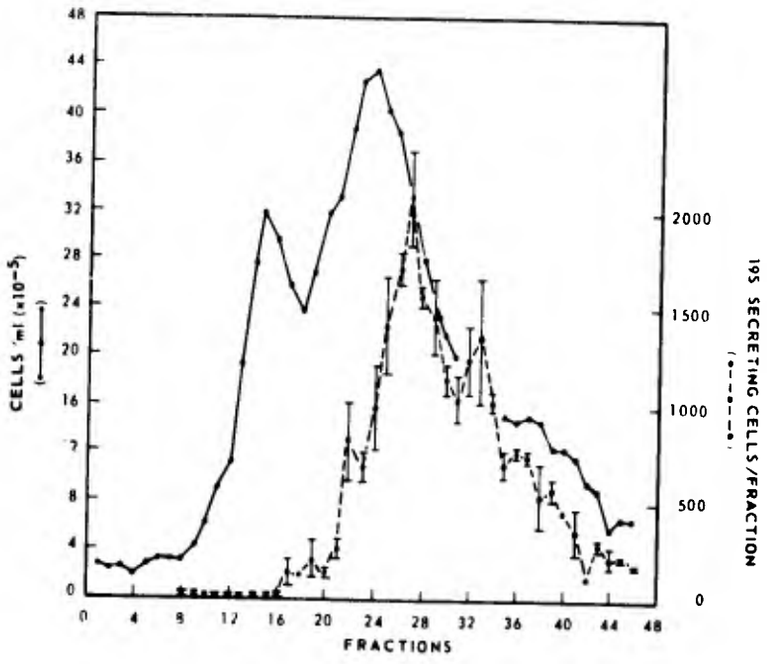

Figure 1. Density profile of 19S antibody-secreting cell population. Fractions of 1.1 ml were collected and two determinations for plaque-forming cells were made per fraction. Error bars represent standard error of the mean.

density profile of the colony forming units in the spleen showed a major peak at a density of 1.0815 g/cm^3 and minor peaks in the light region of the gradient (Figure 2); and (4) the cell population causing the graft versus host disease appeared to be homogeneous and banded at a density of 1.0825 g/cm^3 (Figure 3).

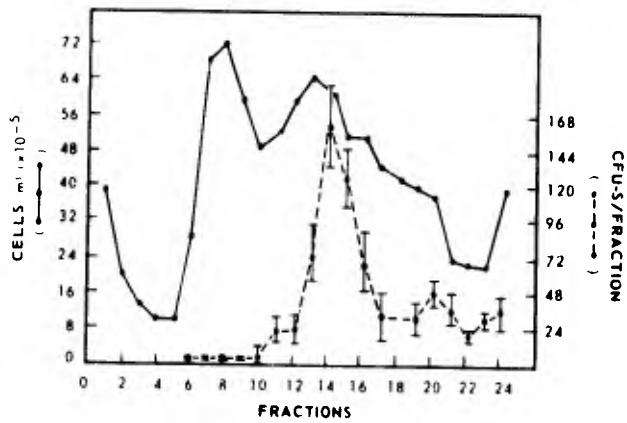

Figure 2. Density profile of CFU-S population. Fractions of 2.2 ml were collected. Error bars represent standard error of the mean.

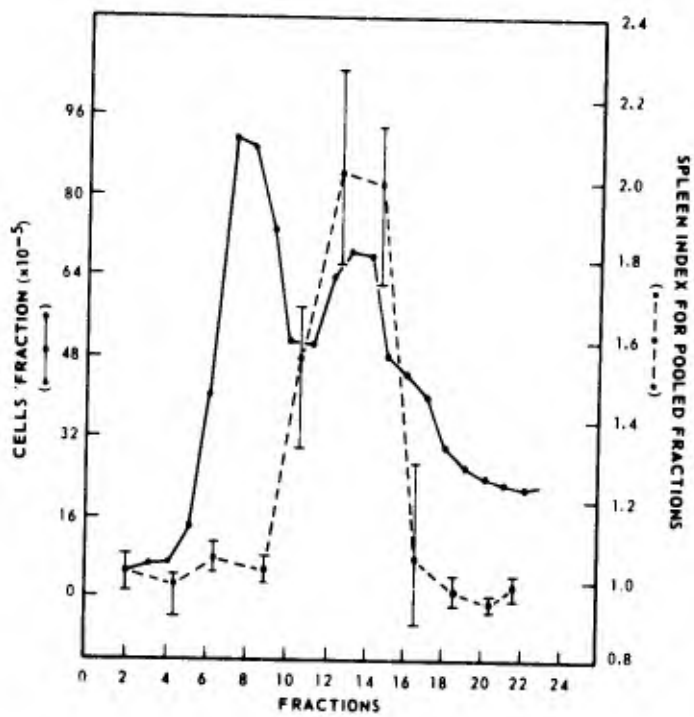

Figure 3. Density profile of cell population eliciting graft versus host reaction disease. Fractions of 2.2 ml were collected and pooled as indicated. Error bars represent standard error of the mean.

In summary, it appears that different functional cell populations give distinct density profiles on iso-osmotic neutral density gradients which contain a reverse salt gradient.

REFERENCE

1. McCarthy, K. F., Nutter, J. E. and MacVittie, T. J. Separation of spleen cells in iso-osmotic Ficoll density gradients. Bethesda, Maryland, Armed Forces Radiobiology Research Institute Scientific Report SR73-4, 1973 (in press).

EFFECTS OF IONIZING RADIATION ON IMMUNE RESPONSES IN LETHALLY IRRADIATED ANIMALS

Principal Investigator: *J. E. Nutter*
Technical Assistance: *E. D. Exum, R. T. Brandenburg, C. L. Cloud, M. P. Fink, N. A. Eaton and P. E. Ewald*

The objective of this study was to assess the efficacy of two antibiotics developed during the past decade, ampicillin and gentamicin, which had not yet been used in irradiated animals.[1] Whenever indicated by signs of internal bleeding, this treatment was augmented by red blood cell and platelet transfusions and fluids.

Beagles exposed to 350 rads bilateral ^{60}Co gamma radiation without subsequent supportive treatment died with an average survival time of 14 days and with the expected signs of the hematopoietic syndrome: leukopenia, fever and bacteremia. Neither the administration of prophylactic antibiotics (sodium ampicillin and gentamicin sulfate) alone nor the transfusion of irradiated erythrocytes and platelets altered the mortality although the antibiotic regimen resulted in a small but significant mean prolongation of life to 18 days (Table IV). When erythrocyte and platelet transfusions

Table IV. The Effect of Various Treatments on the Survival of Beagles Following Exposure to 350 Rads ^{60}Co Gamma Radiation

Group	Number of survivors/ total number	Average day of death (range)
Untreated	0/5	14 (13-15)
Transfusions only	0/5	13 (11-15)
Antibiotics only	0/5	18 (13-21)
Combined treatment	8/9	18

were administered in combination with the parenteral antibiotic regimen during the period of profound leukopenia, eight of nine treated animals survived. This combined regimen allowed autochthonous recovery of marrow function, observed 18-28 days postirradiation. Once myelogenous recovery had begun, the antibiotics were discontinued. Erythrocyte and platelet transfusions could usually be discontinued during the 4th week postirradiation. This simple therapeutic regimen resulted in a greater survival rate for beagles following uniformly lethal doses of irradiation than has been reported previously. This therapy can permit studies of other functional capacities of dogs following usually lethal doses of irradiation and has significance for the management of bone marrow recipients also subjected to immunosuppressive therapy.

REFERENCE

1. Nutter, J. E., Graw, R. G., Jr. and Baum, S. J. Therapy of postirradiation marrow hypoplasia with blood components and antibiotics. Bethesda, Maryland, Armed Forces Radiobiology Research Institute Scientific Report SR73-5, 1973 (in press).

RESTORATION OF IMMUNE CAPABILITIES IN POSTIRRADIATION ANIMALS

Principal Investigators: *C. L. Cloud and J. E. Nutter*

The objective of this study was to develop a method for the prevention of the graft versus host reaction (GVHR) by inducing immunological paralysis of donor tissue to specific host antigens.

A model system was developed for inducing and assaying immunologic unresponsiveness in a localized graft versus host reaction. This assay depends on enlargement of the popliteal lymph node of Lewis-Brown Norway ($LBNF_1$) hybrid rats following injection of parental Lewis lymphoid cells into their footpad. The reaction is immunologically specific, is dependent on the recognition of foreign histocompatibility antigens by immunologically competent lymphocytes, and can be quantitated by determination of the node index (weight of the test node/weight of the contralateral normal node). Prospective donor parental rats were pretreated with hybrid spleen

cells for varying periods of time and the graft versus host reactivity of their spleens was assayed using the above system. The effect of different pretreatment intervals on the subsequent reactivity of the lymphoid cells is shown in Figure 4. The induction of the unresponsive state, following a constant dose of 2×10^8 cells, was an active process as demonstrated by the time dependency; there was no significant difference when the treatment times were 7, 10 or 14 days but these intervals induced greater degrees of unresponsiveness than did 1- or 3-day intervals.

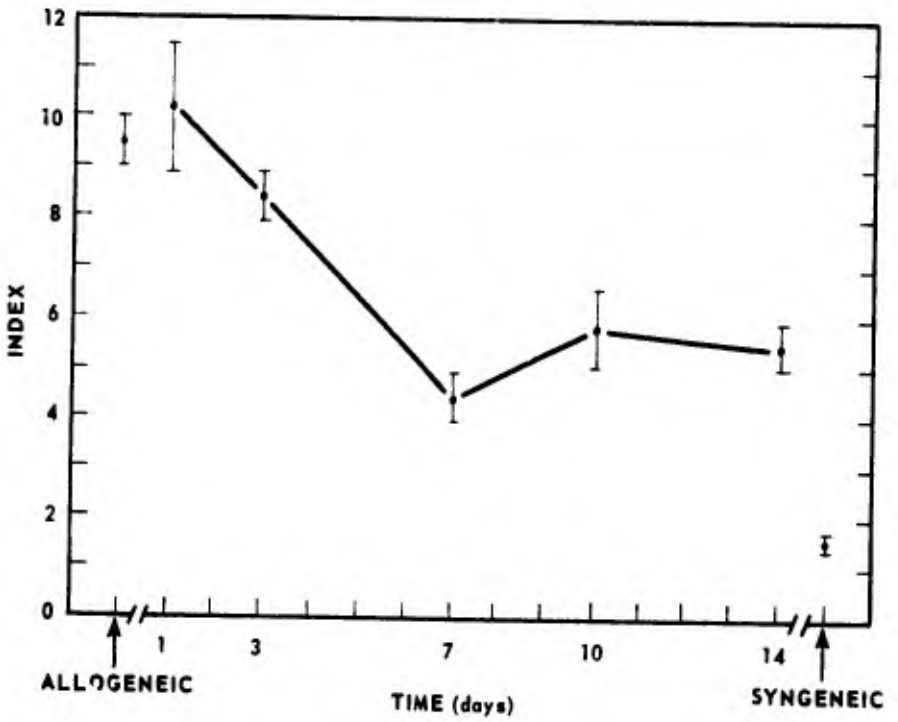

Figure 4. Effect of pretreatment interval on local graft versus host activity of Lewis spleen cells

The results presented in Figure 5 demonstrate the effect of various doses of hybrid cells on the system when assayed at the 7th day. The decrement in the node index was linear throughout the range of doses assayed (1×10^7 to 5×10^8 cells). Maximum reduction of the node index was observed when a dose of 5×10^8 cells was administered 7 days before assay ($p < .001$). Under these conditions the indexes were significantly less than those observed with cells from untreated allogeneic rats and approach those obtained with syngeneic cells.

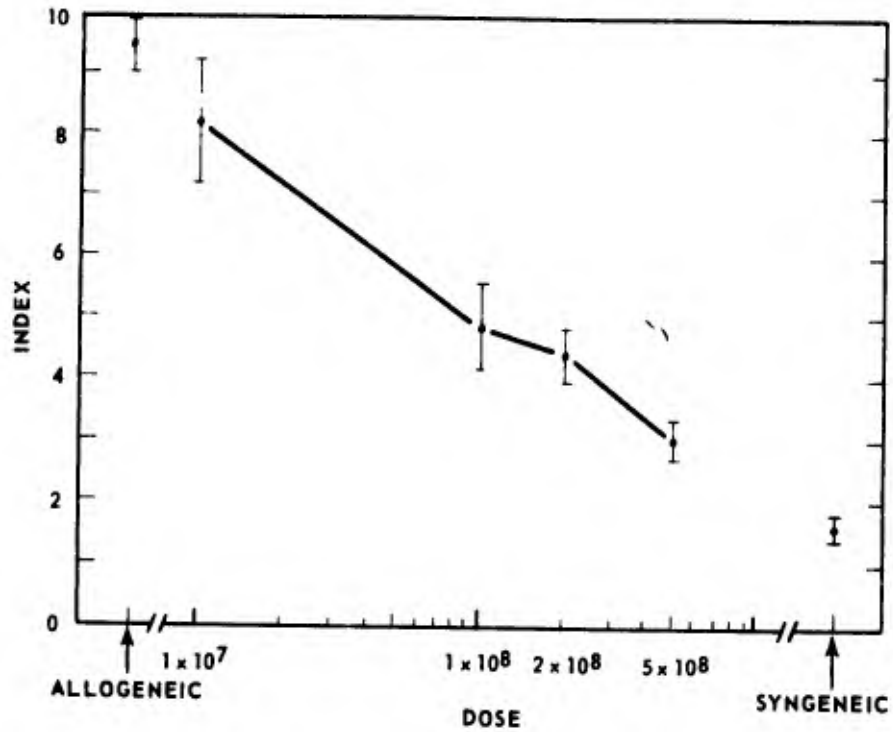

Figure 5. Effect of pretreatment dose on local graft versus host activity of Lewis spleen cells

Techniques for conducting bone marrow grafts and mixed lymphocyte interactions have been developed. These will allow correlation of the graft versus host reactivity in spleen, peripheral blood lymphocytes, and bone marrow and will also assist in ascertaining the efficacy of using a localized GVHR for predicting the severity of secondary disease following marrow engraftment.

MOLECULAR STUDIES OF CELLULAR AND SUBCELLULAR DAMAGE IN THE IRRADIATED ANIMAL

Principal Investigator: *G. N. Catravas*
Technical Assistance: *C. G. McHale*

Supralethally irradiated animals such as monkeys, miniature pigs and rats, shortly after exposure, experience a period of transient performance decrement or early transient incapacitation which is often accompanied by convulsions.[1,2] This

is followed first by a relative improvement in performance and then by a rapid, irreversible deterioration and eventual death.

Since drug-induced convulsions and functional inactivities are associated with changes in the metabolism of neurotransmitters, the objective of this research was to determine whether incapacitating doses of ionizing radiation affect the activities of enzymes involved in neurotransmitter metabolism.

Experiments were performed in which groups of rats were exposed to about 18 krads of mixed neutron-gamma radiation (pulse) rich in neutrons (neutron to gamma ratio 7 to 1) or rich in gamma rays (gamma to neutron ratio about 5 to 1) from the AFRRI-TRIGA reactor. The animals were sacrificed by decapitation at 4, 40 or 180 minutes after exposure with the heads falling into liquid nitrogen to freeze metabolic reactions at the time of decapitation. The brains were then partially thawed in a cold room and the dorsal hippocampus, cerebral cortex, cerebellum and anterior and posterior hypothalami were dissected out and homogenized in the appropriate media. Activity determinations were performed on RNA polymerase (RNA synthesis), choline acetyl transferase (acetyl choline synthesis), acetylcholinesterase (acetyl choline hydrolysis) and monoamine oxidase (inactivation of biogenic amines).

The radiation-induced changes in the activities of the four enzymes under investigation in the hippocampus, cerebellum and cerebral cortex are shown in Figure 6.

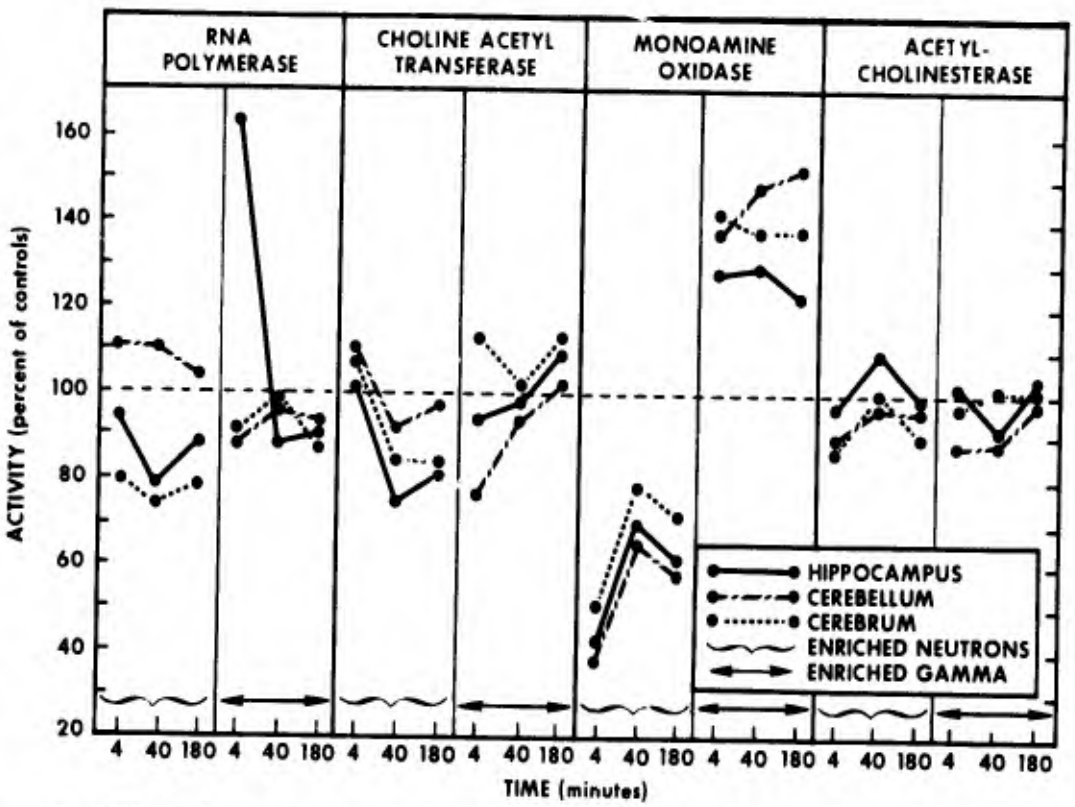

Figure 6. Effect of mixed neutron-gamma radiation (18 krads) on activity of brain enzymes

Figure 7 shows the activity changes observed in the anterior and posterior hypothalami. The results obtained indicate that the activity of the enzyme monoamine oxidase is affected most by irradiation of the animal. More specifically one can see that as early as 4 minutes after enriched neutron irradiation a pronounced (up to 70 percent) decrease in the activity of this enzyme occurred in all brain areas under investigation. In contrast, up to 50 percent increase in its activity was observed when the animals were exposed to radiation rich in gamma rays. RNA polymerase activity also appeared to be inhibited by radiation rich in neutrons and enhanced (during the first 4 minutes) by radiation rich in gamma rays. Relatively minor changes were observed in the activities of choline acetyl transferase and acetylcholinesterase.

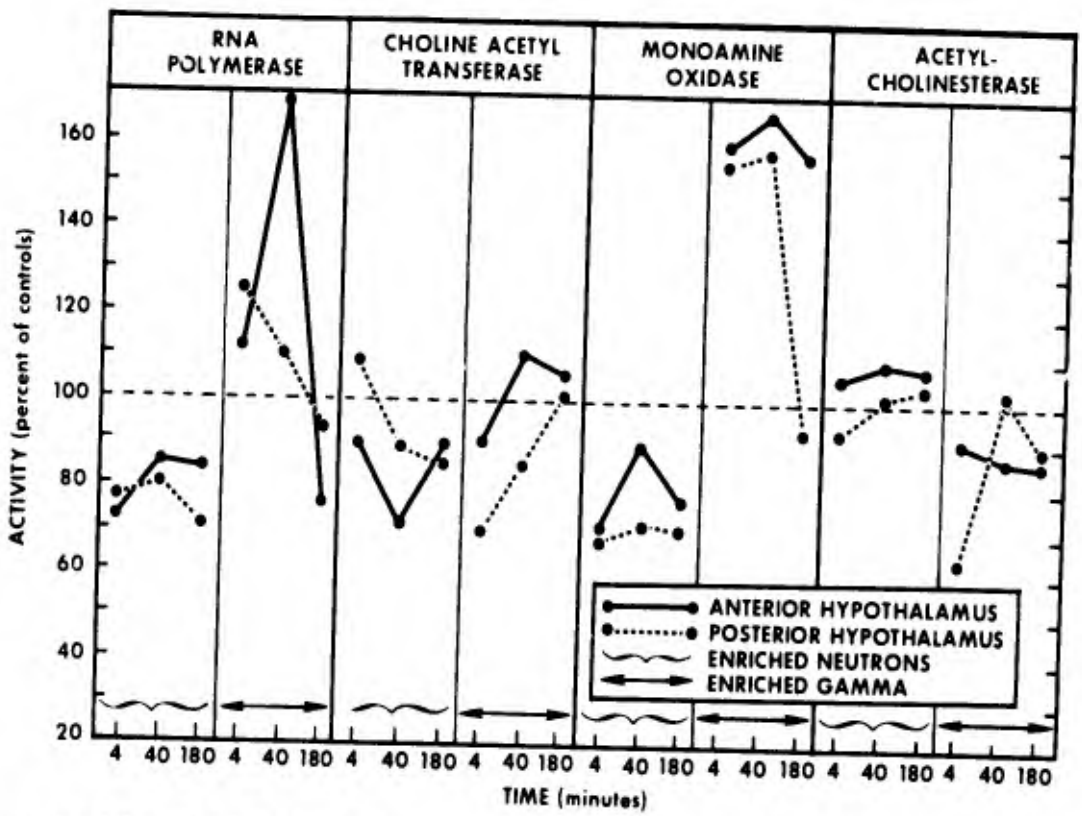

Figure 7. Effect of mixed neutron-gamma radiation (18 krads) on activity of brain enzymes

REFERENCES

1. Chaput, R. L. and Wise, D. Miniature pig incapacitation and performance decrement after mixed gamma-neutron irradiation. Bethesda, Maryland, Armed Forces Radiobiology Research Institute Scientific Report SR69-12, 1969.

2. Seigneur, L. J. and Brennan, J. T. Incapacitation in the monkey (Macaca mulatta) following exposure to a pulse of reactor radiations. Bethesda, Maryland, Armed Forces Radiobiology Research Institute Scientific Report SR66-2, 1966.

EFFECT OF IONIZING RADIATION ON BIOLOGICAL OXIDATION IN MAMMALIAN CELL MEMBRANES

Principal Investigators: *S. L. Cohan and G. N. Catravas*
Technical Assistance: *J. R. Abbott and E. E. Ricks*

The effect of high dose (10,000 and 20,000 rads) electron irradiation upon cerebral mitochondrial respiration has been studied.[1,2] After 20,000 rads there is a transient diminution in ADP-stimulated (state 3) respiration but no alterations in the presence of ATP (state 4) (Table V). There is also a loss of respiratory control (state 3/state 4) which is transient in nature; respiratory control returns to normal by 4 hours after irradiation. These changes are seen only if glutamate (site I) is used as a substrate but not if succinate (site II) is used demonstrating that site I of the respiratory chain is more susceptible to radiation injury and may act as the rate-limiting

Table V. The Effect of High Dose Ionizing Radiation upon Respiration of Cerebral Mitochondria

Substrate and Time	State 3 Respiratory Rate* (+ADP 400 nmoles)			State 4 Respiratory Rate (-ADP)			Respiratory Control (state 3/state 4)			ADP/O		
	20,000 rads	10,000 rads	Control	20,000 rads	10,000 rads	Control	20,000 rads	10,000 rads	Control	20,000 rads	10,000 rads	Control
Glutamate												
5 min	70.1+	80.4	83.5	26.9	21.7	22.5	2.6‡	3.7	3.7	1.82+	2.38	2.40
1 hr	81.3	84.6	86.0	28.0	22.8	22.6	2.9‡	3.7	3.8	2.26	2.47	2.44
4 hr	82.3	78.2	80.2	22.3	20.7	21.1	3.7	3.8	3.8	2.44	2.57	2.40
24 hr	79.4	81.1	80.5	20.9	22.5	21.3	3.8	3.6	3.8	2.28	2.41	2.42
Succinate												
5 min	90.6	92.5	97.0	48.4	45.8	45.2	1.9	2.0	1.9	1.49	1.46	1.54
1 hr	99.7	92.1	95.1	52.8	45.3	46.6	1.9	2.0	2.0	1.53	1.49	1.61
4 hr	96.1	91.5	97.3	52.0	50.1	50.7	1.8	1.8	1.9	1.44	1.52	1.42
24 hr	91.1	96.0	94.4	45.2	44.1	49.7	2.0	2.1	1.9	1.58	1.56	1.49

* Respiratory rate in nmoles oxygen/mg mitochondrial protein per minute
+ $P < .05$
‡ $P < .02$

segment in respiratory function under these circumstances. No abnormalities in cerebral mitochondrial respiration are seen after irradiation with 10,000 rads.

We have investigated the role of mitochondrial lipid peroxide formation and swelling in the transient radiation-induced abnormalities in respiration observed. Brain mitochondria are extremely resistant to peroxidation (Table VI) and swelling (Table VII); no significant differences in peroxidation or swelling of irradiated and nonirradiated mitochondria are seen. This is in striking contrast to the rapid swelling and peroxidation seen in mitochondria from organs other than the brain. Addition of ascorbate and $FeNH_4SO_4$, both strong oxidizing agents, failed to produce any differences in swelling or peroxidation between irradiated and control mitochondria (Tables VI and VII).

Table VI. The Effect of Ionizing Radiation upon Lipid Peroxidation of Cerebral Mitochondria

Time*	Control†			$FeNH_4SO_4$‡			Ascorbate‡		
	20,000 rads	10,000 rads	Sham irradiated	20,000 rads	10,000 rads	Sham irradiated	20,000 rads	10,000 rads	Sham irradiated
5 min	.090§	.100	.099	.603	.623	.614	.450	.439	.436
1 hr	.071	.075	.087	.591	.594	.618	.434	.399	.416
4 hr	.093	.078	.090	.608	.585	.606	.450	.410	.453
24 hr	.080	.065	.077	.616	.601	.593	.434	.423	.405

* Time after irradiation
† Mitochondria incubated for 90 minutes in 175 mM KCl + 20 mM Tris HCl at pH 7.4
‡ Mitochondria incubated for 90 minutes in the presence of $FeNH_4SO_4$ or ascorbate
§ D532

Table VII. The Effect of Ionizing Radiation upon Swelling of Cerebral Mitochondria

Time*	Control†			$FeNH_4SO_4$‡			Ascorbate‡		
	20,000 rads	10,000 rads	Sham irradiated	20,000 ra is	10,000 rads	Sham irradiated	20,000 rads	10,000 rads	Sham irradiated
5 min	.460§	.470	.470	.465	.445	.450	.380	.380	.390
1 hr	.470	.480	.470	.420	.440	.430	.390	.390	.390
4 hr	.481	.475	.460	.465	.440	.415	.390	.410	.385
24 hr	.460	.460	.450	.422	.425	.450	.390	.410	.410

* Time after irradiation
† Mitochondria incubated for 90 minutes in 175 mM KCl + 20 mM Tris HCl at pH 7.4
‡ Mitochondria incubated for 90 minutes in the presence of $FeNH_4SO_4$ or ascorbate
§ D520

Addition of DPNH, a nonbound portion of the respiratory chain which is required for entrance of site I substrates, to irradiated and nonirradiated mitochondria does not influence respiratory function, probably ruling out the loss of unbound portions of the respiratory chain through leaking mitochondrial membranes as an explanation for the abnormal respiratory function seen with site I substrates.

REFERENCES

1. Cohan, S. L., Catravas, G. N., Abbott, J. R. and Ricks, E. E. The effect of supralethal doses of ionizing radiation upon mitochondria of the rat central nervous system. Bethesda, Maryland, Armed Forces Radiobiology Research Institute Scientific Report SR72-12, 1972 (in press).

2. Cohan, S. L., Abbott, J. R. and Catravas, G. N. The effect of ionizing radiation upon mitochondria of the central nervous system. Bethesda, Maryland, Armed Forces Radiobiology Research Institute Scientific Report SR72-17, 1972 (in press)

RESPIRATORY CONTROL AND SWELLING IN RAT LIVER MITOCHONDRIA: EFFECT OF ^{60}Co GAMMA RADIATION AND INJECTED NUTRIENT

Principal Investigator: *W. D. Skidmore*
Technical Assistance: *E. E. Ricks and O. Z. Williams*

The effects of whole-body irradiation on the structural and functional integrity of rat liver mitochondria were investigated.

The objective of this study[1] was to compare the relative effects of three treatments with that of radiation on the lag time for mitochondrial swelling and the respiratory control during oxidation of succinate. The three treatments were dietary supplementation with ethyl linoleate, time of feeding, and an intraperitoneal injection of a soluble diet. Control and experimental rats from each of the eight different treatment groups were bilaterally exposed to 1000 rads of ^{60}Co gamma rays. Liver mitochondria were collected from the 16 different groups 24 hours later for assay. Iron-induced mitochondrial swelling was used as an index of structural integrity. Respiratory control of adenosine diphosphate stimulated oxidation of succinate was selected as an index of functional integrity. Results indicate that the intraperitoneal injection of a soluble diet significantly increased the lag time for swelling in every

group given the injection in comparison with uninjected controls (Table VIII). The effect of radiation that tends to decrease the lag time is reversed by the dominant effect of the injection. In the assay for respiratory control, either whole-body irradiation or injection of a soluble diet significantly increased the respiratory control values above those for untreated controls. The significant effects were consistently observed in all treated groups. A direct and injurious effect of irradiation was not found in rat liver mitochondria.

Table VIII. Mitochondrial Swelling and Respiratory Control Mean Value with Associated Standard Error for Each of the Combined Treatment Groups*

Treatment group		Assay	
Code	Description	Swelling (minutes)	Respiratory control
1. $X^0L^0F^0D^0$	Untreated control	76.0 ± 13.8	2.11 ± 0.10
2. $X^1L^0F^0D^0$	Exposure to radiation	55.4 ± 8.3	2.43 ± 0.14
3. $X^0L^1F^0D^0$	Linoleate supplementation	49.4 ± 8.2	2.19 ± 0.10
4. $X^1L^1F^0D^0$	Radiation and linoleate	40.7 ± 10.5	2.55 ± 0.10
5. $X^0L^0F^1D^0$	Feeding	68.7 ± 9.0	2.13 ± 0.05
6. $X^1L^0F^1D^0$	Radiation and feeding	63.6 ± 7.6	2.58 ± 0.13
7. $X^0L^1F^1D^0$	Linoleate and feeding	74.8 ± 10.8	2.21 ± 0.09
8. $X^1L^1F^1D^0$	Radiation, linoleate, and feeding	56.1 ± 9.9	2.62 ± 0.09
9. $X^0L^0F^0D^1$	Diet injection (I.P.)	122.0 ± 12.9	2.60 ± 0.15
10. $X^1L^0F^0D^1$	Radiation and I.P. diet	133.0 ± 11.8	2.84 ± 0.13
11. $X^0L^1F^0D^1$	Linoleate and I.P. diet	121.0 ± 15.9	2.69 ± 0.08
12. $X^1L^1F^0D^1$	Radiation, linoleate, and I.P. diet	118.0 ± 9.4	2.87 ± 0.12
13. $X^0L^0F^1D^1$	Feeding and I.P. diet	134.0 ± 10.4	2.79 ± 0.07
14. $X^1L^0F^1D^1$	Radiation, feeding, and I.P. diet	133.0 ± 10.7	3.05 ± 0.05
15. $X^0L^1F^1D^1$	Linoleate, feeding, and I.P. diet	129.0 ± 14.8	2.75 ± 0.13
16. $X^1L^1F^1D^1$	Radiation, linoleate, feeding, and I.P. diet	133.0 ± 11.7	3.11 ± 0.07

* Treatments and assays are defined in referenced report[1]

REFERENCE

1. Skidmore, W. D. Respiratory control and swelling in rat liver mitochondria: effect of ^{60}Co gamma radiation and injected nutrient. Bethesda, Maryland, Armed Forces Radiobiology Research Institute Scientific Report SR72-11, 1972.

DRUG RESPONSIVENESS IN THE POSTIRRADIATION ANIMAL

Principal Investigators: *T. A. Strike and T. F. Doyle*
Technical Assistance: *W. G. Ewald*

The effectiveness of the histamine and the serotonin antagonist cyproheptadine in preventing or ameliorating the cardiovascular response observed in monkeys and the role of histamine in radiation-induced early transient incapacitation (ETI) were investigated.

Monkeys were given cyproheptadine hydrochloride (1 mg/kg) 30 minutes before they were irradiated with a single, pulsed 4000-rad dose of mixed gamma-neutron radiation. The postirradiation hypotension was similar to that observed in saline-treated controls but an earlier and greater recovery of blood pressure occurred in the cyproheptadine-treated monkeys. The mean survival time of the cyproheptadine-treated irradiated monkeys (34.3 ± 9.7 hours) was significantly longer than that of the saline-treated irradiated controls (2.9 ± 1.2 hours). The effect of cyproheptadine on the hypotension observed in monkeys following a 4000-rad dose of mixed gamma-neutron radiation was similar to that of the antihistamine chlorpheniramine.[1]

The amount of histamine released in the monkey at various times after a 4000-rad dose of mixed gamma-neutron radiation was measured. Four monkeys were treated with chlorpheniramine (20 mg) before irradiation. These monkeys were also injected with aminoguanidine (1 mg/kg), a histidine decarboxylase inhibitor, to prevent the rapid metabolism of histamine and permit its measurement in this species. Post-irradiation blood pressure changes were also monitored. At 5 minutes postirradiation hypotension was maximum and, at the same time, histamine concentration reached a maximum value of approximately five times the preirradiation value (Figure 8).

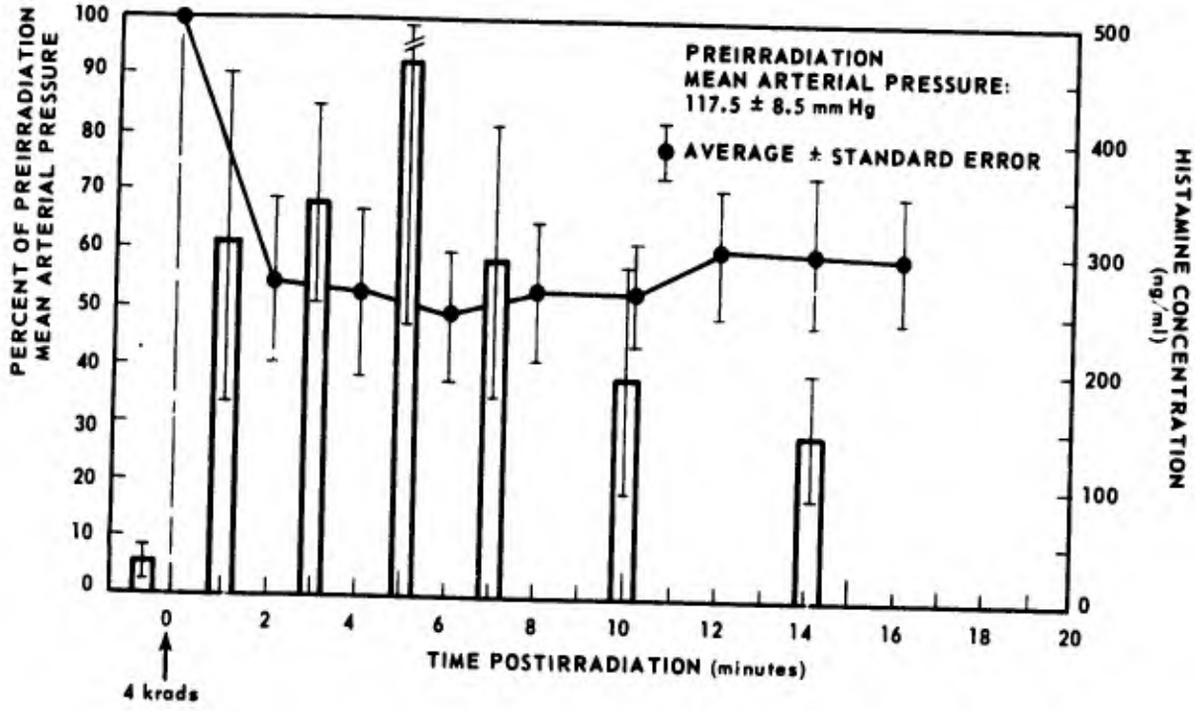

Figure 8. Changes in histamine concentration and arterial pressure of four monkeys given aminoguanidine and chlorpheniramine 30 minutes before receiving a 4000-rad dose of mixed gamma-neutron radiation

Monkeys were given daily injections of Compound 48/80 (1 mg/kg), a histamine releaser specific for mast cells, for 4 days prior to irradiation. A marked fall in blood pressure occurred immediately after the first injection of Compound 48/80. The degree of hypotension was less following the second dose of Compound 48/80 and appeared to stabilize after the third injection. Thirty minutes after the fourth injection of Compound 48/80, the monkeys were given chlorpheniramine and aminoguanidine then irradiated 30 minutes later. The postirradiation hypotension in these mast cell histamine-depleted animals (Figure 9) was similar to that observed in the saline controls; however, histamine increased only slightly above the preirradiation value.

The chlorpheniramine- and aminoguanidine-treated monkeys were irradiated with a 4000-rad dose of mixed gamma-neutron radiation. Twenty minutes later they were injected with Compound 48/80 (1 mg/kg). Blood pressure decreased after injection of Compound 48/80 to approximately 62 percent of preinjection value and at the same time a twofold increase in histamine was noted (Figure 10).

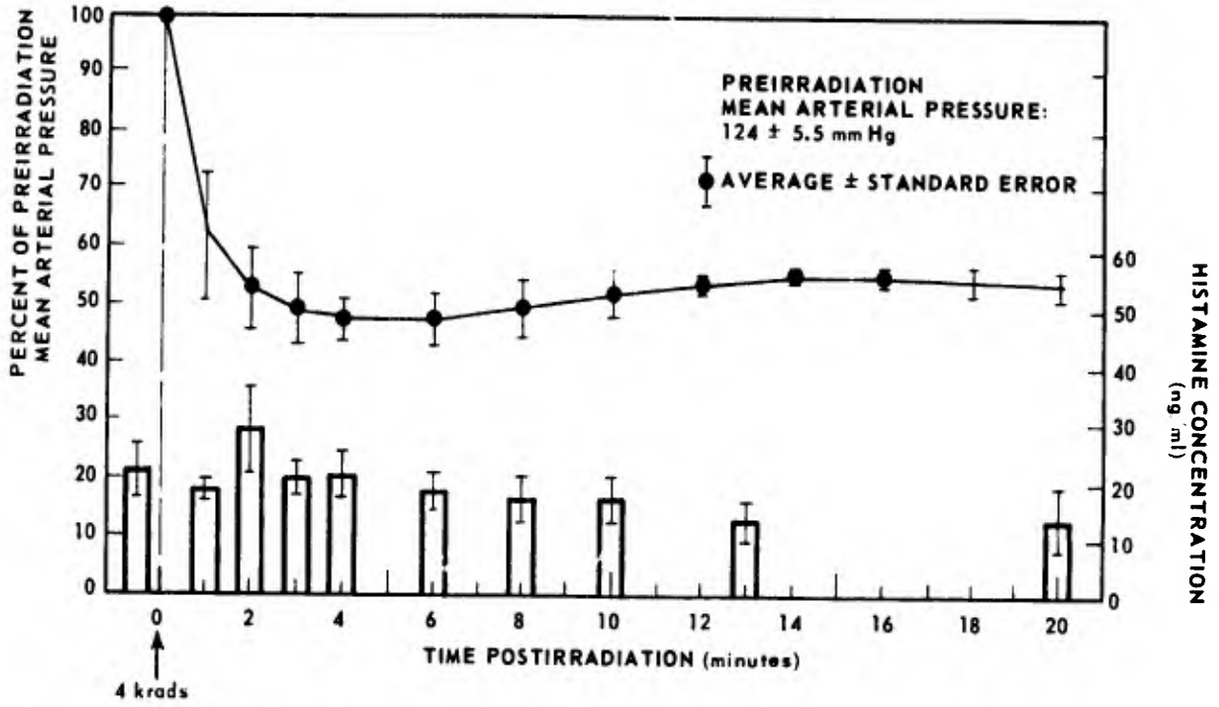

Figure 9. Changes in histamine concentration and arterial pressure of four monkeys after four consecutive days of mast cell histamine depletion and a 4000-rad dose of mixed gamma-neutron radiation given after aminoguanidine

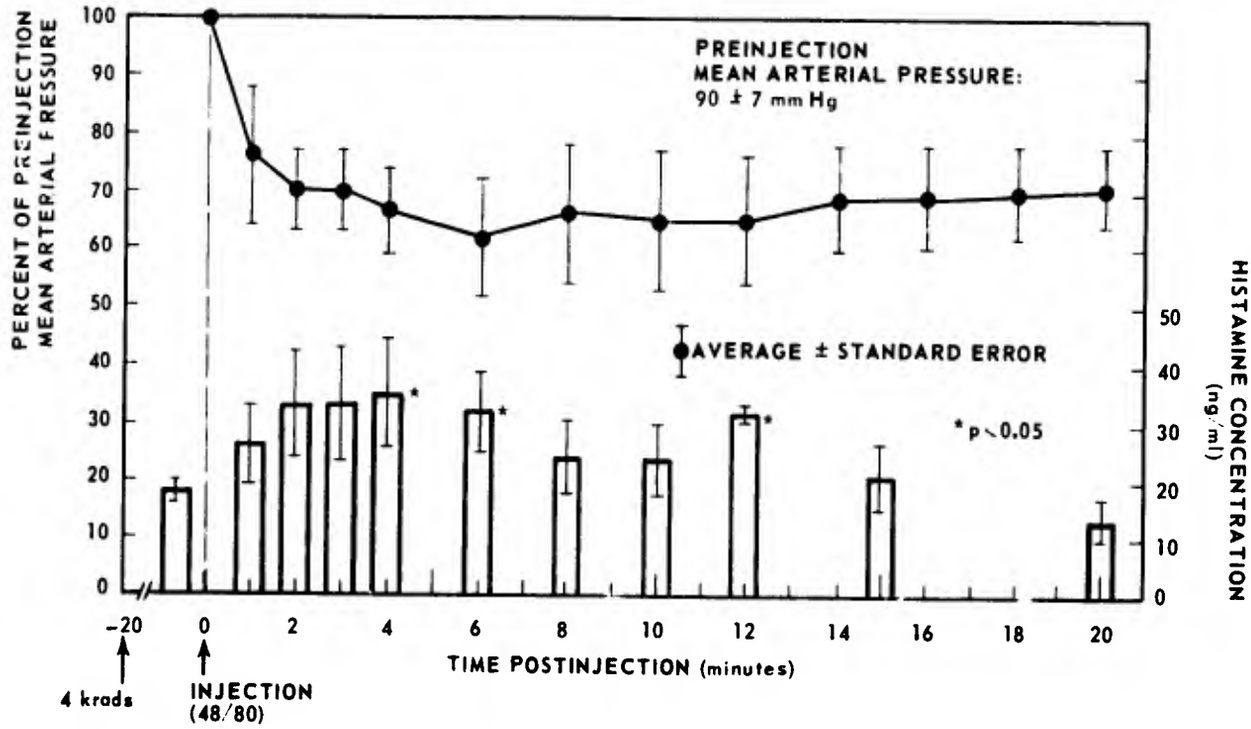

Figure 10. Blood histamine concentrations and arterial pressure changes of four monkeys given a 4000-rad dose of mixed gamma-neutron radiation and 20 minutes later injected with aminoguanidine and Compound 48/80

It is difficult to assess the role of histamine from the results obtained in these preliminary studies. It appears that ionizing radiation causes the release of both mast cell and nonmast cell histamine. Monkeys apparently depleted of their mast cell histamine still show a slight increase in plasma histamine after irradiation, which appears to correlate with the fall in blood pressure. Irradiated monkeys that are then treated with the mast cell histamine releaser (Compound 48/80) show a twofold increase in plasma histamine, which also appears related to the decreased blood pressure. Further work is necessary to determine the relationship between plasma histamine levels and the degree of hypotension that is produced. This preliminary work, of course, does not rule out the possibility that radiation releases vasodepressor substances other than histamine.

REFERENCE

1. Doyle, T. F., Curran, C. R. and Turns, J. E. Chlorpheniramine as a prophylaxis to radiation-induced performance decrement in the monkey. Bethesda, Maryland, Armed Forces Radiobiology Research Institute Scientific Report SR73-9, 197[illegible] (in press).

THE RELATIONSHIP OF BLOOD-BRAIN BARRIER DAMAGE TO SURVIVAL TIME AFTER ACUTE RADIATION INJURY

Principal Investigators: *D. E. Wyant, J. Kabal, S. J. Baum and L. J. Parkhurst*

The purpose of this study was to investigate whether a relationship exists between alterations of the blood-brain barrier (BBB) and the survival time of rats exposed to supralethal irradiation.[1] BBB alterations were produced by injection of glycerol, mercuric chloride, or by lymphatic cervical blockade. Animals were subsequently exposed to a supralethal dose of radiation, and the survival times of various groups were compared.

The results of the study with and without lymphatic cervical blockade (LCB) are presented in Figure 11. LCB alone induced no deaths. In irradiated rats there was no difference in the 50 percent mortality time between LCB and sham operated rats.

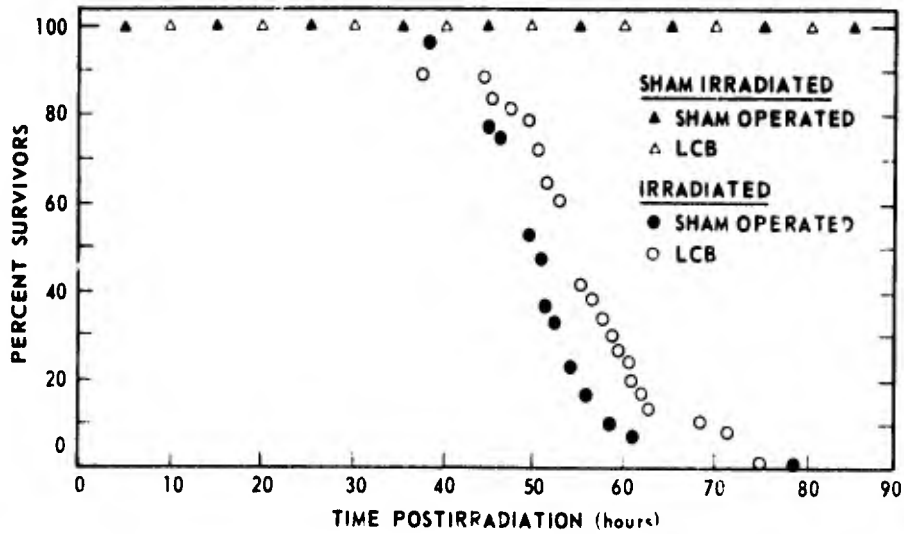

Figure 11. Survival time of rats with and without lymphatic cervical blockade (LCB) after exposure to 20,000 rads of whole-body mixed gamma-neutron radiation

In the glycerol treated rats, the survival of the irradiated sham operated rats was nearly linear with time (Figure 12). Fifty percent mortality was reached approximately 32 hours postirradiation, and all rats died within 75 hours. The 50 percent mortality time of the LCB group was approximately 57 hours after exposure, but all rats in this group were dead 79 hours after exposure.

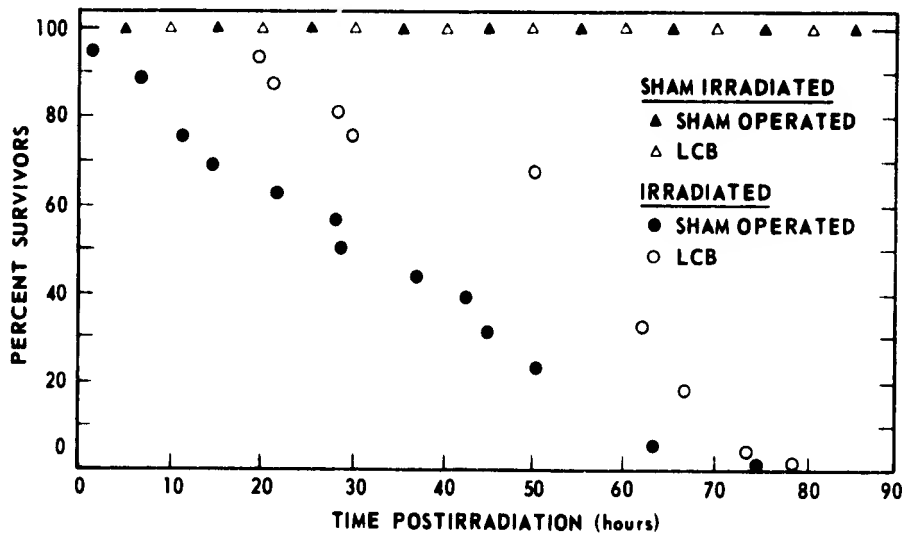

Figure 12. Survival time of glycerol pretreated rats with and without lymphatic cervical blockade (LCB) after exposure to 20,000 rads of whole-body mixed gamma-neutron radiation

The 50 percent mortality time of the irradiated LCB and sham operated mercuric chloride pretreated rats did not differ significantly from each other (Figure 13).

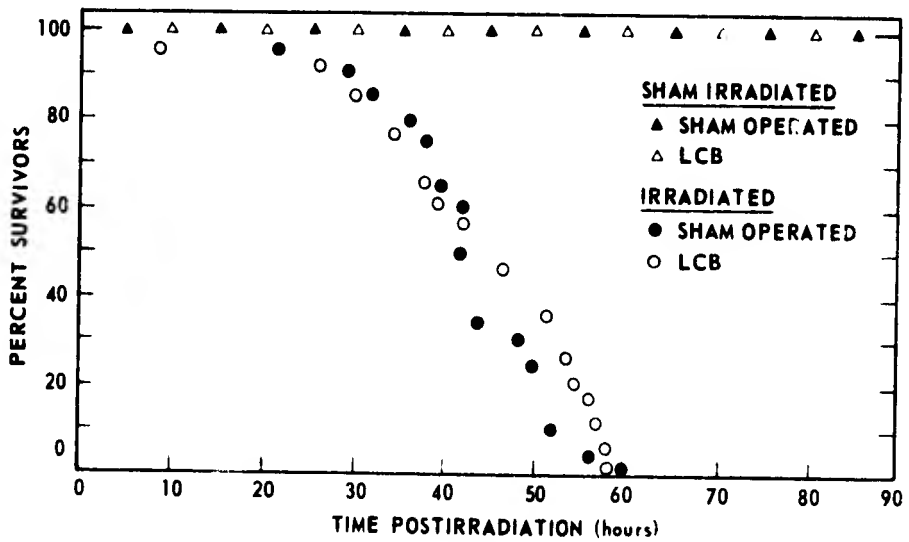

Figure 13. Survival time of mercuric chloride pretreated rats with and without lymphatic cervical blockade (LCB) after exposure to 20,000 rads of whole-body mixed gamma-neutron radiation

The BBB alterations thus induced by LCB and glycerol or mercuric chloride injection, when followed by irradiation, did not significantly shorten survival when compared to animals receiving irradiation alone. This suggests that BBB alteration prior to irradiation does not contribute significantly to mortality, further suggesting that BBB damage may bear no direct relationship to survival after acute radiation injury.

REFERENCE

1. Wyant, D. E., Kabal, J., Baum, S. J. and Parkhurst, L. J. The relationship of blood-brain barrier damage to survival time after acute radiation injury. Bethesda, Maryland, Armed Forces Radiobiology Research Institute Scientific Report SR72-18, 1972 (in press).

EFFECTS OF IONIZING RADIATION ON THE ULTRASTRUCTURE OF MAMMALIAN TISSUES

Principal Investigators: *A. A. Rene' and J. H. Darden*
Technical Assistance: *M. L. Guimond*

The existence of a blood-brain barrier (BBB) in the central nervous system has been well established. Under experimental conditions, alterations in the BBB have been induced by various means including radiation, allowing the uncontrollable escape of vascular fluid into the brain tissue. Although a number of studies have been devoted to BBB changes in irradiated recipients, the mechanism of brain edema formation has not been completely established.

The objective of this study[1] was to determine how edema may possibly develop in the brain tissue of animals exposed to relatively high doses of radiation. Electron microscopy was employed to study a low molecular weight protein, horseradish peroxidase (HRP), as a tracer suitable for locating permeability changes in the BBB. Increased permeability may be the cause of possible fluid loss from blood vessels and edema of certain tissue.

Sprague-Dawley rats were subjected to a whole-body dose of 15 krads of mixed gamma-neutron radiation. Following irradiation the animals were intravenously injected with HRP and sacrificed. The medulla of these animals was fixed either by perfusion or by immersion, incubated in a substrate medium and processed for electron microscopic examination. In control animals subjected to the same procedures, the reaction product of the enzyme HRP and its substrate was confined to the lumina of the blood vessels in the brain fixed by immersion (Figure 14) and completely washed out of the blood vessels of the brain fixed by perfusion. The brain tissue of the irradiated animals injected with HRP and fixed by immersion exhibited a dense reaction product in the lumina of the blood vessels, in invaginations of the luminal surface, and in micropinocytotic vesicles of the endothelial cell cytoplasm (Figure 15). The electron dense material was also observed in the outer margin of the basement membrane and in areas beyond this membrane (Figures 15 and 16). The brain tissue of the irradiated animals fixed by perfusion was similar to the tissue fixed by immersion except for the presence of reaction products within blood vessels. The most significant alteration in the medullary tissue of the irradiated animals was an increase in the number of micropinocytotic vesicles in the endothelial cells. This was viewed as the mode of transcapillary passage of substances from the vascular tissue to the parenchymal tissue of the brain. It appears, then, that damage caused by high doses of radiation initiates increased vascular permeability which may lead to the edematous condition observed in the irradiated animal.

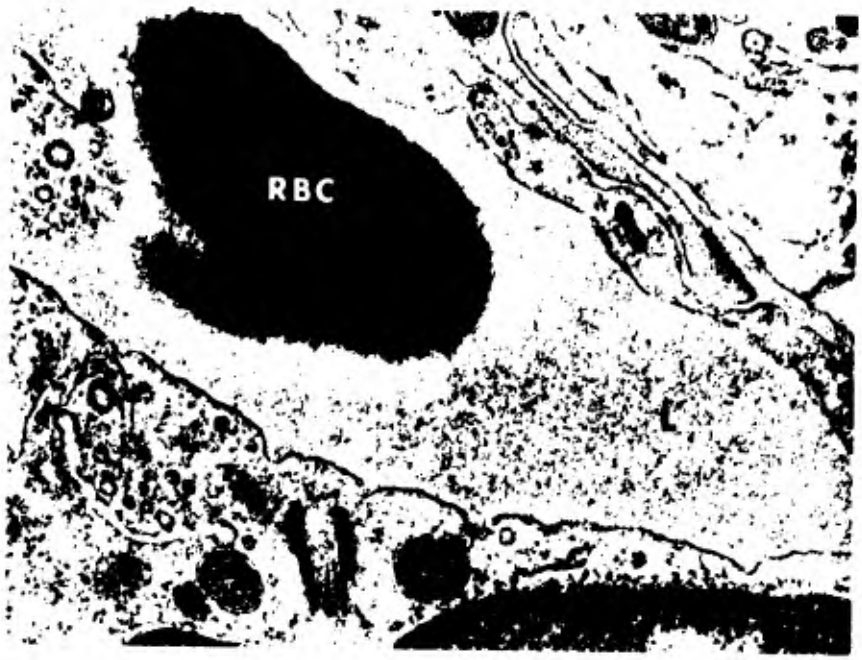

Figure 14. A cross section of a medullary capillary of a control rat. The reaction product and a red blood cell may be seen in the lumen (L) of the vessel. A red blood cell (RBC) may also be seen in the capillary lumen. X 28,500

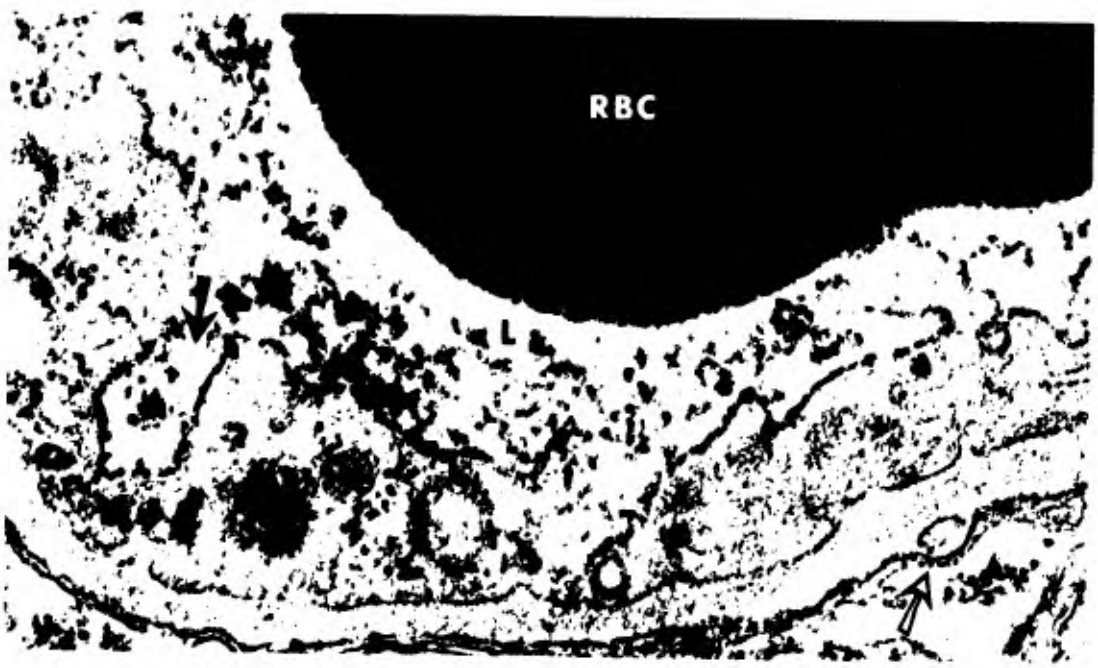

Figure 15. A cross section of a medullary capillary of a rat exposed to 15 krads of whole-body mixed gamma-neutron radiation. The reaction product may be seen in invaginations of the endothelial cell (solid arrow), in the lumen (L) of the vessel and in a vesicle on the contraluminal margin of the basement lamina (open arrow). A red blood cell (RBC) may also be seen in the capillary lumen. X 48,750

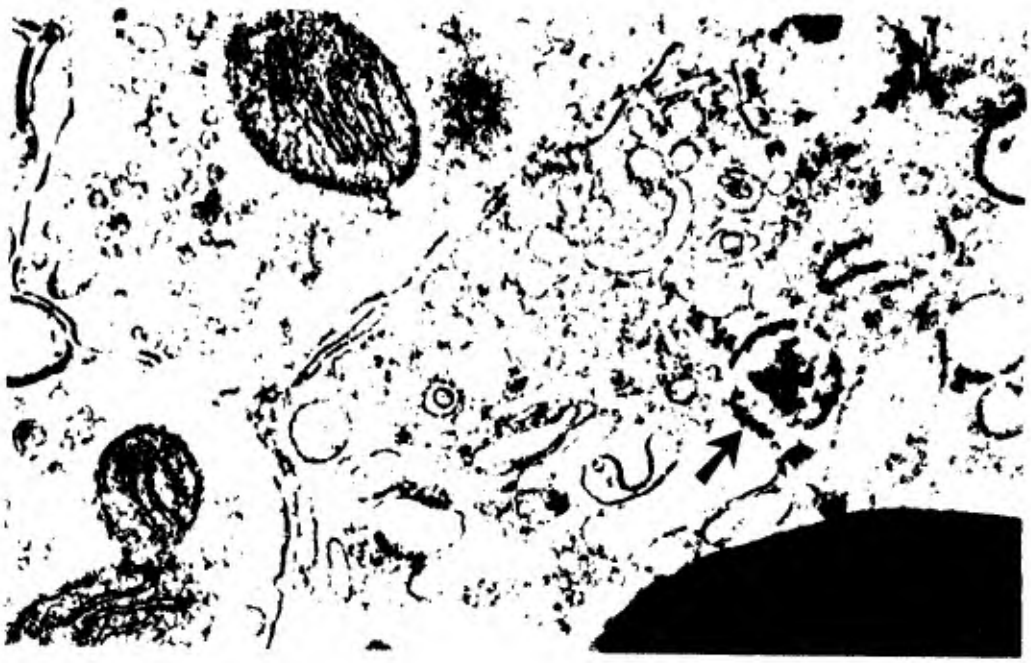

Figure 16. A section of medullary parenchymal tissue of a rat exposed to 15 krads of whole-body mixed gamma-neutron radiation. Reaction product in a vesicle may be seen in what appears to be glial cell cytoplasm (arrow). X 43,125

REFERENCE

1. René, A. A., Parker, J. L., Darden, J. H. and Eaton, N. A. Effect of a supra-lethal dose of radiation on the blood-brain barrier. Bethesda, Maryland, Armed Forces Radiobiology Research Institute Scientific Report SR73-2, 1973 (in press).

THE DEPENDENCE OF MINIATURE PIG PERFORMANCE DECREMENT UPON GAMMA RAY DOSE RATE

Principal Investigators: *R. E. George and R. L. Chaput*
Technical Assistance: *E. L. Barron, W. W. Wolfe, J. K. Warrenfeltz, M. E. Flynn, N. L. Fleming and T. K. Dalton*

To test the hypothesis that performance decrement varies with gamma ray dose rate even at hundreds to thousands of rads per minute, trained miniature pigs were irradiated in a nuclear reactor-produced gamma ray field.[1] The dose rate at the

midline of the brain was 470, 1000, 1500, 2000, or approximately 10,000,000 (pulsed irradiation) rads/minute. Doses ranged from 1500 to 14,700 rads. Postirradiation performance data were used to calculate for each dose rate the most probable dose that would cause 50 percent of the animals to perform unsatisfactorily (ED_{50}). The miniature pigs' response varied markedly with dose rate. ED_{50}'s were 10,570, 7780, 4480, 2500, and 2380 rads, respectively, for 470, 1000, 1500, 2000, and 10^7 rads/minute (Figure 17).

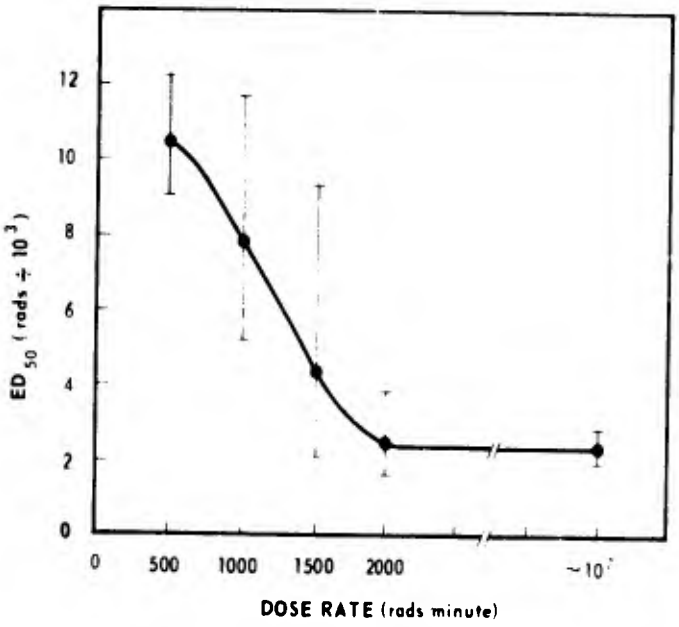

Figure 17. The most probable dose that would cause 50 percent of trained miniature pigs to perform unsatisfactorily (ED_{50}) versus gamma ray dose rate

Survival times did not appear to be dependent upon dose rate.

REFERENCE

1. George, R. E., Chaput, R. L. and Barron, E. L. The dependence of miniature pig performance decrement upon gamma ray dose rate. Bethesda, Maryland, Armed Forces Radiobiology Research Institute Scientific Report SR72-20, 1972 (in press).

INVESTIGATION OF INCAPACITATING DOSES OF RADIATION IN THE LARGER MAMMALS

Principal Investigators: *R. L. Chaput and G. H. Zeman*
Technical Assistance: *E. L. Barron, W. W. Wolfe, J. K. Warrenfeltz, M. E. Flynn, N. L. Fleming and T. K. Dalton*

Previous work indicated that miniature pigs, trained to a shuttlebox problem, performed better after the second of two 4400-rad doses of ionizing radiation.[2] These results were unaffected by changing the time interval between the two equal dose fractions over the range of 1/2 to 51 hours. It is evident that mechanisms responsible for the reduced response of the pigs to the second dose were clearly effective within 30 minutes. The objective of this research was to resolve the "recovery" or kinetics of these mechanisms and to evaluate the role of the central nervous system in these processes.

Five groups of eight pigs each received two 4400-rad doses of high energy electrons from the AFRRI electron linear accelerator.[1] The radiation was delivered mainly to the brain and the doses were separated by time intervals of 10^{-4} to 30 minutes.

Average performance decrement (percent omission) observed during the first 15 minutes after the second dose of radiation is presented in Figure 18. The contribution of the initial dose to the total decrement observed after the second dose is also shown.

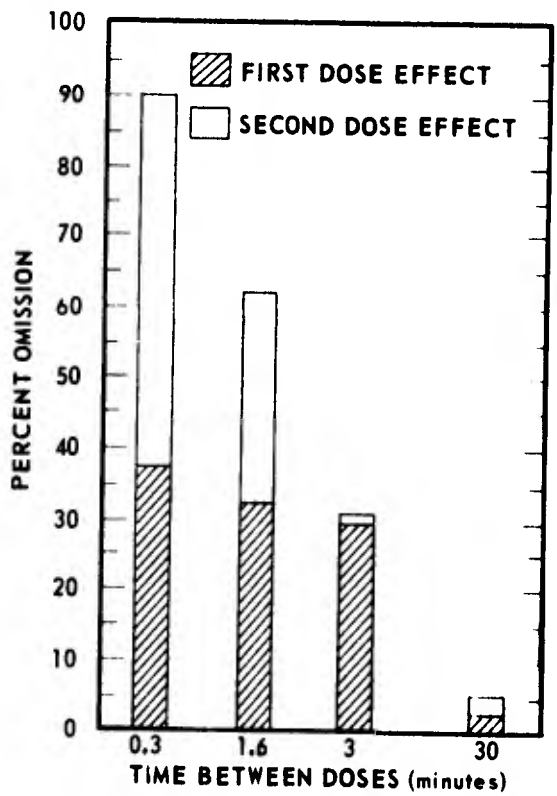

Figure 18 The contribution of the first and second doses to early performance decrement as a function of time between doses

The most notable finding was the marked reduction in percent omission after the second dose when the time interval between doses was increased from 0.3 to 3 minutes. The second dose apparently contributed to performance decrement only when the two doses were no more than 1.6 minutes apart. At longer time intervals, the residual injury from the initial dose of radiation could account for essentially all of the performance decrement seen after the second dose of radiation.

Because the radiation was delivered primarily to brain structures, it was concluded that the increased radioresistance to the second dose was initiated by changes in the central nervous system. These and results of earlier studies prompted an investigation on the effects of supralethal doses of radiation on the metabolism of the central nervous system.

Grand mal type seizures consistently occur immediately after miniature pigs are exposed to a supralethal dose of ionizing radiation. Gamma-aminobutyric acid (GABA), a putative neuroregulating transmitter, has been implicated in the etiology of seizures observed in a variety of clinical and stress situations. Therefore, the metabolism of this compound is being investigated in animals exposed to high radiation doses to determine if it also plays a role in radiation-induced seizures.

The only known pathway for GAB[illegible] metabolism in brain tissue is as follows:

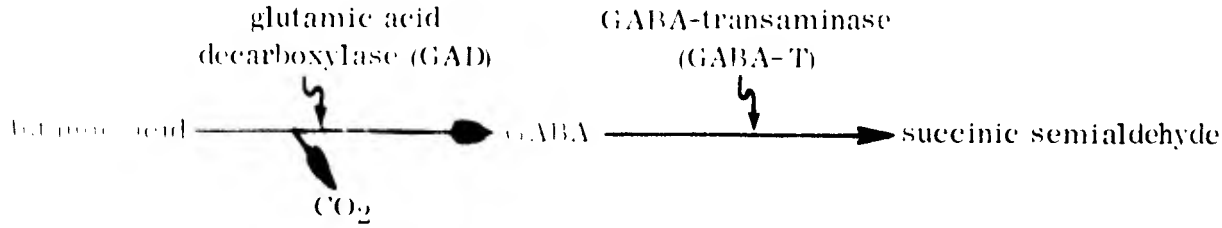

The rate-limiting step appears to be that regulated by GAD.

An enzymic assay system based on the method of Scott and Jakoby[4] was used to analyze brain GABA levels. A radiometric method is currently being used to estimate GAD activity.[3] However, the procedures are cumbersome and an automated system for assay of GAD has been developed.[5]

The technique is based on measurements of the partial pressure of CO_2 evolved in the conversion of glutamate to GABA. The PCO_2 for various GAD concentrations, shown in Figure 19, is linear over the entire range of concentrations used. Figure 20 shows the results of PCO_2 assays of various GAD solutions plotted against the results of radiometric assays of the same solutions. There is a high linear correlation coefficient between the two methods ($r = 0.9959$).

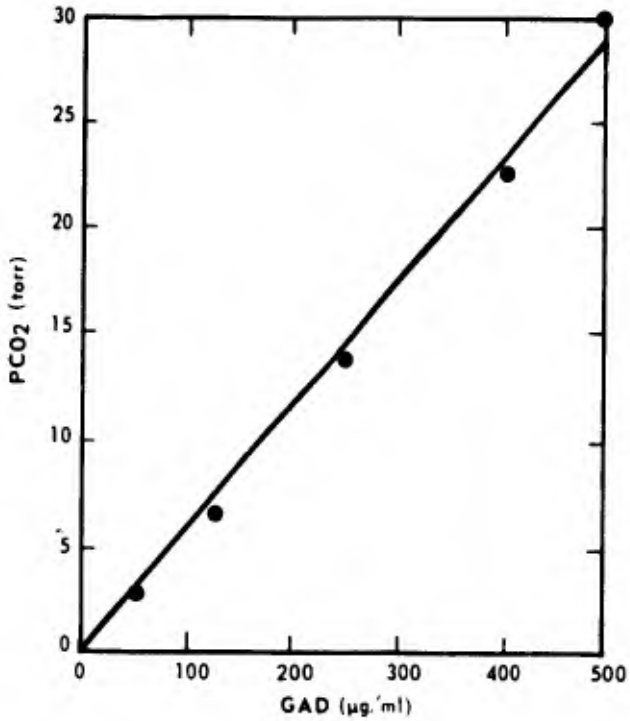

Figure 19. PCO_2 versus GAD concentration

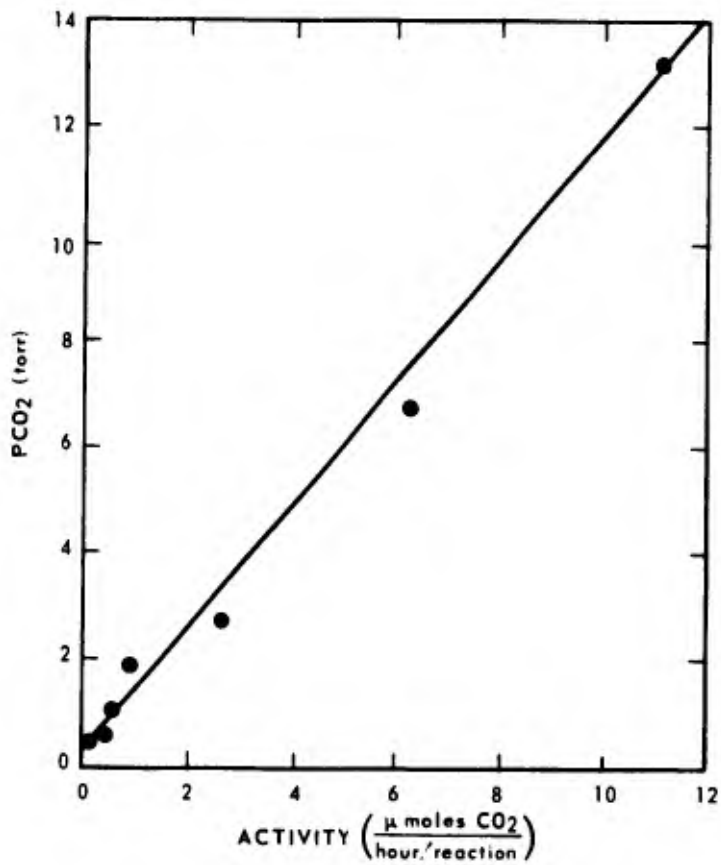

Figure 20. PCO_2 changes versus radiometrically determined activity

Brain homogenates prepared in our laboratory have yielded typical GAD activities of 2 μmoles CO_2/hour per reaction when assayed radiometrically. This is well within the range of sensitivity of the PCO_2 method. Thus, the PCO_2 automated method provides the desired high sensitivity and handling speed (30 samples per hour) required to process large numbers of samples. Slight modifications of this procedure are required, however, before tissue homogenates can be assayed.

A radiometric method for assay of GABA-T is currently being developed.

Whole brain GABA in rats exposed to 10,000 or 20,000 rads mixed gamma-neutron radiation is compared to laboratory controls and sham irradiated animals in Table IX. These data indicate that brain GABA levels rose markedly when animals were sham irradiated and that a slight additional increase occurred after irradiation.

Table IX. Whole Brain GABA in Control and Irradiated Ra

Number of rats	Treatment	Time after irradiation (min)	GABA (μmole/g wet weight brain)
12	Control	-	2.09 ± 0.26*
	10,000 rads		
4	sham	-	2.37 ± 0.086
4	irradiated	1	2.31 ± 0.144
4	irradiated	5	2.48 ± 0.073
4	irradiated	20	2.56 ± 0.053
	20,000 rads		
4	sham	-	2.48 ± 0.13
3	irradiated	1	2.69 ± 0.08
3	irradiated	5	2.61 ± 0.10

* ± Standard error

Preliminary data indicate that GAD activity declines after irradiation. The average value from 12 control rats is 5.13 ± 0.36 μmoles glutamate converted to GABA/100 mg brain wet weight/hour. One minute after 10,000 rads, the average value from six irradiated rats was 4.78 ± 0.09.

The results obtained thus far are not inconsistent with the hypothesis that GABA metabolism may be involved in the etiology of radiation-induced seizures. Rats spontaneously convulse within 20 minutes after irradiation only after doses of about 30,000 rads. They do not convulse after 10,000 rads but will do so several hours after a 20,000-rad dose. It is anticipated, therefore, that changes in GABA metabolism will be more closely related to radiation doses that clearly show convulsive effects.

Studies have shown that an increased brain GABA level can be correlated with an increased resistance to seizures induced by a variety of stress situations and by drugs such as hydrazides. Thus, it is interesting to note that the increased GABA levels are consistent with previous findings that, after receiving a 4000-rad dose of radiation, miniature pigs show an increased resistance to the convulsant effects of a subsequent supralethal dose.

REFERENCES

1. Chaput, R. L. and Berardo, P. A. Increased brain radioresistance after supralethal irradiation. Bethesda, Maryland, Armed Forces Radiobiology Research Institute Scientific Report SR73-7, 1973 (in press).

2. Chaput, R. L. and Kovacic, R. T. Miniature pig performance after fractionated supralethal doses of ionizing radiation. Radiation Res. 44:807-820, 1970.

3. Roberts, E. and Simonsen, D. G. Some properties of L-glutamic decarboxylase in mouse brain. Biochem. Pharmacol. 12:113-134, 1963.

4. Scott, E. M. and Jakoby, W. B. Soluble γ-aminobutyric-glutamic transaminase from Pseudomonas fluorescens. J. Biol. Chem. 234:932-940, 1959.

5. Zeman, G. H., Sobocinski, P. Z. and Chaput, R. L. An automated PCO_2 assay for glutamic acid decarboxylase. Bethesda, Maryland, Armed Forces Radiobiology Research Institute Technical Note TN72-4, 1972 (in press).

INTERMEDIATE FACTORS INVOLVED IN THE DEVELOPMENT OF BRAIN EDEMA

Principal Investigators: *L. S. Solomon and T. F. Doyle*
Technical Assistance: *W. L. Stringfield*

Brain edema is a major cause of mortality. It is either the principal or a contributing cause of death from open or closed head injuries, massive radiation exposures, brain tumors, brain inflammations, subdural hematomas, vascular accidents, hypercarbic hypoxia and some types of poisoning.

Several factors could in principle produce the morphological and biochemical features of brain edema (Figure 21).

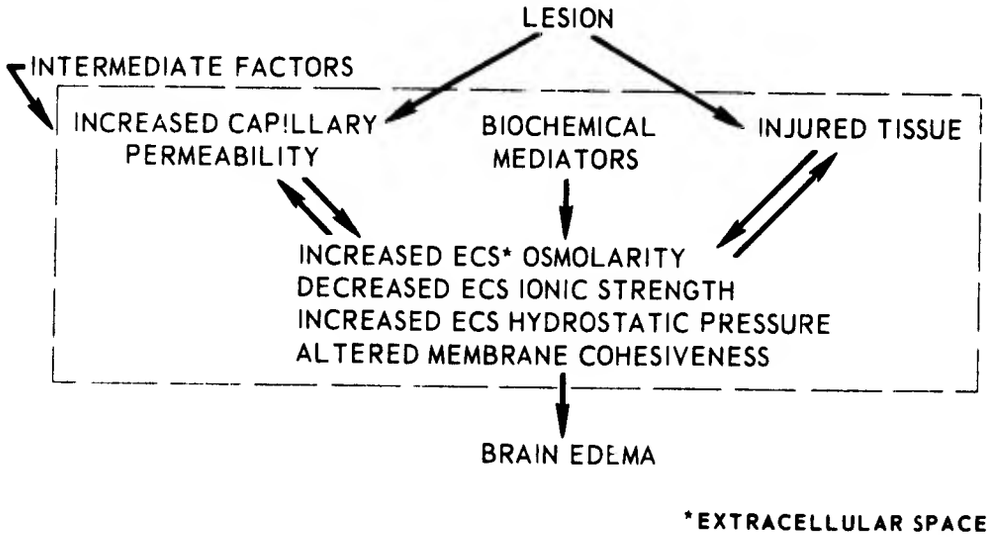

Figure 21. Schema showing possible role of intermediate factors

Lesions associated with brain edema usually involve injury to both brain parenchyma and its microcirculation, thus raising important questions regarding the relative roles of injured tissue and traumatized capillaries in producing the final morphological picture described above. Both of these events are potentially capable of altering the osmotic and ionic strength of the extracellular fluid, increasing its hydrostatic pressure or decreasing membrane cohesiveness; any one of which could be the physical-chemical basis of the observed morphological changes.

Previous work has been mostly concerned with the creation of an experimental lesion and assessing the result by viewing the fixed tissue in the electron microscope, following the course of various tracer substances or by making biochemical measurements on tissue samples. The body of information thus developed has resulted in a fairly good description of the edema produced by a variety of lesions, but gives little information about the interplay of intermediate factors.

The technique of continuous ventricular perfusion with serial sampling of the periventricular tissue was developed at the National Institutes of Health by Rall et al.[1] Fluid is infused at a constant rate through a needle in the lateral ventricle, flows through the ventricular system and out a cisternal needle. This technique maintains a known constant intraventricular concentration of any test substances that are added to the perfusion fluid and allows a steady-state concentration gradient to develop in the periventricular tissue. Samples of grey or white matter sectioned serially outward from the ventricular surface are taken when the animal is sacrificed and concentration profiles of the test substances can be obtained.

These serial samples can also be examined by histological or tracer techniques for the presence of brain edema and the presence of edema can be thus correlated with the concentration of test substances. The unique feature of this approach is that neither brain microcirculation nor brain metabolism is interrupted by a lesion, and thus the relationship of observed effects to test substances will be established in the absence of complicating factors.

The technique of ventricular-cisternal perfusion has been successfully duplicated in our laboratory. Trial perfusions with 5-hydroxytryptamine as the first in a series of test substances have been encouraging.

REFERENCE

1. Rall, D. P., Oppelt, W. W. and Patlak, C. S. Extracellular space of brain as determined by diffusion of inulin from the ventricular system. Life Sci. 2:43-48, 1962.

NUCLEAR MEDICINE AND RADIOPHARMACY RESEARCH

Principal Investigators: *J. S. Stevenson, G. L. Dunson, J. E. West, V. L. McManaman,, M. D. Sinclair and C. M. Cole*

Collaborators: *J. F. Taylor, S. L. Cohan, AFRRI; M. C. Johnson, S. M. Pinsky, R. B. Grove, T. L. Brown, N. Ghaed, Walter Reed General Hospital; L. L. Heck, P. T. Kirchner, R. E. George, J. W. Duley, R. H. Adams, U. S. Naval Hospital; R. W. Bright, Naval Medical Research Institute; W. C. Eckelman, Washington Hospital Center; F. Hosain, Johns Hopkins Medical Institutions; and L. S. August, Naval Research Laboratory*

Consultants: *R. C. Reba, Washington Hospital Center; G. S. Johnston, R. P. Chandler, National Institutes of Health· J. C. Harbert, Georgetown University Hospital; C. B. Cook, Northern Virginia Pathology Laboratories, Fairfax Hospital; M. Goldman, University of California, Davis; and H. S. Winchell, Donner Laboratory, Berkeley*

Technical Assistance: *E. L. Barron, N. L. Fleming, J. K. Warrenfeltz, W. W. Wolfe, M. E. Flynn and M. K. Mellor*

The objectives of the AFRRI nuclear medicine research program are: to conduct fundamental and applied biomedical research in support of clinical diagnosis and organ function studies, to implement and expand the radiopharmaceutical research program

initiated at Walter Reed General Hospital, to acquire essential instrumentation for on-line clinical nuclear medicine research, and to develop a recognized training program to meet residency research requirements for specialty board certification in nuclear medicine. Regulations and controls promulgated by the Food and Drug Administration for safety and effectiveness of radiopharmaceuticals intended for clinical use are followed carefully during all phases of research, development, test and evaluation of the radiopharmacy research operations.

Major progress during the early developmental phase of this new research area consisted of establishing liaison with nuclear medicine experts from local, area, and regional military medical centers and institutions, personnel staffing, instrumentation and laboratory space programming and acquisition, research protocol development, and initiation of preliminary biomedical studies with radiopharmaceuticals. Several consultants of national reputation were named.

A major portion of the instrumentation required for nuclear medicine research was received and assembled for on-line operational use. This includes a radionuclide rectilinear scanner and a stationary imaging gamma camera with a computerized data acquisition system and a 35-mm Nikon photography attachment. Arrangements were made for the use of an attachment to the gamma camera to detect positron-emitting radionuclides, e.g., ^{52}Fe. Additionally, two small animal whole-body counters were acquired: one, an NaI(Tl) annulus-shaped crystal, can accommodate specimens of a size up to 2.5 inches in diameter; the other, a portable unit having a scintillation detection system with greater comparative sensitivity for counting deposited radiopharmaceuticals, can accommodate samples of sizes up to 4.5 inches in diameter. Space for a special, fully-equipped radiopharmacy laboratory was allocated. Installation of a radioisotope fume hood, a laminar airflow biological unit, and a pressurizable glove box is expected to be completed soon. A radiochromatogram scanner and a radiation dose calibrator also will be located in this research laboratory. The operational readiness of a major part of the nuclear medicine instrumentation described has been demonstrated during preliminary research investigations.

Several research investigations were initiated in collaboration with nuclear medicine and radiopharmacy personnel from other military medical and civilian medical centers in the area. Early results appear highly promising and will be intensively pursued.

The unique biomedical research assets at AFRRI, including its scientific staff encompassing a wide range of disciplines in the medical, biological and physical sciences, its radiation sources, radioisotope production and handling facilities, research laboratories, and laboratory animal medicine and surgery program, promise to be effectively utilized in this new clinically addressed research effort.

RADIOPHARMACEUTICALS AS SCANNING AGENTS

Principal Investigator: *G. L. Dunson*
Collaborators: *J. E. West, C. M. Cole, AFRRI; L. S. August, Naval Research Laboratory; and W. C. Eckelman, Washington Hospital Center*
Technical Assistance: *E. L. Barron and M. K. Mellor*

Technetium-99m polyphosphate as a bone imaging agent. Toxicity studies are being carried out in two species, in accordance with Food and Drug Administration guidelines. Studies have been done on polyphosphate complexes made by Calgon and Monsanto Corporations and on ^{99m}Tc, tin, polyphosphate preparations from kits made in-house and from kits furnished by Walter Reed General Hospital (WRGH) and Upstate Medical Center, Syracuse, N. Y. Rabbits and rats are used for LD_{50} and LD_{100} studies. Dogs, monkeys and pigs are used for acute toxicity studies. The rate, route, site and volume of injection is designed to parallel patient administration.

Results to date indicate an LD_{50} of approximately 40 mg/kg, differing markedly from the 100 mg/kg LD_{50} reported in the literature.

Various methods of preparation of kits are being developed and tested to achieve the goal of developing a stable, high-quality, reproducible, one-step kit that can be prepared in batch lots without the use of lyophilizers and can be terminally autoclaved. Radioscintigraphic and radiochromatographic testing indicated that an apparently successful kit has been prepared in small lots. The shelf life, reproducibility and large lot production testing of the kit is in progress.

Lot samples of polyphosphate kits compounded at WRGH and freeze-dried at the Walter Reed Army Institute of Research are tested for radiochemical tagging, biological safety and effectiveness prior to their use in patients by the U. S. Naval Hospital, National Naval Medical Center, and WRGH. Radioscintigraphic quality in miniature pigs using a scintillation camera and a rectilinear scanner has been the determining factor in accepting or rejecting a production lot. Toxicity has not been a factor. Polyphosphate kit shelf life under varying storage conditions will continue to be studied for at least a year.

Reticuloendothelial system (RES) bone marrow imaging as an indicator of erythron marrow. Feasibility studies were done on a large miniature pig that had erythron marrow damage due to exposure to high-level irradiation. RES marrow radioscintigraphic imaging using a technetium-99m minicolloid that has been shown in another project to be superior for RES marrow imaging was done on a scintillation camera and a rectilinear scanner. Erythron marrow imaging was done on a rectilinear scanner using ^{59}Fe. The results indicate that the study is worth continuing and that ^{52}Fe production at the Naval Research Laboratory (NRL) cyclotron would be required in order to produce quality images.

Chemical and pharmaceutical processing of iodine-123. A target holder and target material of natural tellurium was irradiated in the NRL cyclotron, successfully producing a mixture of radioactive xenon gases. Separation of the gases in the hot laboratory at AFRRI showed that the procedure could be accomplished with a minimum of time and equipment. The travel distance between the NRL cyclotron and AFRRI is so great that the chemical processing of ^{123}I from ^{123}Xe at AFRRI is impractical. Therefore, arrangements were made for the chemical separation and gamma spectrum analysis to be accomplished at the radiation safety laboratory at NRL. An enriched tellurium material is on hand at NRL.

Iodinated streptokinase has been compounded using ^{131}I as a practice starting material. Various methods and modifications of labeling techniques are being developed and tested. Preliminary results indicate that a high purity ^{131}I will be used instead of ^{123}I for labeling streptokinase for animal studies.

Evaluation of technetium-99m radiopharmaceuticals for bone marrow scanning. Technetium-99m sulfide colloid radiopharmaceuticals were compounded from either hydrogen sulfide gas or thiosulfate kit methods developed by the principal investigator or from commercial kits furnished by E. R. Squibb & Sons or New England Nuclear Corporation. The radiopharmaceuticals were administered to rats by femoral vein injection, the rats were sacrificed at various intervals, and body tissue distribution was determined by dissection and scintillation counting. Preliminary results indicate that there is significantly higher marrow uptake and lower spleen uptake with the hydrogen gas produced radiopharmaceutical.

Miniature pigs and dogs were scanned on a rectilinear scanner using the various radiopharmaceuticals. The scans agreed with tissue distribution studies and patient scans done at WRGH.

Distribution studies and scintillation camera imaging in connection with lymphangiographic studies will be completed.

TECHNETIUM ORTHOPHOSPHATE

Principal Investigator: *W. C. Eckelman, Washington Hospital Center*

The objective of this work is to determine the factors which control the uptake of reduced technetium orthophosphate in the bone in order to take advantage of the low toxicity and routine availability of the orthophosphate as compared to the presently used polyphosphate.

Carrier free technetium polyphosphate was first suggested by Subramanian et al. as a bone scanning agent in nuclear medicine.[1,2] Because of the carrier free nature of the technetium used, the chemical species are not identified. Both the tripolyphosphate and a polyphosphate of chain length 46 have been suggested with the latter giving faster blood clearance and lower liver uptake. A preliminary report concerning the use of technetium orthophosphate has been submitted. The technetium orthophosphate showed higher bone uptake in mice than did the polyphosphate but also slightly higher blood and liver uptake. Gamma camera images of technetium orthophosphate in rabbits showed good bone visualization but high liver uptake.

The major factor in the preparation of tin and technetium orthophosphate complexes is the use of a nitrogen purged glove box for all preparative manipulations. Preparation of components immediately before use also increases the reproducibility of the final product. Although instant kits with 1-month stability are the ultimate end, it is important at this point to eliminate the stability aspect and concentrate on the other variables. The variables studied are the pH of the final solution, the molar concentration of the phosphate, the molar concentration of the phosphate injected relative to the in vivo molar concentration and the molar ratio of phosphate to stannous chloride. It appears that low pH solutions are superior to high pH solutions with a maximum at 5.5, that high molar concentrations of phosphate are superior to low phosphate concentration with a maximum at 1 M and that the phosphate to stannous chloride ratio is critical to prevent liver uptake.

The general procedure is to prepare a stannous chloride solution in 1 N HCl, add pertechnetate in 3 ml saline and finally 3.5 ml of phosphate buffer. This technetium complex was studied in swine by I.V. injection and gamma camera imaging at 1-3 hours. The eight experiments carried out to date involved work in the following areas:

1. The comparison of rabbits and swine to correlate the present project with previous work carried out at Brookhaven National Laboratory. In this experiment the stability of the technetium tin phosphate complex was the same for all animals because the same phosphate-tin ratio was used for all preparations with various amounts injected on a per kilogram basis. This experiment showed that the use of 1.0 M phosphate solution gives good images in rabbits and fair images in swine. Injection of amounts of phosphate greater than the in vivo concentrations appeared to give better bone uptake. In the swine the head bone was evident.

2. The standardization of collected counts in comparison imaging. In this project different solutions of the same phosphate concentration were prepared so that larger amounts of activity could be injected in both rabbits and swine. These preparations kept the phosphate concentration constant, kept the activity injected equal and allowed for injection of subconcentrations and superconcentrations of phosphate relative to the in vivo phosphate concentration. All images showed a high blood background due to the presence of free pertechnetate in the blood.

3. The preparation of compounds with various orthophosphate concentrations. Technetium compounds were prepared with total phosphate concentrations of 0.5 M and 1.5 M. The camera images again showed high blood background. On the 0.5 M phosphate complex the pelvic region was visible.

4. The effect of pH variation on bone concentration of technetium. All previous experiments were at a final pH of 6.5. Three experiments were run with final pH of 2.1, 5.6 and 6.5 in a 1 M phosphate solution. All camera images were poor with high blood background. In one swine (pH 6.5) a blood sample at 3 hours indicated 10 percent of the injected dose remaining in the plasma, and silica gel chromatography indicated that the majority of the activity was pertechnetate. The low pH image was superior to the others due to the greater stability of the stannous solutions at low pH.

5. Variation of tin concentration to determine the existence of a carrier effect. Since most other bone scanning elements are subject to carrier effects due to protein binding, increasing amounts of tin chloride ranging from a total of 250 μg to 1000 μg $SnCl_2 2H_2O$ at a phosphate concentration of 1 M phosphate were prepared. These solutions were made prior to injection and bone uptake appeared to be comparable to that of experiment 1 in which samples were also made up prior to injection. The high tin concentration also had liver uptake. The blood of this swine contained approximately 20 percent of the technetium dose at 3 hours. Bone visualization of the pelvic region was better for increasing amounts of tin.

6. The effect of variation of pH on bone localization of technetium with samples prepared prior to injection. Experiment 4 was repeated with samples prepared prior to injection because of the improved image quality observed in experiment 5. Three samples were run in swine at final pH values of 4.7, 6.1 ard 7.4 at a final phosphate concentration of 1 M. A total of 500 μg $SnCl_2 2H_2O$ were used and liver uptake was observed as in experiment 5 at that level. The bone image at pH 6.1 was the clearest which prompts further investigations in the pH range of 4.7 to 6.1. The pH 7.4 image had high liver concentration indicating the strong hydrolysis of the stannous ion.

7. The effect of the variation of pH on bone localization of technetium in the pH range 4.7 to 6.1. In this experiment a higher phosphate concentration (1.5 M) was used in an attempt to form a more stable complex. However precipitation seemed to occur and caused high blood background. Although the pelvic region and vertebrae were visible they were not as distinct as those of experiment 6.

8. The effect of phosphate and tin concentration on bone localization of technetium. To test the possibility of a K_{sp} effect causing precipitation of stannous phosphate and subsequently technetium phosphate, two solutions were prepared with varying tin phosphate concentrations. The preparation of tin phosphate using 500 μg $SnCl_2 2H_2O$ in 1 M phosphate produced a good bone visualization with individual vertebrae distinguishable. Further work in this area seems warranted.

Three of the experiments seemed to be controlled by the instability of the technetium tin phosphate complex. The remaining five experiments show that good bone visualization can be achieved if the preparations are carried out immediately before use and the pH, tin concentration and phosphate concentration are maximized at the points shown. Further work in better defining each of these maxima is planned.

REFERENCES

1. Subramanian, G. and McAfee, J. G. A new complex of ^{99m}Tc for skeletal imaging. Radiology 99:192-196, 1971.

2. Subramanian, G., McAfee, J. G., Bell, E. G., Blair, R. J., O'Mara, R. E. and Ralston, P. H. ^{99m}Tc-labeled polyphosphate as a skeletal imaging agent. Radiology 102:701-704, 1972.

THE RELATIVE EFFECTIVENESS OF FISSION NEUTRONS FOR GASTROINTESTINAL DAMAGE

Principal Investigators: *G. H. Zeman, S. R. Jones and R. E. George*
Collaborators: *J. E. West and S. G. Levin*
Technical Assistance: *G. D. Lee and D. F. Trainor*

Characterization of the relative effectiveness of fission neutrons for intestinal damage has continued. Following the study in miniature swine[1] the relative effectiveness of fission neutrons for gastrointestinal lethality and jejunal crypt response in mice was investigated.[2] Analysis of the jejunal crypt stem cell survival data has been completed.[3]

The numbers of surviving jejunal crypt stem cells have been calculated for mice irradiated in either a neutron field (incident neutron to gamma ratio of 5) or a gamma ray field (incident gamma to neutron ratio of 9). The radiations were delivered in a single pulse (approximately 20 msec duration) or at 40 or 250 rads/minute.

The multitarget single-hit cellular survival model was used to analyze the crypt stem cell survival data. Survival curves were fitted by computer using a nonlinear least squares program. The model provided excellent fitting curves for both the neutron and gamma irradiated mice at the three dose rates used. These curves are shown in Figure 22.

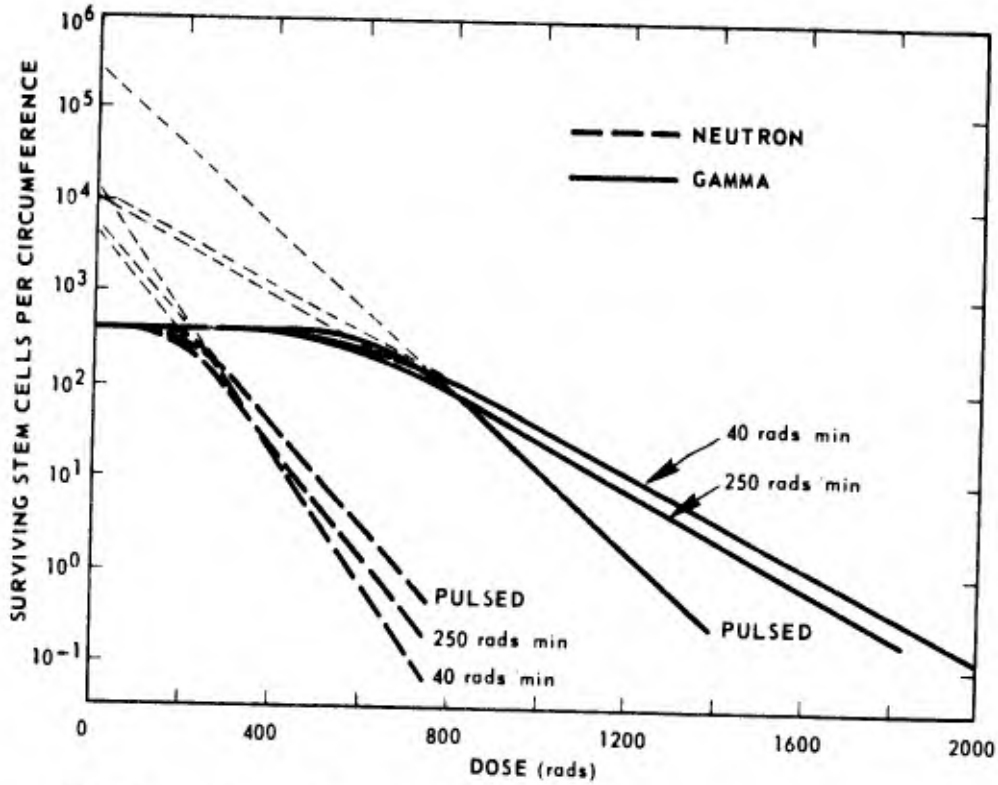

Figure 22. Stem cell survival after neutron and gamma irradiation

The broader shoulders and more gradual slopes of the gamma ray curves are a characteristic of low LET radiations. At low levels of stem cell survival, i.e., 1 percent, the pulsed neutrons were approximately 1.9 times as effective as the pulsed gamma rays, and the pulsed gamma rays were approximately 20 percent more effective than the lower dose rate gamma rays. An apparent reverse dose rate effect was seen for the neutrons, however, with the pulsed neutrons being approximately 10 percent less effective than those at lower dose rates.

REFERENCES

1. Jones, S. R., George, R. E., West, J. E. and Verrelli, D. M. The relative effectiveness of fission neutrons for gastrointestinal death in miniature pigs. Bethesda, Maryland, Armed Forces Radiobiology Research Institute Scientific Report SR71-17, 1971.

2. Zeman, G. H., Jones, S. R., George, R. E. and Levin, S. G. The relative effectiveness of fission neutrons for gastrointestinal damage in mice: lethality and jejunal crypt response. Bethesda, Maryland, Armed Forces Radiobiology Research Institute Scientific Report SR72-15, 1972 (in press).

3. Zeman, G. H., Jones, S. R., George, R. E. and Levin, S. G. The relative effectiveness of fission neutrons for gastrointestinal damage in mice: jejunal crypt stem cell survival. Bethesda, Maryland, Armed Forces Radiobiology Research Institute Scientific Report SR73-3, 1973 (in press).

◆◆◆◆◆◆◆◆◆

THE EFFECT OF EXERCISE ON RADIATION RESPONSE IN DOGS

Principal Investigator: *J. L. Terry, Jr.*
Technical Assistance: *E. L. Barron, W. W. Wolfe, J. K. Warrenfeltz, N. L. Fleming, M. E. Flynn and T. K. Dalton*

One of the major causes of death following irradiation in the midlethal range is infection. Any procedure that stimulates the regeneration of white blood cells should have a beneficial effect on an individual's recovery subsequent to radiation exposure. It was theorized that if an animal was exercised until in very good physical condition the white blood cell-forming system might recover faster following radiation exposure and, thus, be able to better combat the infection and, therefore, increase survival. This study was designed to test the effect of exercise on radiation survival.

Thirty-six healthy, AKC registrable beagles of both sexes, 2-3 years of age, were the experimental animals. They were trained to run on a motor-driven treadmill, starting initially at slow speeds for short periods of time until becoming accustomed to the procedure. Within 2 weeks the animals were able to run for 15 minutes at 2-1/2 miles per hour at a 10^{0} slope. This procedure was continued every working day for 5 months to achieve maximum physical fitness. Routine hematological procedures were performed twice weekly. All animals received a midline tissue dose (MTD) of 240 rads at 40 rads/minute, an estimated $LD_{33/30}$, from the AFRRI cobalt-60 irradiator.

The greater number of deaths in the physically conditioned animals was unexpected (Table X). It was thought that the better physical condition of the animal would enhance its chance of survival rather than decrease it. A recent report[1] stated that physical conditioning resulted in a faster turnover of red cells and also stimulated red cell production. Although hematological values of the exercised and nonexercised dogs were not significantly different, in the physically conditioned animal, red cells may have been replaced at the expense of the white cells, thus making it more susceptible to a midlethal radiation exposure.

Table X. Beagle Mortality Data

Exercise schedule	Mortality*	Survival time (days)	
		Mean	Range
Preexposure and postexposure	12/10	18.6	15 - 24
Postexposure	6/2	26	18 - 34
Postexposure+	6/5	17.6	17 - 19
Controls	12/5	23	17 - 33

* Number exposed/number of deaths
\+ Exercised three times more postexposure than other exercised groups

Although the precise mechanism responsible for this adverse effect is unknown, results of this preliminary investigation suggest that physical conditioning by exercise prior to irradiation under the conditions of this study was detrimental to postirradiation survival.

REFERENCE

1. Yoshimura, H. Anemia during physical training (sports anemia). Nutr. Rev. 28: 251-253, 1970.

FACTORS AFFECTING THE PERFORMANCE OF PRIMATES FOLLOWING A 2700-RAD PULSED DOSE OF IONIZING RADIATION

Principal Investigators: *C. R. Curran and D. M. Verrelli*
Collaborators: *G. C. Brown, S. J. Allen and D. J. Barnes, USAF School of Aerospace Medicine*

A study was designed to facilitate a comparison of the behavior of primates trained by the USAF School of Aerospace Medicine (SAM) with the behavior of primates trained by the Armed Forces Radiobiology Research Institute (AFRRI).[1]

The performance of eight monkeys (Macaca mulatta), trained at SAM to operate a primate equilibrium platform (PEP), was tested following a single pulse, whole-body 2700-rad (± 200 rads) dose of neutron-gamma radiation at the AFRRI-TRIGA reactor (n/g = 0.5:1, pulse half-width of 50 msec). The results were compared to: (1) PEP-trained animals exposed to a 2500-rad pulse of neutron-gamma radiation at the White Sands Missile Range fast burst reactor (n/g = 9:1, pulse half-width of 40 μsec), and (2) animals trained at AFRRI to perform a simple discrete avoidance task and then irradiated (2800 rads) in the AFRRI-TRIGA reactor. The two groups of animals exposed in the higher gamma field of the TRIGA reactor exhibited a behavioral decrement soon after irradiation (Figures 23 and 24) which was more severe than the decrement observed in animals exposed to the higher neutron field of the White Sands reactor (Figure 25). Stimulus response differences in the behavioral tasks employed were manifested in a slower recovery rate for the *PEP*-trained animals exposed in the TRIGA reactor compared to the AFRRI animals trained to perform the discrete avoidance task and irradiated in the same reactor.

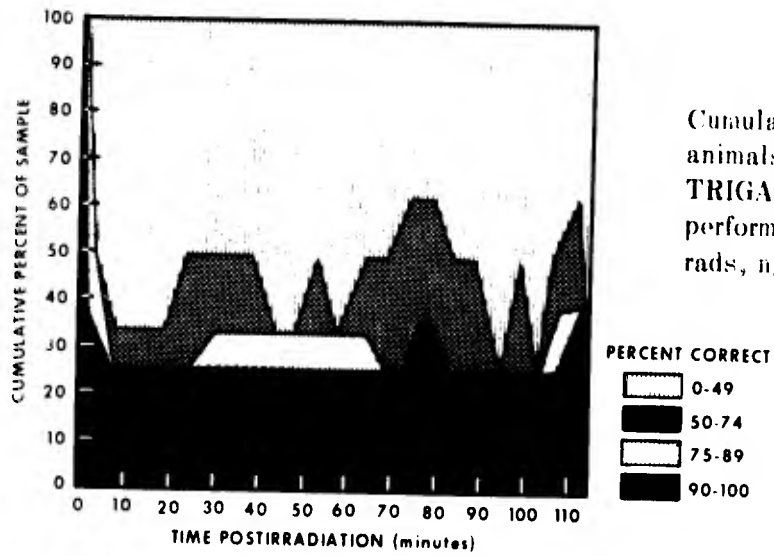

Figure 23.
Cumulative percent of the PEP-trained animals (8) exposed in the AFRRI-TRIGA reactor that fall within four performance ranges (mean dose = 2700 rads, n/g = 0.5 : 1)

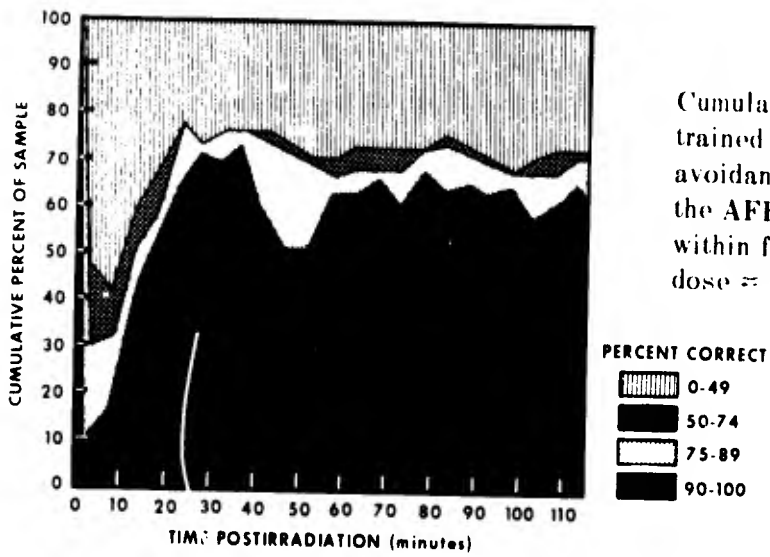

Figure 24.
Cumulative percent of the animals (39) trained at AFRRI to perform a discrete avoidance task and then irradiated in the AFRRI-TRIGA reactor that fall within four performance ranges (mean dose = 2800 rads, n/g = 0.5 : 1)

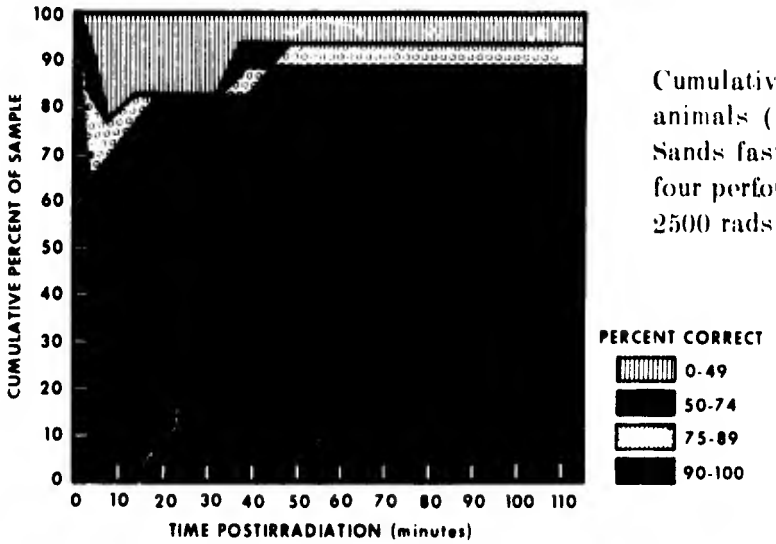

Figure 25
Cumulative percent of the PEP-trained animals (16) exposed in the White Sands fast burst reactor that fall within four performance ranges (mean dose = 2500 rads, n/g = 9 : 1)

REFERENCE

1. Brown, G. C., Curran, C. R., Verrelli, D. M., Allen, S. J. and Barnes, D. J. Factors affecting the performance of primates following a 2700-rad pulsed dose of ionizing radiation. Bethesda, Maryland, Armed Forces Radiobiology Research Institute Scientific Report SR72-14, 1972 (in press).

THE PERFORMANCE OF PRIMATES FOLLOWING EXPOSURE TO PULSED WHOLE-BODY GAMMA-NEUTRON RADIATION

Principal Investigators: *C. R. Curran, R. W. Young and W. F. Davis*
Technical Assistance: *C. G. Franz, P. Mannon, J. R. Harrison and G. G. Kessell*

This study[1] consolidates the data from a relatively large test sample of monkeys trained to a common behavioral task and exposed in the AFRRI-TRIGA reactor.

Eighty-eight monkeys (Macaca mulatta) were trained to perform a shock motivated visual discrimination task and were exposed to a single supralethal dose of pulsed gamma-neutron radiation. The postirradiation performance of these animals

is presented in a manner which facilitates group comparisons of performance following doses of approximately 1100, 1700, 2600, 4900, 8900 or 15,200 rads. At these dose levels, group performance declined within minutes after exposure. For some subjects, the decline was so severe that the animals appeared comatose. The frequency with which a behavioral decrement was observed and the severity of the initial decrement appeared to be dose dependent (Figure 26). After the initial decrement, most animals at least partially regained their ability to perform the discrimination task. Performance was generally maintained at recovery levels until shortly be ore death. Factors which appeared capable of modifying observed postirradiation behavior include the gamma-neutron ratio of the radiation source and the nature of the behavioral task employed.

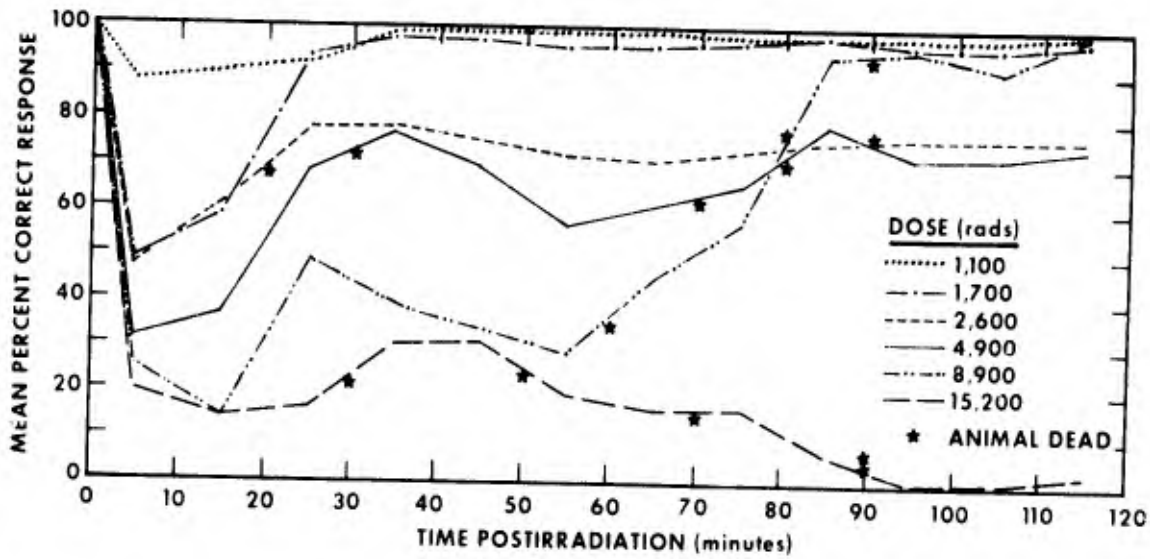

Figure 26. Mean percent correct response for all groups exposed to mixed gamma-neutron radiation

REFERENCE

1. Curran, C. R., Young, R. W. and Davis, W. F. The performance of primates following exposure to pulsed whole-body gamma-neutron radiation. Bethesda, Maryland, Armed Forces Radiobiology Research Institute Scientific Report SR73-1, 1973 (in press).

LATERAL VENTRICULAR PRESSURE CHANGES IN THE MONKEY INDUCED BY SUPRALETHAL DOSES OF MIXED GAMMA-NEUTRON RADIATION

Principal Investigators: *C. L. Turbyfill, J. H. Flinton, R. M. Roudon and V. A. Kieffer*

To test the hypothesis that increased intracranial pressure, following irradiation, may result in subsequent behavioral deficiencies if there was a sufficient decrease in perfusion pressure to produce cerebral ischemia despite normal carotid flow, a study[1] was initiated to measure intracranial pressure in the monkey following irradiation with doses reported to produce early transient incapacitation.

Monkeys were surgically implanted with catheters to monitor lateral ventricular pressure of the brain, aortic and venous pressures, carotid flow, and respiratory and heart rates and were irradiated with a pulse of 4000 rads of mixed gamma-neutron whole-body radiation. Immediately following irradiation the lateral ventricular pressure increased to approximately 1.4 times the preirradiation level (Figure 27). The

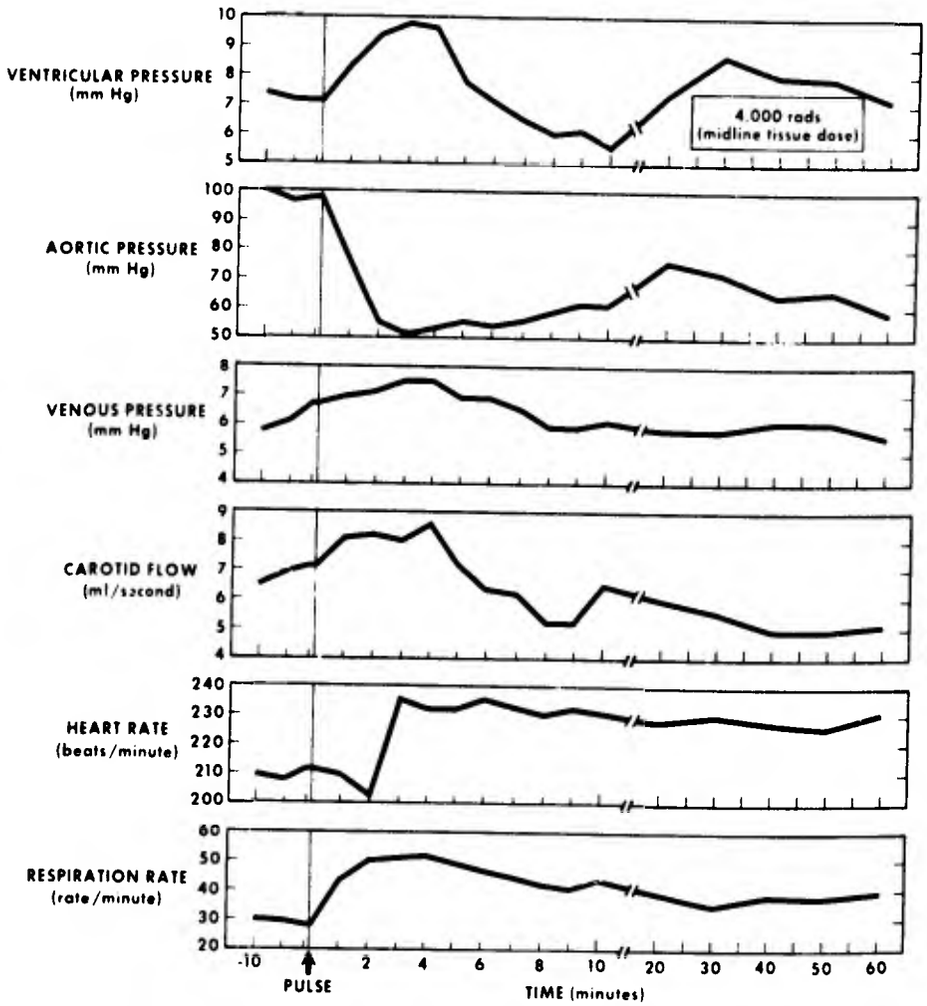

Figure 27. Mean physiological values for irradiated monkeys

lateral ventricular pressure returned to preirradiation levels by 6 minutes postirradiation. The aortic pressure decreased following irradiation and did not return to preirradiation levels during the 1-hour postirradiation monitoring period. The respiratory and heart rates were increased following irradiation. The increase observed in the lateral ventricular pressure of the monkey, following irradiation, does not appear to approach levels that would effectively limit cerebral capillary perfusion and induce or sustain behavioral incapacitation, providing normal autoregulatory vasoactive mechanisms are maintained.

REFERENCE

1. Turbyfill, C. L., Flinton, J. H., Roudon, R. M. and Kieffer, V. A. Lateral ventricular pressure changes in the monkey induced by supralethal doses of mixed gamma-neutron radiation. Bethesda, Maryland, Armed Forces Radiobiology Research Institute Scientific Report SR72-21, 1972 (in press).

AUTOMATED ANALYTICAL METHODS

Principal Investigator: *P. Z. Sobocinski*
Technical Assistance: *W. J. Canterbury and K. M. Hartley*

Two automated methods have been developed to increase the efficiency and precision of analytical determinations required for current research projects.

Determination of L-fucose in serum glycoproteins.[4] Studies of serum glycoprotein fucose levels in radiation therapy patients and of glycoprotein biosynthesis in irradiated animals produced a requirement for a specific and highly sensitive procedure for fucose analysis having a capability for large numbers of assays.

The determination of the methylpentose L-fucose (6-deoxy-L-galactose) in glycoproteins is usually performed by Winzler's[5] modification of the cysteine-sulfuric acid reaction described by Dische and Shettles;[1] however, it has been demonstrated at this laboratory and by other investigators that nonfucose moieties of glycoproteins contribute spurious chromogens to the reaction. An enzyme assay employing L-fucose dehydrogenase isolated from pork liver has been proposed, but the enzyme is not commercially available and its preparation is time consuming and beyond the capability of most clinical laboratories.

To circumvent this problem and thereby obtain a better estimation of the true fucose content of glycoproteins, a preliminary acid treatment of the glycoprotein material to hydrolyze terminal fucose residues has been suggested by Gyorky and Houck[2] and forms the basis of the automated method.

The procedure utilizes the cysteine-sulfuric acid reaction. Correction for the chromogens produced by the small amount of nonfucose sugars present in the acid hydrolysate is achieved by using the absorption at 420 nm as a measure of these chromogens rather than 430 nm or 427 nm as reported by Dische and Shettles.[1]

Fucose levels are calculated by comparing the increment in optical density, O. D. 400 nm - O. D. 420 nm, of the unknowns with that obtained with a series of standards. Figure 28 shows the linear relationship between the increment in optical density (400 nm - 420 nm) and fucose concentration obtained with the automated technique.

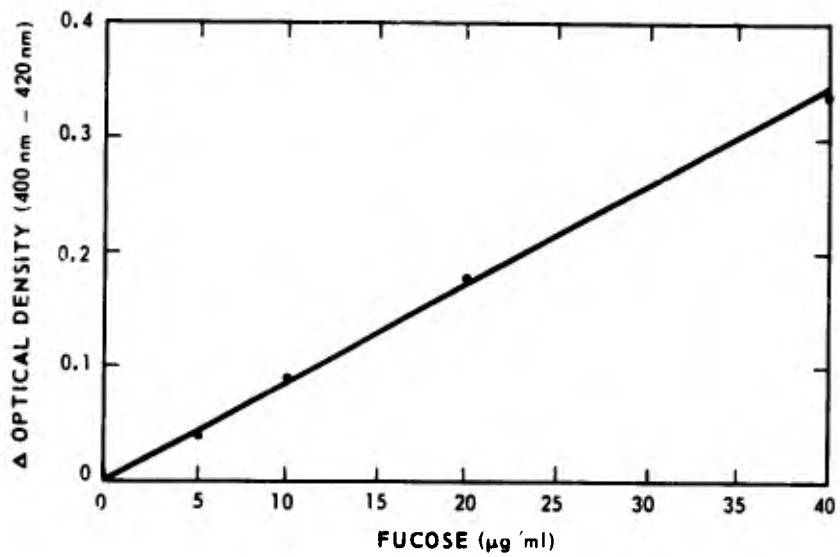

Figure 28. Positive increment in optical density, 400 nm – 420 nm, produced by various concentrations of L-fucose in an automated analytical system

Table XI shows the results obtained when a human serum pool sample was assayed by the proposed automated method and by a manual enzyme method employing L-fucose dehydrogenase (FDH). There is no significant difference between the mean values obtained by the two methods. The standard deviation for the automated method is one-half that of the enzyme method.

Unlike the manual method originally proposed by Dische and Shettles, the automated method does not require that optical density readings be obtained with and without cysteine. This is attributable to the elimination of many protein-bound organic substances from the reaction by the hydrolysis procedure used in the preliminary

Table XI. Fucose Content of a Human Serum Pool Obtained by Two Different Analytical Methods

Method*	Fucose (mg/100 ml)†
Automated (10)	7.2 ± 0.7
Manual, FDH‡ (10)	6.6 ± 1.4

* Number of replicate analyses is shown in parentheses

† Value shown is the mean ± the standard deviation

‡ L-fucose dehydrogenase methodology has been previously described

treatment of the serum glycoprotein samples. This latter advantage is in addition to the following advantages: (1) a reduction in standard deviation, and (2) a reduction in the amount of interference produced by nonfucose moieties so that a fucose value is obtained which more closely resembles the "true" fucose level than the manual procedure published by Winzler.

Simultaneous determination of inulin and para-aminohippuric acid (PAH) in plasma and urine.[3] The simultaneous infusion of inulin and para-aminohippuric acid and subsequent determination of their plasma clearance is a widely used method for the evaluation of kidney function. The laboratory determination of inulin and PAH in plasma and urine by manual techniques is tedious and time consuming.

A simultaneous automated technique has been developed which greatly increases the efficiency and precision of the laboratory determinations required for the evaluation of kidney function in dogs after exposure to ionizing radiation.

Para-aminohippuric acid is determined by coupling diazotized PAH with N-(1-naphthyl) ethylenediamine hydrochloride. Inulin is determined by the indolylacetic acid reaction in the presence of concentrated hydrochloric acid.

The linear relation between concentration and absorbance obtained by the simultaneous method is shown in Figure 29.

The effect of normal and elevated glucose levels on the inulin determination is shown in Figure 30. Interference by glucose (210 mg%) is approximately 2 percent when the plasma inulin concentration is 25 mg%. At low levels of inulin, glucose interference is significant; however, glucose may be eliminated from low level inulin samples by treatment with glucose oxidase.

Recovery of added inulin (20-40 mg%) in plasma and urine ranged from 97.2 percent to 100.9 percent with a mean of 98.0 percent for plasma and 100.5 percent for

urine. The recovery of added PAH in plasma (2.4 - 4.8 mg%) and urine (12 - 24 mg%) ranged from 96.9 percent to 100.7 percent with a mean of 99.1 percent for plasma and 99.0 percent for urine.

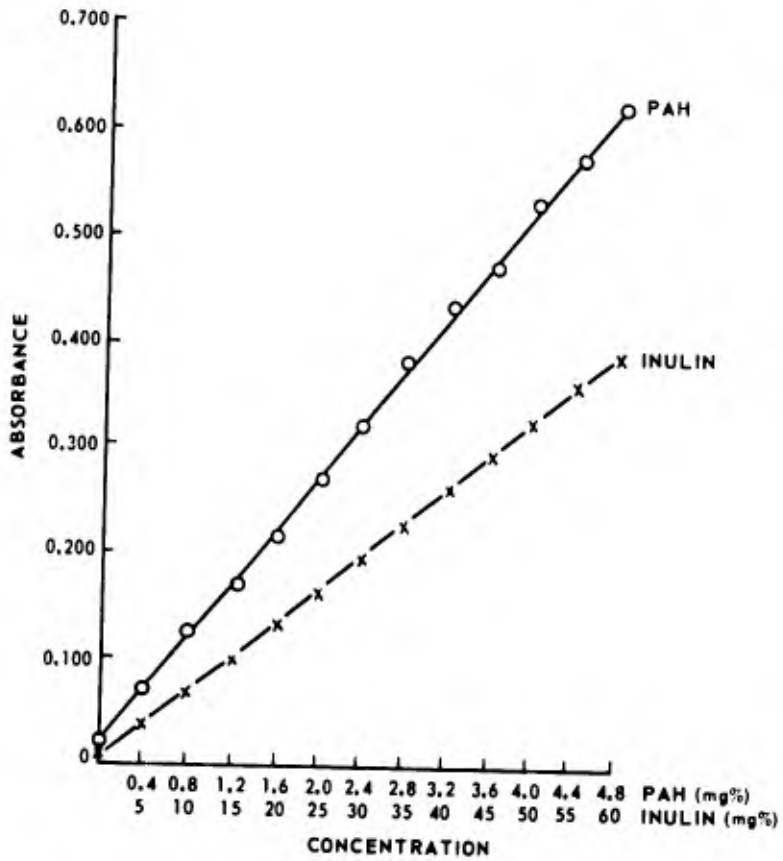

Figure 29 Calibration curve for the simultaneous determination of inulin and PAH

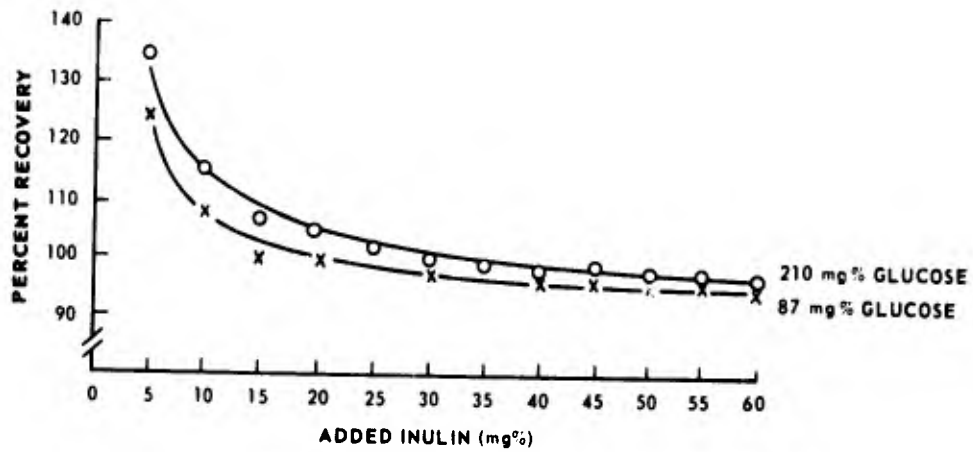

Figure 30. Effect of normal and abnormal levels of glucose on the recovery of plasma inulin

Replicate analysis produced a coefficient of variation of 0.5 percent for inulin and 3.4 percent for PAH.

The use of a 40 per hour sampling cam (2:1 sample to wash ratio) plus a water wash between actual specimens yields maximum separation between samples and allows the performance of 40 determinations per hour.

REFERENCES

1. Dische, Z. and Shettles, L. B. A specific color reaction of methylpentoses and a spectrophotometric micromethod for their determination. J. Biol. Chem. 175:595-603, 1948.

2. Gyorky, G. and Houck, J. C. The determination of terminal protein-bound fucose. Canad. J. Biochem. 43:1807-1811, 1965.

3. Sobocinski, P. Z. Simultaneous determination of inulin and para-aminohippuric acid in plasma and urine by an automated technique. Bethesda, Maryland, Armed Forces Radiobiology Research Institute Technical Note TN72-5, 1972 (in press).

4. Sobocinski, P. Z., Canterbury, W. J. and Hartley, K. M. Determination of L-fucose in glycoproteins. II. An automated method for the determination of L-fucose in serum glycoprotein hydrolysates. Bethesda, Maryland, Armed Forces Radiobiology Research Institute Scientific Report SR72-7, 1972.

5. Winzler, R. J. Determination of serum glycoproteins. Meth. Biochem. Anal. 2:279-311, 1955.

PARTIAL CHARACTERIZATION OF CARBOHYDRATE RESIDUES OF SERUM GLYCOPROTEINS IN NEOPLASTIC DISEASE

Principal Investigators: *P. Z. Sobocinski and A. S. Evans*
Technical Assistance: *K. M. Hartley and W. J. Canterbury*

Recent evidence suggests that the level of L-fucose in serum glycoproteins may serve as a diagnostic aid for the detection of malignancy. However, these findings are equivocal due to the lack of specificity in the analytical method most commonly used for fucose determination.

The objective of this investigation[2] was primarily to establish whether the apparent increase in fucose levels in patients with malignant tumors is real, or related to lack of specificity in the analytical method, and, if the increase is real, to obtain data as to its source.

Data obtained by borate ion-exchange chromatographic (BIC) estimation of carbohydrate residues released by mild acid hydrolysis of serum glycoproteins confirm the elevation of fucose levels in certain malignancies. The fucose levels obtained by BIC and two other methods are shown in Table XII. Elevated fucose levels occurred in three of the serum specimens. These three patients had the following diagnoses: 223, carcinoma of the larynx with metastases; 222, carcinoma of the prostate with metastases; and 143, anaplastic carcinoma of the lung with metastases. The remaining two specimens contained fucose levels below that found for a normal human pool. These latter patients had the following diagnoses: 139, invasive squamous cell carcinoma of the skin; and 154, rectal mass, benign.

Table XII. Serum Fucose Levels Obtained by Various Methods in Normal and Pathological States

Sample*	Fucose content (peak area)				Fucose assay* (mg/100 ml)			
	Peak area / mg protein	% NHP	Peak area / ml serum	% NHP	A	B	C	D
NHP	28.2	100.0	1866	100.0	6.6‡	6.6‡	5.7	9.2
223	38.2	135.8	3017	161.7	9.0	10.7	11.7	17.2
222	38.5	136.9	2377	127.4	9.0	8.4	9.3	14.2
139	22.2	78.9	1379	73.9	5.2	4.9	3.8	7.3
154	21.5	76.2	1249	67.0	5.0	4.4	4.1	6.9
143	62.4	221.7	3558	192.3	14.6	12.7	15.2	20.4

* NHP, normal human pool; 223, carcinoma (Ca) of the larynx with metastases; 222, Ca prostate with metastases; 139, invasive squamous cell Ca skin; 154, rectal mass, benign; 143, anaplastic Ca lung with metastases

* Values calculated on mg protein (A) and ml serum (B) bases according to the following method:

$$\frac{\text{peak area/mg or ml (sample)}}{\text{peak area/mg or ml (NHP)}} \times 6.6;$$

values for C and D were obtained by Winzler's modification of the cysteine-sulfuric acid reaction with C representing the fucose value obtained after correction of D for hexose interference

‡ Values determined by a method employing L-fucose dehydrogenase

In an effort to explain the net increase in fucose levels we have calculated the "expected" levels due to specific serum glycoproteins present in normal and pathological states (cancer). The results are shown in Table XIII. The calculated mean values for total fucose concentration are in good agreement with those obtained in this study (Table XII).

Table XIII. Fucose Content of Specific Serum Glycoproteins in Normal and Pathological States

Glycoprotein*	Fucose+ (%)	Concentration‡ (mg/100 ml)		C/N
		Normal (N)	Cancer (C)	
Ceruloplasmin	0.2	0.044	0.100	2.27**
Transferrin	0.07	0.213	0.160	0.75
α_2-Macroglobulin	0.1	0.247	0.251	1.02
IgA	0.22	0.464	0.521	1.12
IgD	--§	--	--	--
IgG	0.2	2.460	2.220	0.90
IgM	0.7	1.330	0.917	0.69
α_1-Acid Glycoprotein	0.7	0.483	1.785	3.70**
α_1-Antitrypsin	0.2	0.420	1.260	3.00**
α_2 HS-Glycoprotein	0.2	0.112	0.076	0.68**
β_2-Glycoprotein	0.2	0.066	0.048	0.73**
GC-Globulin	0.2	0.064	0.060	0.94
Haptoglobin	0.2	0.340	0.800	2.35**
Hemopexin	0.4	0.300	0.348	1.16**
Prealbumin	0.0	--	--	--
Total fucose concentration and ratio (C/N)		6.5‡	8.6‡	(1.32)

* Glycoproteins present in normal and pathological states

\+ From Schultze and Heremans

‡ Calculated from the data of Snyder and Ashwell[1] according to the following method:

$$[\text{mean glycoprotein (mg/100 ml)}]_i \left[\frac{\%\ \text{fucose}}{100}\right]_i = \sum_i^m [\text{fucose (mg/100 ml)}]$$

§ Value not available

** Significant based on P values obtained for concentration difference

The glycoprotein material which we have analyzed is of course a heterogeneous mixture of many different glycoproteins and the values obtained for the relative amounts

of fucose are therefore an average value. Alterations in the relative amount of any single glycoprotein species might be expected to affect the average value. Recent evidence presented by Snyder and Ashwell[1] indicates that several specific glycoproteins are elevated in malignancy, while others are depressed. Using Snyder and Ashwell data, we have calculated the theoretical fucose content of these glycoproteins present in normal and neoplastic states to determine whether the increase in fucose content we obtained in sera of patients with malignancy could be accounted for by the net increase in these specific glycoproteins.

The data presented in Table XIII suggest that the alterations in the concentrations of ceruloplasmin, α_1-acid glycoprotein, α_1-antitrypsin, haptoglobin, and hemopexin in sera of cancer patients are sufficient to elevate the serum fucose levels. The ratio of mean fucose values, cancer patients/normals, of 1.32 is of a similar order of magnitude as the 1.39 found in this study (see Table XII column labelled peak area/ml serum, % NHP, 223, 222, 139, and 143).

In view of these findings, it appears that the serum fucose level may serve as a diagnostic aid for the detection of malignancy since it provides an indirect index to alterations in the glycoprotein profile which may be pathognomonic for certain diseases. Current studies are being performed to determine whether the changes in the relative amounts of other residues present in the prosthetic carbohydrate structure of serum glycoproteins may provide criteria for differentiating various neoplasms.

REFERENCES

1. Snyder, S. and Ashwell, G. Quantitation of specific serum glycoproteins in malignancy. Clin. Chim. Acta 34:449-455, 1971.

2. Sobocinski, P. Z., Hartley, K. M., Evans, A. S. and Canterbury, W. J. Partial characterization of carbohydrate residues of serum glycoproteins in neoplastic disease. Bethesda, Maryland, Armed Forces Radiobiology Research Institute Scientific Report SR72-13, 1972 (in press).

PROTEIN-BOUND CARBOHYDRATES AS BIOCHEMICAL CRITERIA IN DIFFERENTIAL DIAGNOSIS OF VARIOUS DISEASE STATES

Principal Investigator: *A. S. Evans*
Collaborator: *M. F. Dolan, U. S. Naval Hospital*
Technical Assistance: *F. A. Quinn, G. E. Routzahn and M. H. Gobbett*

The present study was designed to investigate the glycoprotein profile of patients with various diseases at progressive stages of their treatment regimens and to relate those profiles with the individual's response to therapy to define the feasibility of such a test battery (a) as an objective diagnostic aid to estimate disease activity, and (b) as a prognostic tool to aid the physician in in-hospital management and outpatient follow-up.

To date, 507 serum specimens from 390 individuals have been examined. One hundred and twenty of these samples were from 111 individuals with no clinical disease (controls) and 39 were from patients with normal, uncomplicated pregnancies, approximately evenly divided amongst the trimesters. The remaining 348 specimens from 240 individuals were from patients in (or outpatients of) the Cincinnati General Hospital, Cincinnati, Ohio (66 specimens, 29 individuals) or the U. S. Naval Hospital, Bethesda, Maryland (282 specimens, 211 individuals).

The patients were categorized in accordance with the diagnostic nomenclature of the International Classification of Diseases, Eighth Revision, Adapted for Use in the United States (Public Health Service Publication No. 1693). Practically all the disease classes, as set forth therein, were represented in the sampling, with a considerable preponderance of class II, Neoplasms.

The test battery consisted of total protein, total serum globulins, protein-bound neutral hexoses, hexosamines, sialic acid, and fucose. From these analytical data, a number of additional parameters which are still in the process of interpretation were derived.

A major portion of the effort during this preliminary phase of the work has been directed toward critical evaluation and standardization of analytical methods, with especial reference to elimination of or correction for influences of extraneous substances including other carbohydrates on specificity of the various procedures. Consistency in results of protein-bound neutral hexoses was considerably enhanced by automation of the procedure, while interferences in testing for protein-bound hexosamines and sialic acid were apparently minimized by the simple expedient of utilizing a narrow band-pass spectrophotometer.

The most important technical modification, however, was derived from the work of Sobocinski et al.[1] Analyses of a matrix varying neutral hexoses (as galactose and mannose = G-M) and fucose concentrations over each of their ranges enabled derivation

of a correction factor to eliminate the influence of the neutral hexoses on the optical density readings and to obtain values for "true" fucose. Derivation of such a correction factor was made possible by the fact that each of the family of parallel lines generated by increasing amounts of neutral hexoses in the reaction mixture (Figure 31) was displaced by a distance proportionate to the added concentration of galactose-mannose throughout the ranges tested. To our knowledge, this is the first laboratory to be able to correct for nonfucose interference in analysis and to measure such true fucose values.

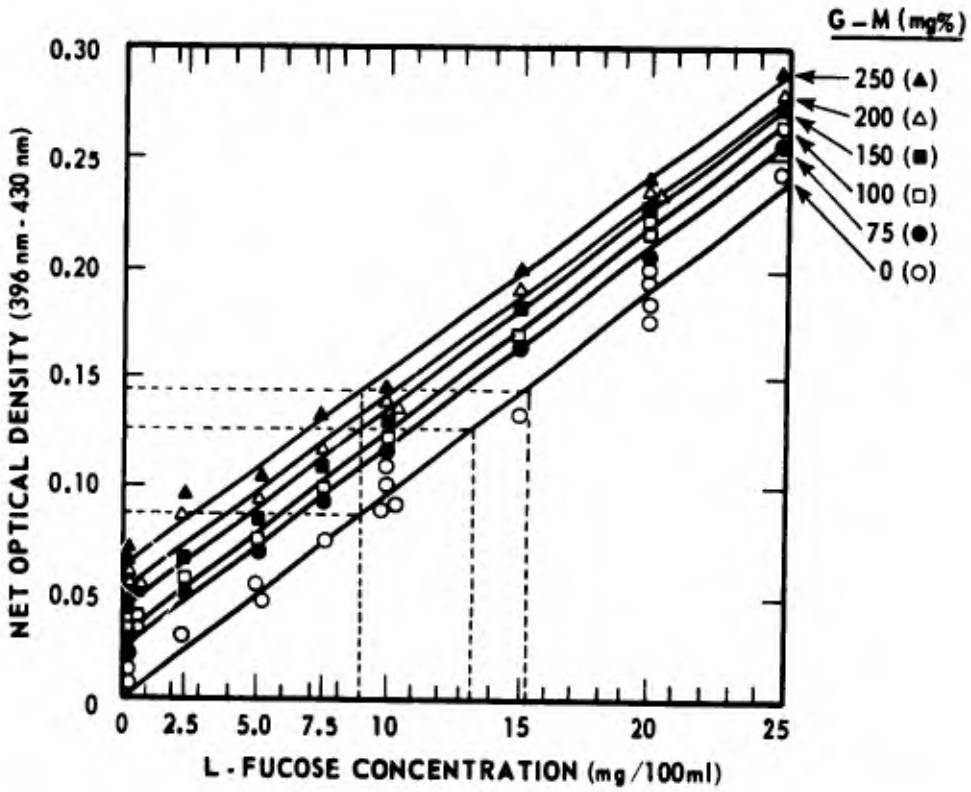

Figure 31. Influence of various concentrations of galactose and mannose (G-M) on the apparent concentration of L-fucose as estimated by the Dische-Shettles CyR3 reaction. Each data point represents the mean of duplicate determinations. Regression lines were fitted by the method of least squares.

Interpretation of the data thus far has been empirical and dependent on two basic considerations. Thus, effects of changes in blood volume on the analytical concentration of the various carbohydrate classes were eliminated by calculating the amount of carbohydrate bound per 100 mg protein. More importantly, since albumin is not a glycoprotein, derivation of the carbohydrate to globulin ratio enabled differentiation of absolute from relative changes in the glycoprotein profile in disease states where hypoproteinemia results from loss of circulating albumin.

Figure 32 illustrates two of the 27 analytical and derived parameters under study in patients afflicted with a number of diseases who were not receiving treatment at the time of sampling. The most obvious and striking feature of this plot is the distribution of the values of patients with malignant neoplasms, with respect to the fucose content of their serum globulins. Thus, while only 61 of the 79 cases (77.2 percent) had elevated values, of those who were later found to have had some degree of dissemination of their disease, 58 of 62 (93.5 percent) had abnormal fucose to globulin ratios. By contrast, only 3 of 17 cases (17.6 percent) who were clinically or surgically assessed to have localized, potentially resectable tumors were found to have increased values. Such a dichotomy indicates excellent potential for presurgical estimation of the extent of the tumor process. The symbols to the right of the upper limit of normal of the neutral hexose to globulin ratio are interpreted as indicating concurrent infections or inflammatory processes or a proportionately greater metastatic involvement. The fact that 12 of the 50 cases (24.0 percent) with diagnoses other than cancer were abnormal in this test system indicates that these two parameters are not, by themselves, sufficient for original differential diagnostic application. It should be noted, however, that most of these individuals returned rapidly to the normal range with treatment.

Of interest, also, was the finding that, contrary to other biochemical criteria for assessment of tumor activity, normal, uncomplicated pregnancies did not give false positives.

When patients were treated and they experienced varying degrees of amelioration of their disease, their values tended to return toward the norm. The full significance of this finding is yet to be determined, but it appears at this stage to promise objective criteria for at least short-term prognosis.

A unique effort is being made to generate total glycoprotein profiles on these patients, utilizing the entire gamut of the 27 parameters mentioned previously. While trends are evident visually which enable differentiation of some disease classes from others, computer analyses will be necessary to relate the profile of the individual with the medical history and current status of that person.

Comparison of these studies with results with carcinoembryonic antigen and phosphohexoisomerase determinations, which are to be added to the test battery, may give clues to the mechanism of the changes seen and therefore enable refinement of its ultimate (clinical) application.

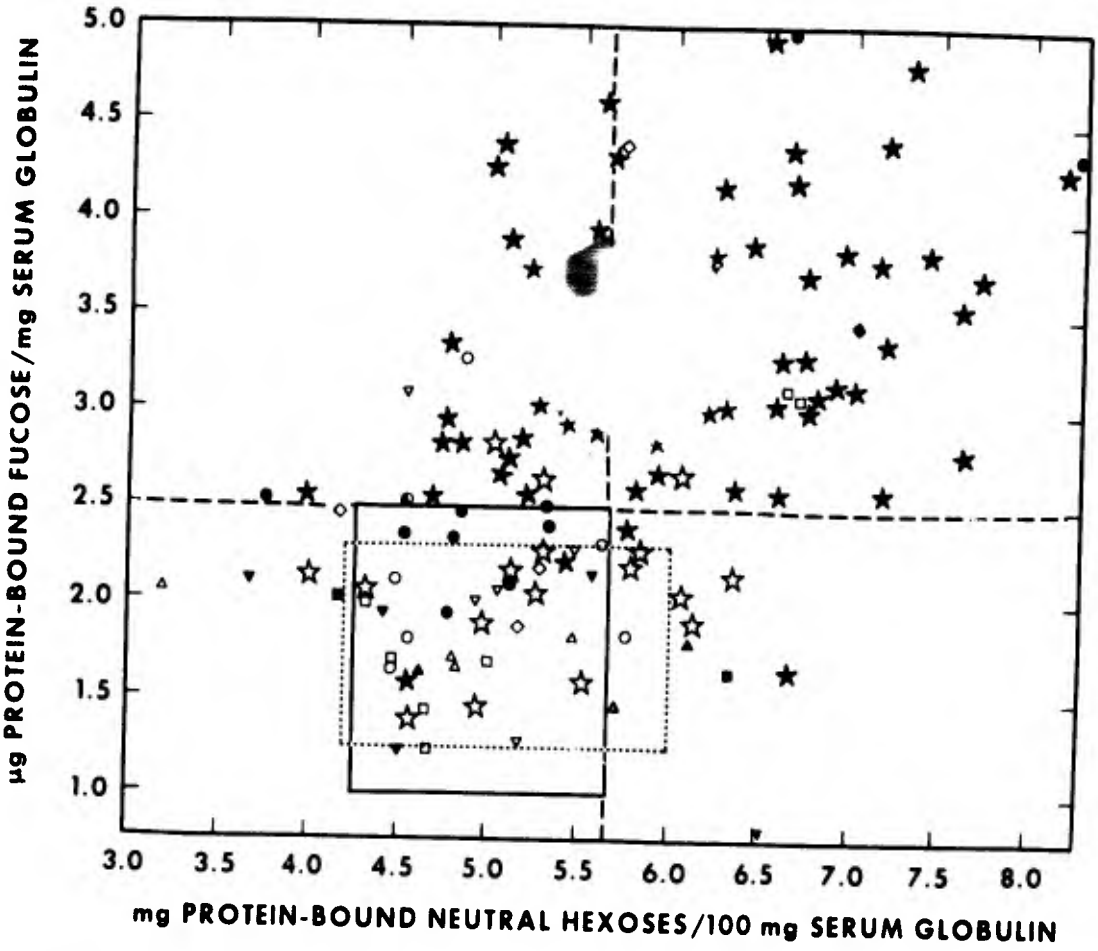

INTERPRETATION OF SYMBOLS

(THE NUMBERS IN PARENTHESES ARE NUMBER OF PATIENTS IN EACH DISEASE CATEGORY.)

——— THE SOLID RECTANGLE DELIMITS THE RANGE OF THE NORMAL CONTROLS (120)

····· THE DASHED RECTANGLE REPRESENTS THE LIMITS OF THE PREGNANCIES (39)

★ = METASTATIC MALIGNANT NEOPLASIA (62)

☆ = LOCALIZED MALIGNANT NEOPLASIA (17)

○ = ENDOCRINE, NUTRITIONAL, AND METABOLIC DISEASES (6)

■ = DISEASES OF THE BLOOD AND BLOOD-FORMING ORGANS (2)

◐ = DISEASES OF THE NERVOUS SYSTEM AND SENSE ORGANS (1)

□ = DISEASES OF THE CIRCULATORY SYSTEM (7)

▲ = DISEASES OF THE RESPIRATORY SYSTEM (2)

● = DISEASES OF THE DIGESTIVE SYSTEM (10)

△ = DISEASES OF THE GENITOURINARY SYSTEM (5)

▼ = DISEASES OF THE MUSCULOSKELETAL SYSTEM AND CONNECTIVE TISSUE (7)

◆ = CONGENITAL ANOMALIES (1)

▽ = INFECTIVE AND PARASITIC DISEASES (5)

◇ = ACCIDENTS, POISONINGS, AND VIOLENCE (4)

Figure 32. Distribution of pretreatment serum protein-bound fucose to globulin and neutral hexose to globulin ratios in 79 patients with primary diagnoses of malignant neoplasia and 50 patients with a variety of nonneoplastic diseases.

REFERENCE

1. Sobocinski, P. Z., Canterbury, W. J. and Hartley, K. M. Determination of L-fucose in glycoproteins. I. Effect of nonfucose moieties of serum glycoproteins. Bethesda, Maryland, Armed Forces Radiobiology Research Institute Scientific Report SR72-6, 1972.

DEVELOPMENT OF A HYPOTHROMBOGENIC BLOOD OXYGENATOR MEMBRANE

Principal Investigator: *P. K. Weathersby*
Collaborator: *T. Kolobow, National Institutes of Health*

Despite its current sporadic performance, the membrane oxygenator holds the greatest promise for long-term pulmonary assistance.[1] Most of the remaining problems concern the membrane itself. Prominent among these is thrombogenicity. The development of nonthrombogenic or even hypothrombogenic membranes has been impeded by the use of poorly characterized industrial products rather than homogeneous, pure materials.

The objectives of this research are to produce pure materials, study their chemical and physical nature and evaluate their blood compatibility. The family of silicone rubbers has been chosen since they have a very high permeability to gases and a history of relative inertness toward blood.

Commercially obtained silicone polymers were analyzed for average (viscosity) molecular weight and chemical composition. A computer-controlled, pulse infrared spectrometer at the National Institutes of Health was used to detect contaminant substituents; in some cases the sensitivity reaches one group per average polymer chain.

The polymer is applied to suitable substrates and cured by ionizing radiation in a controlled gaseous environment. Mechanical tests and infrared spectra determine the type of cure and the occurrence of side products, such as oxidation residues. Radiation curing produces a purer product than traditional peroxide catalysts, but side groups can nevertheless be changed.

The cured silicone rubbers are tested for thrombogenicity. Fresh human blood requires over 45 minutes to clot in test tubes coated with these silicone rubbers, rather than the 15-25 minutes in commercial silicones (Lee and White test). Additional

static clotting and platelet activation assays are being evaluated as part of this research. A simple in vivo test, the Kolobow "Mini-Lung," will be used for advanced testing of the new membranes.

Anticipating the problems associated with poor mechanical properties of nonreinforced silicone polymers, studies are underway to bond the cured polymer to strong, permeable substrates. Other techniques for increasing strength such as filler incorporation and fabric backing will be examined for chemical and biologic effects. Processing variables associated with large scale membrane production will be evaluated by the same methods.

REFERENCE

1. Kolobow, T., Spragg, R. G., Pierce, J. E. and Zapol, W. M. Extended term (to 16 days) partial extracorporeal blood gas exchange with the spiral membrane lung in unanesthetized lambs. Trans. Am. Soc. Artif. Internal Organs 17:350-354, 1971.

CHEMICAL RESPONSE OF BIOLOGICAL SYSTEMS TO IONIZING RADIATION: FREE RADICAL INTERACTIONS

Principal Investigator: *G. M. Meaburn*
Collaborator: *G. W. Donaldson*
Technical Assistance: *P. J. Ferry*

Pulse radiolysis studies of dilute aqueous solutions of deoxyribonucleic acid (DNA). A major effort was made to examine the spectral region below 300 nm for transient optical absorptions in irradiated DNA solutions. The aim of the experiment was twofold: (1) to determine the existence of new absorption arising from the formation of secondary free radicals localized in the DNA, and (2) to find evidence for or against rapid changes in hypochromicity in the first optical absorption band of DNA centered at 260 nm. This spectral region is a difficult one in which to work because of poor instrumental sensitivity and low signal-noise ratio of the photoelectric detector. A device for pulsing the xenon arc has been made to operate reliably for this series of experiments. The pulser has permitted us to increase the analyzing light output by about two orders of magnitude for periods of several hundred microseconds, thereby improving the signal to noise ratio considerably in the spectral region 300 - 250 nm.

The results of this work are most interesting: (1) No new absorptions are observed in the spectral region under consideration at times up to 300 μsec after the pulse of ionizing radiation (~0.5 μsec). This is a clear indication that a significant hyperchromic shift is not occurring over this time range. (2) There is a significant decrease in optical absorption at 260 nm over the first few microseconds following the pulse, indicating a rapid destruction of chromophoric groups in the DNA, probably as a result of hydroxyl radical attack.

Analysis of gaseous products of DNA radiolysis. Using the methods of gas-solid chromatography, hydrogen yields have been determined for ^{60}Co gamma irradiated DNA solutions under a variety of experimental conditions. The experimental data so far obtained can be interpreted as follows: (1) Solvated electron (e^-_{aq}) attack of DNA does not result in the production of H_2, i.e., we can rule out the possibility of abstraction reactions involving this species, a not altogether surprising result. (2) The reaction of hydroxyl-free radicals with DNA is an efficient process, again not resulting in the formation of H_2.

The reaction of hydrogen atoms (the neutral form of e^-_{aq}) with DNA is currently being investigated. Preparations are also being made to examine the yield of CO_2 from DNA solutions.

Production of labile phosphate esters in ^{60}Co gamma irradiated DNA solutions. The determination of inorganic phosphate yield via radiation-induced production of labile phosphate esters is being continued. Samples of oxygen-free 0.01 w/v DNA solutions in phosphate buffer are irradiated at dose rates of ~400 rads/minute. The radiation yield of phosphate, G(phos), has been determined to be 0.5 ± 0.1 over the dose range 3 - 20 krads. At lower doses (1 - 3 krads) there is an indication that G(phos) is somewhat higher, 0.6 - 0.7. No explanation can yet be offered for this increased sensitivity of the phosphate-sugar band in DNA at low doses.

STATISTICAL METHODS FOR EEG-BEHAVIORAL STUDIES

Principal Investigator: *S. G. Levin*
Technical Assistance: *E. E. Sereno*

The object of this work is to develop an overall general purpose system that handles large amounts of EEG data, extracts the relevant information, develops measures that show changes in the patterns, summarizes information from a number of epochs, and calculates quantities necessary for comparisons and tests of hypotheses.

In using this system, a set of EEG epochs from one lead is selected that is representative of the conditions of interest and to the eye is free of artifacts. The power spectra are obtained by first calculating the autocorrelation function and then the smoothed power spectral density function using a weighted cosine transform.

The power spectral density is plotted using the computer line printer and, although the original data have been reduced in volume, the system must then provide quantitative measures to compare salient features of the plot. Since the power density spectrum has the characteristics of a statistical distribution function, we can characterize the spectrum by its moments. The first moment (M1) is indicative of the location of the center of mass of a distribution function and the second moment (SD) is a measure of spread of a distribution. The implications in terms of EEG configuration are that if the first moment (center of mass) is low, then slow waves are predominant in the EEG. If the second moment is small, then the EEG shows a regular wave form synchronized around the frequency band indicated by the value of the first moment. The shape of the EEG spectrum is not symmetrical and often looks like Figure 33A. Since this is reminiscent of the log normal distribution often encountered in biostatistical data, plotting the data on a log frequency scale tends to make it symmetrical and would make the moments of the log frequency spectra easier to interpret. The measures found to be most representative of change are the antilogs of the moments (AM1L, ASDL) of the spectra of amplitude versus log frequency. The median frequency is also computed since it gives the point that divides the area of the power spectral density function in half and has the same meaning regardless of the shape of the spectrum. A final measure that is used to characterize the power spectral density function is the total power which is the sum of all of the intensities without regard to frequency. It is an indication of the average amplitude of the EEG signal during the time of the epoch.

Figure 33A and B illustrates the location of the AM1L and ASDL values on two power spectral density plots. That frequency (W) at which the 50 percent point is located is called the median frequency (MED). If the median point was between two frequencies, linear interpolation was used to estimate the median.

The moment concepts were developed to permit quantification and summarization of the data on a large number of epochs in any given category for several animals. The basic comparisons were between preirradiation and postirradiation periods, between "go" and "no go" conditions, and between correct and incorrect responses. The EEG epochs were categorized to allow these comparisons to be made. A computer program was developed that lists the time; the category of epoch, e.g., preirradiation, "go", correct; the response latency for the 10-second epoch; and the value of power, M1, SD, MED, AM1L and ASDL, for each epoch. The values of heart rate (beats per minute) and blood pressure (millimeters of mercury) are listed as well for each epoch. The program groups all of the epochs of a particular type, e.g., postirradiation, "go", correct, and for each condition gives average values of each EEG measure and physiological variable.

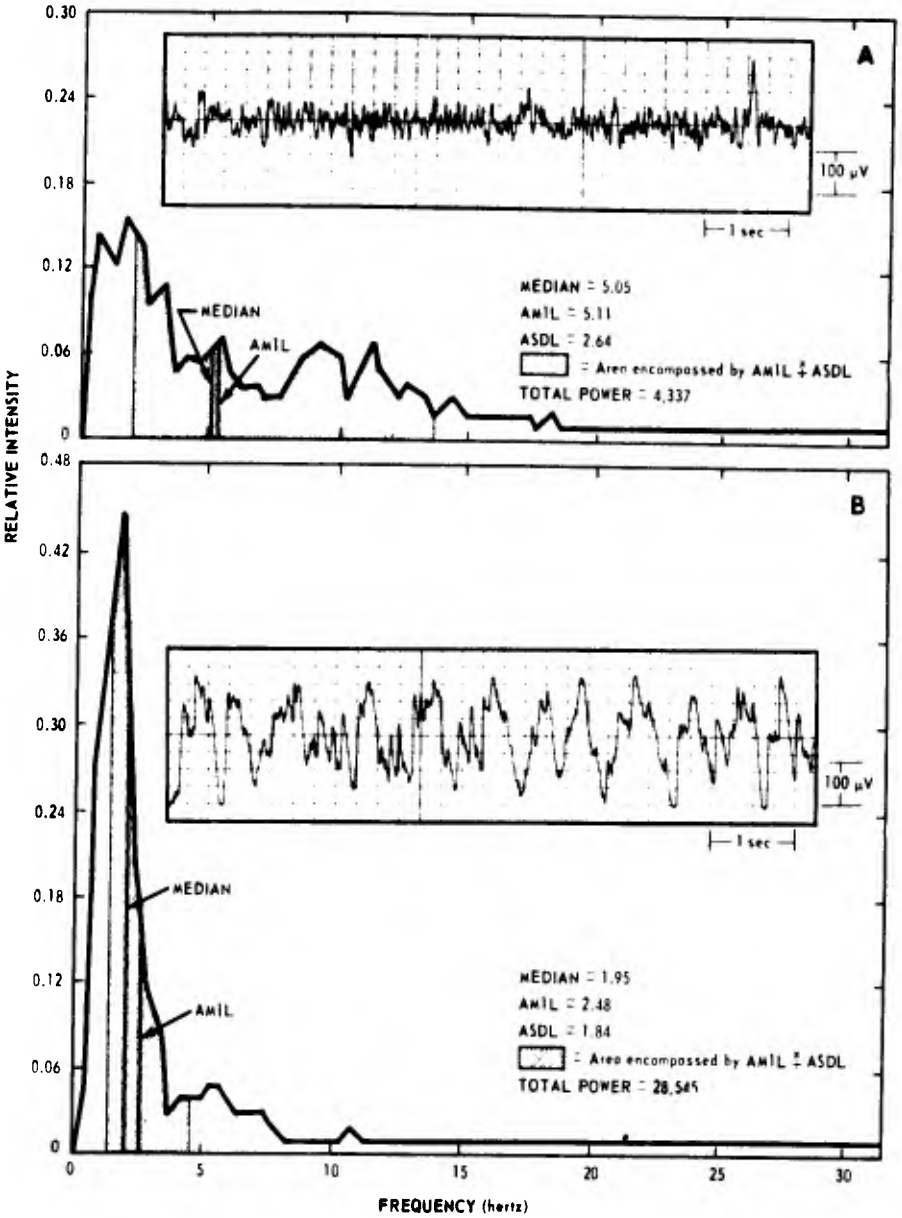

Figure 33. Samples of "raw" EEG epochs and their associated power spectral density plots. A. From a time period prior to irradiation. Three measures used to characterize the spectral density plot are illustrated. The median indicates the point at which 50 percent of the total power lies below and 50 percent above; AM1L is analogous to the mean of the power distribution and ASDL is a measure of spread. Note the multi-peaked nature of the distribution and the rather large spread indicated by ASDL in the shaded area. B. From the ETI period of incapacitation after irradiation. Note relative to the normal EEG in A that now most of the power is shifted into a large peak at around 1 5 Hz with corresponding downward shifts in the median and AM1L measures: ASDL is reduced; and the total power in the epoch has increased relative to preirradiation.

EEG data from seven monkeys were analyzed using this system.[3] It was possible to average data from several animals or type of stimulus; graphs of the values of the moments at fixed intervals preirradiation and postirradiation clearly showed trends; and shifts in the moments and power generally coincided with behavioral (ability to perform) changes.

Adey et al.[1] showed that, for cats, pairs of subcortical electrodes could be used to discriminate between correct and incorrect responses. The relation between electrodes in different parts of the brain showed the best ability to discriminate. The present course of this project has pursued that line of reasoning. A computer program utilizing the fast Fourier transform[2] calculates autocorrelations, power density spectra (auto spectra), and total power for two electrodes at a time, and also calculates other quantities that show relationships between data from the pair of leads. Cross spectra show the frequencies that the two leads have in common, coherence spectra indicate the strength of the relation between the leads, and phase angle shows the phase relationship of the data over the frequency range. The general approach is to select several leads and examine all pair relationships in this way. The need for measures to characterize becomes essential in this case since, for example, five leads would result in 15 auto and cross spectra for a single epoch. A similar number of coherence and phase angle plots are obtained for each of the 10 epochs which would require the examination of 450 graphs.

The improved system calculates the moments for each graph and presents them in matrix form for each epoch, which again reduces the mass of data to manageable proportions. The intention has been to use multivariate statistical methods on those matrices of moments which have replaced single moments in the preliminary study. In the multilead case, the moments characterize the auto spectra satisfactorily, but cross spectra, coherence and phase might require a different type of measure. Work is proceeding in the thorough check of the revised system and in the development of different measures to characterize the cross spectral data.

REFERENCES

1. Adey, W. R., Walter, D. O. and Hendrix, C. E. Computer techniques in correlation and spectral analyses of cerebral slow waves during discriminative behavior. Exptl. Neurol. 3:501-524, 1961.

2. Cooley, J. W., Lewis, P. A. W. and Welch, P. D. Application of the fast Fourier transform to computation of Fourier integrals, Fourier series, and convolution integrals. IEEE Trans. Audio and Electroacoustics AU-15(2):79-84, 1967.

3. McFarland, W. L. and Levin, S. G. Effects of pulsed gamma-neutron irradiation on the EEG and behavior of the monkey. Bethesda, Maryland, Armed Forces Radiobiology Research Institute Scientific Report SR72-8, 1972.

AFRRI COBALT-60 IRRADIATOR

Principal Investigators: *D. M. Verrelli and R. E. Carter*
Technical Assistance: *J. T. Istock and G. C. Weiss*

The exposure room of the AFRRI cobalt irradiator is approximately 35 feet square by 25 feet 8 inches high. The irradiator is a versatile facility capable of providing whole-body exposures at rates up to 400 R/minute. Exposure rates can be controlled by source strength as well as by varying source to specimen distances. The design of the facility permits either unilateral or bilateral irradiations.

Calibration of the AFRRI cobalt-60 irradiation facility consisted of a determination of parameters governing operating practices of the facility and programmed biological irradiations. Source to specimen distances are controlled by lateral positioning of the source elevators. Exposure parameters have been measured for both unilateral and bilateral irradiations. These parameters include: (1) exposure rates for a number of source to specimen distances, and (2) source rise time exposure, i.e., the total exposure that a specimen would receive as the sources are raised (or are lowered) from the bottom of the storage pool to their elevated positions.

Exposure rates and total exposures were measured using the AFRRI transfer standard, a 3 cm^3 air-equivalent ionization chamber.[1]

The exposure rate at 12-1/2 feet above the floor of the exposure room was measured for a loading of 30 rods (15 in each elevator cage) and at a number of source to specimen distances. A least squares fit of the data to a simple power function, $\dot{X} = X_0 d^{-x}$, gave a slope of -1.946. Normalized to the exposure rate at 1 meter, these data indicate a scatter component of < 8 percent at a source to specimen distance of 4 meters.

To accommodate large animal irradiations, a portable, general purpose irradiation table is positioned over the 6-ft diameter tank as illustrated in Figure 34. Exposure rates for a number of source positions were remeasured. A least squares fit of these data (see Figure 35) gave a slope of -1.925. By comparison with the exposure rate data at 12-1/2 ft, it is determined that the scatter component at 5-1/2 ft above the floor is increased less than 3 percent.

All experiments will receive a "constant exposure" during the movement of the sources up to their irradiation positions. An additional constant exposure will occur as the sources are lowered into their underwater storage position. For short irradiation times, this constant exposure can be an appreciable fraction of the total exposure. For ease of calculations it is assumed that the exposure during elevation of the

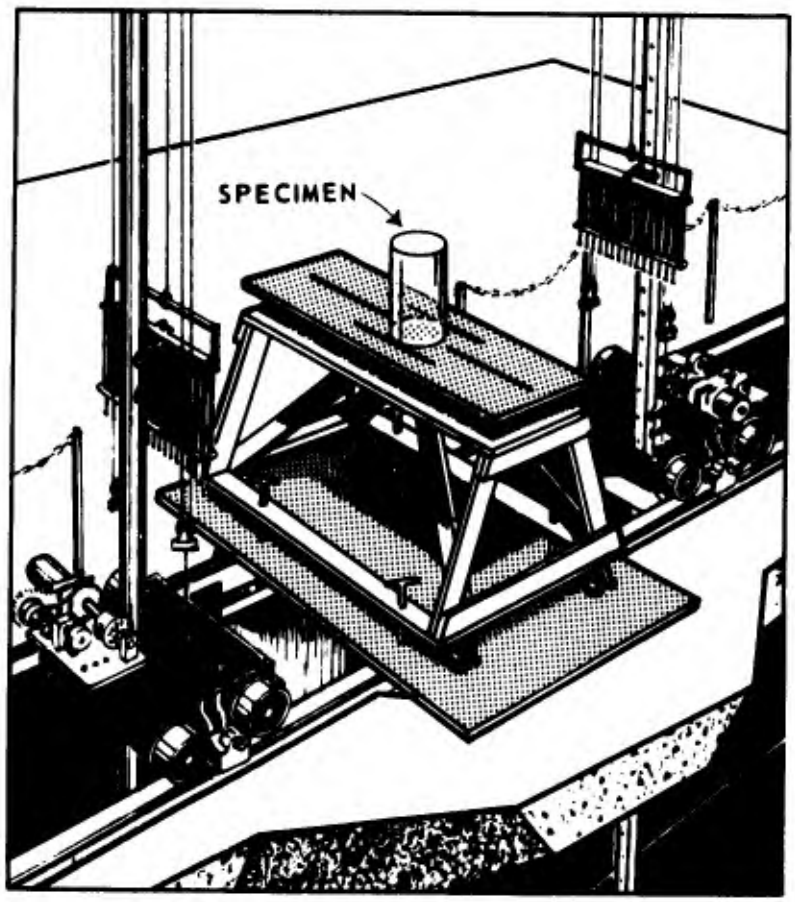

Figure 34. Irradiation geometry for cobalt 60 facility

sources is equal to the exposure while lowering them. In addition, it is assumed that the sources are idealized point sources, that there is no attenuation of the primary photon flux, and that the scatter component is a constant fraction of the exposure rate. The exposure rate during this transient period can be expressed as:

$$\dot{X}(r,t) = \frac{\dot{X}_o d_o^2}{r^2} = \frac{\dot{X}_o d_o^2}{\dot{y}} \quad \frac{\dot{r}}{r(r^2 - d_o^2)^{1/2}} \tag{1}$$

where $\dot{X}_o$ is the exposure rate at a source distance of d_o; $\dot{y}$ is the speed of the source. The speed of the elevators was measured to be 300 cm/min. The constant exposure for elevation of the sources, X_c, can be obtained by integration of equation (1). This integration yields

$$X_c = \frac{-X_o d_o^2}{300} \frac{1}{d_o} \cos^{-1}\left(\frac{d_o}{r}\right) \Bigg|_{\substack{r = d_o \\ r = (y_o^2 + d_o^2)^{1/2}}} \tag{2}$$

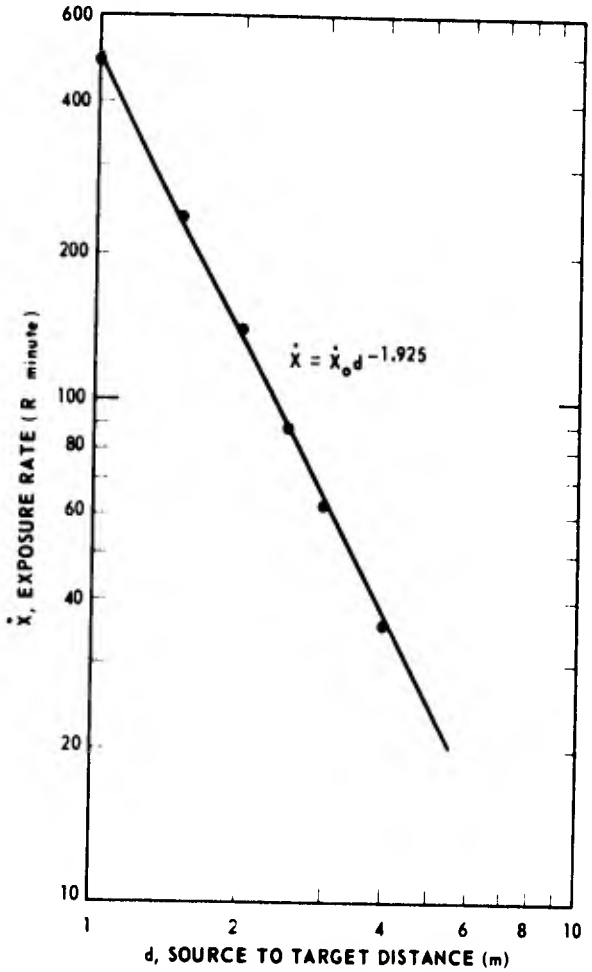

Figure 35 Cobalt irradiator exposure capability

If it is assumed that the constant exposure is delivered over 190 cm of vertical travel (from approximately 7-1/2 inches below water level), equation (2) can be evaluated as a function of source to target distance. A comparison of calculated and measured constant exposures is shown in Table XIV.

STD*	$2X_c$ (rads) Full loading	
	Calculated	Measured
150	212	213
200	137	136
250	95	94
300	70	69
400	42	40

Table XIV. Constant Exposures for Bilateral Irradiations

* Source to target distance in centimeters

For purposes of calculation, measured values of $\dot{X}_0$ were used. The measured values for constant exposure were obtained by integration of ion chamber current over the full length of travel of the elevators from the bottom of the pool to the 5-ft position above the floor.

REFERENCE

1. Attix, F. H., Roesch, W. C. and Tochilin, E., editors. Radiation Dosimetry, 2nd ed., Vol. II. New York and London, Academic Press, 1966.

REDUCTION OF ^{41}Ar ENVIRONMENTAL RELEASES FROM THE AFRRI-TRIGA REACTOR

Principal Investigators: *D. M. Verrelli, R. E. Carter and L. A. Slaback*
Collaborator: *B. E. Leonard*

The release of radioactive argon-41 to the environment is of concern to operators of research reactors whose facility has air cavities subjected to intense neutron fluences. It was reported earlier[1] that significant reduction in the production of argon-41 may be accomplished by minimizing the thermal neutron component of the radiation field in the AFRRI-TRIGA exposure rooms. The purpose of this paper is to report the reduction of environmental releases as a consequence of installing gadolinium-painted panels in the reactor exposure rooms.

Activation of argon-40 is primarily due to the thermal portion of the neutron spectrum.[2] Therefore, radiation field measurements were limited to thermal neutron measurements as determined by the cadmium difference method with thin gold foils. Data on the release of argon-41 were obtained by the facility's stack gas monitoring system. This detection system consists of two gas-flow proportional counters that have a sensitivity of approximately $3 \times 10^{-10} \mu Ci\ cm^{-3} CPM^{-1}$.

The original spatial distributions of the thermal neutron flux density in the reactor exposure rooms are plotted in Figures 36 and 37. Since the mean free path of a thermal neutron in air is on the order of 6 meters, it was assumed that the spatial distribution could be expressed by an unscattered and a scattered component in the form:

$$\phi(r) \quad Ar^{-2} + Br^{-x} \qquad (1)$$

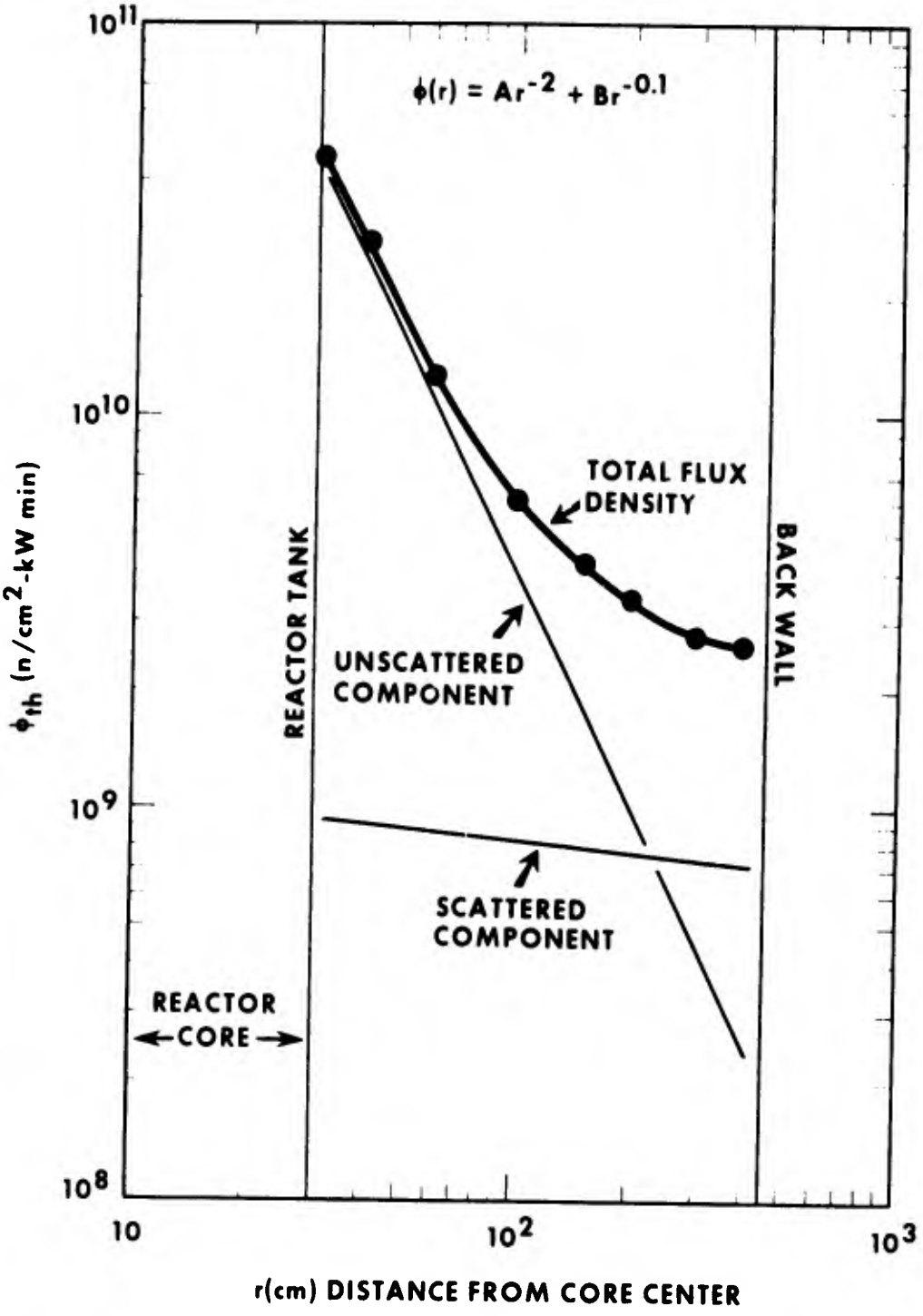

Figure 36. Thermal neutron spatial distribution in ER1

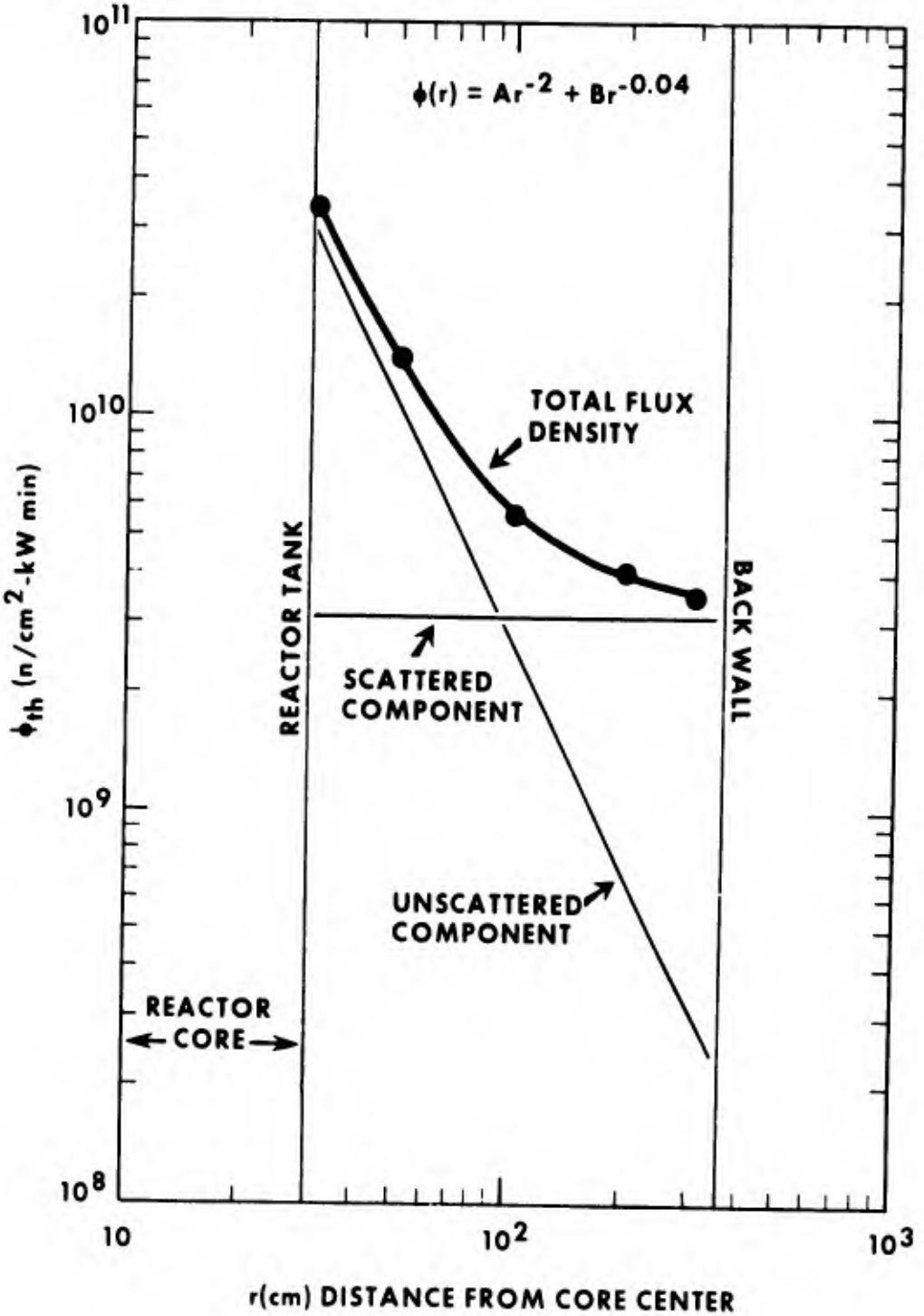

Figure 37. Thermal neutron spatial distribution in ER2

The best fit of the data gave values for x of 0.10 and 0.04 for Exposure Rooms 1 (ER1) and 2 (ER2), respectively. ER1 measures 20' x 20' x 10' high while ER2 measures 13' x 12' x 8' high. These small values for x indicate that the wood walls of the

rooms are nearly perfectly reflective. The greater negative slope for the larger exposure room (ER1) suggests that there is thermal neutron absorption before there are enough wall scatters to produce a constant component. A least squares fit of the data was used to determine the coefficients A and B.

Since the center of the core is only 120 cm above the floor, we assumed that the volume of each room could be expressed as a quarter of a sphere with radii of 460 and 323 cm. By integrating equation (1) over these volumes, we obtained estimates of the two fractions of the ϕ_{th} (unscattered and scattered components). We recognize that this technique will overestimate the unscattered component but will have small effect on the scattered component since this is nearly constant. Nevertheless, the results of the integration indicated that, in ER1 and ER2, only 40 percent and 20 percent, respectively, of the total argon-41 producing neutrons are from unscattered neutrons from the reactor core. Thus, to minimize the generation of ^{41}Ar, it is not sufficient to minimize the thermal neutron leakage into the exposure volume. The wood linings of the rooms, while protecting concrete from activation, serve as an excellent fast neutron thermalizer.

To minimize the thermal neutron leakage into the exposure room, a 16-mil aluminum sheet, sprayed with eight coats of gadolinium paint ($\sim$ 22 mg/cm^2) was wrapped around the reactor core tank projection. A 40-mil cadmium sheet was then placed over the gadolinium-coated aluminum sheet to absorb ^{159}Gd beta radiation and to further attenuate thermal neutrons. ϕ_{th} measurements on the room side of the cadmium shield indicated that there was negligible transmission (.1 percent) of the primary neutrons at the room lobe. One-eighth inch Masonite panels were painted with the gadolinium paint (approximately 11 mg/cm^2) and were installed on the surfaces of the room. The transmission of thermal neutrons through 11 mg/cm^2 of gadolinium was calculated to be .30. Table XV summarizes calculations and measurements of the effectiveness of our action to reduce the ^{41}Ar environmental releases.

Table XV. Argon-41 Production

Room condition	ϕ_{th} Calculations (% initial total ϕ_{th})			Stack effluent measurements	
	Primary	Scattered	Total	Release rate (μCi/kWh)	% Initial
Initial condition					
ER1	44	56	100	5.4	100
ER2	20	80	100	5.6	100
Core shield + 5 surfaces					
ER1	4	8	12	.86	16
ER2	3.5	1.5	5	.36	6.5

Measurements of ^{41}Ar releases were in reasonable agreement with the estimated values for the smaller of the two exposure rooms. However, it is evident that the larger the exposure room, the more important is the unscattered component for generating argon-41. Accordingly, the degree to which the thermal neutron flux density can be decreased will depend on the size and shape of the exposure volume.

In summary, the AFRRI has reduced the amount of radioactive argon-41 released to the environment by minimizing the thermal neutron component of the radiation field in its reactor exposure rooms. This was accomplished by reducing not only the thermal neutron leakage from the core but also the scatter component. In the particular examples cited, the major fraction of the thermal neutron flux density was the scattered component (thermalized fast neutrons). Experimental data on release rates show that the effectiveness has been to decrease the effluent release to the environment by a factor of 10 to 20 depending on the operational configuration of the reactor.

REFERENCES

1. Leonard, B. E. Basic mechanisms and control of the DASA-TRIGA dose. Bethesda, Maryland, Armed Forces Radiobiology Research Institute Annual Research Report ARR-2, pp. 37-43, 1 July 1967 - 30 June 1968.

2. McManaman, V. L. and Leonard, B. E. Experimental data on the production of argon-41 in reactor exposure rooms. Health Phys. 14(5):515-517, 1968.

LINAC REAL-TIME FIELD MONITOR

Principal Investigator: *P. A. Berardo*
Collaborator: *J. A. Willis*
Technical Assistance: *J. L. Rouch*

Real-time monitoring of the AFRRI LINAC field shape and intensity usually is done with a single detector remotely controlled to scan the field along a line perpendicular to the beam. The disadvantages of this approach are that considerable time is required for a complete area scan and that the data collected are rarely in the best form for ready interpretation unless relatively expensive equipment, such as a computer, is used as an aid. Another approach is to use wire planes operating in air as current detectors. The main limitation of this approach is that only profiles are obtained. An ideal monitor would provide an immediate and quantitative indication of the intensity at every point in the field.

A simple, low cost, field monitor has been designed which provides the following: (1) continuous real-time operation, (2) discrete detector inputs, (3) independence of field size and number or type of detector, (4) quantitative three-dimensional cathode-ray tube (CRT) image of field shape and intensity, and (5) quantitative two-dimensional CRT image of multiple profiles displayed concurrently.

Concept. To determine the field intensity at a point, a detector, such as a miniature ionization chamber, a diode, or any other current producing device, is used. If the current is collected and measured for each device, then a grid of such devices provides information on the field shape and intensity. The individual detector output levels are strobed in sequence and superimposed on a CRT background display of rows of the detector grid.

CRT display and strobe signal generation. Three levels of pulse generators (gates) are imbedded to produce the desired clock pulses and the CRT background display of the detector grid (Figure 38). A LINAC, free-running clock pulse, L1,

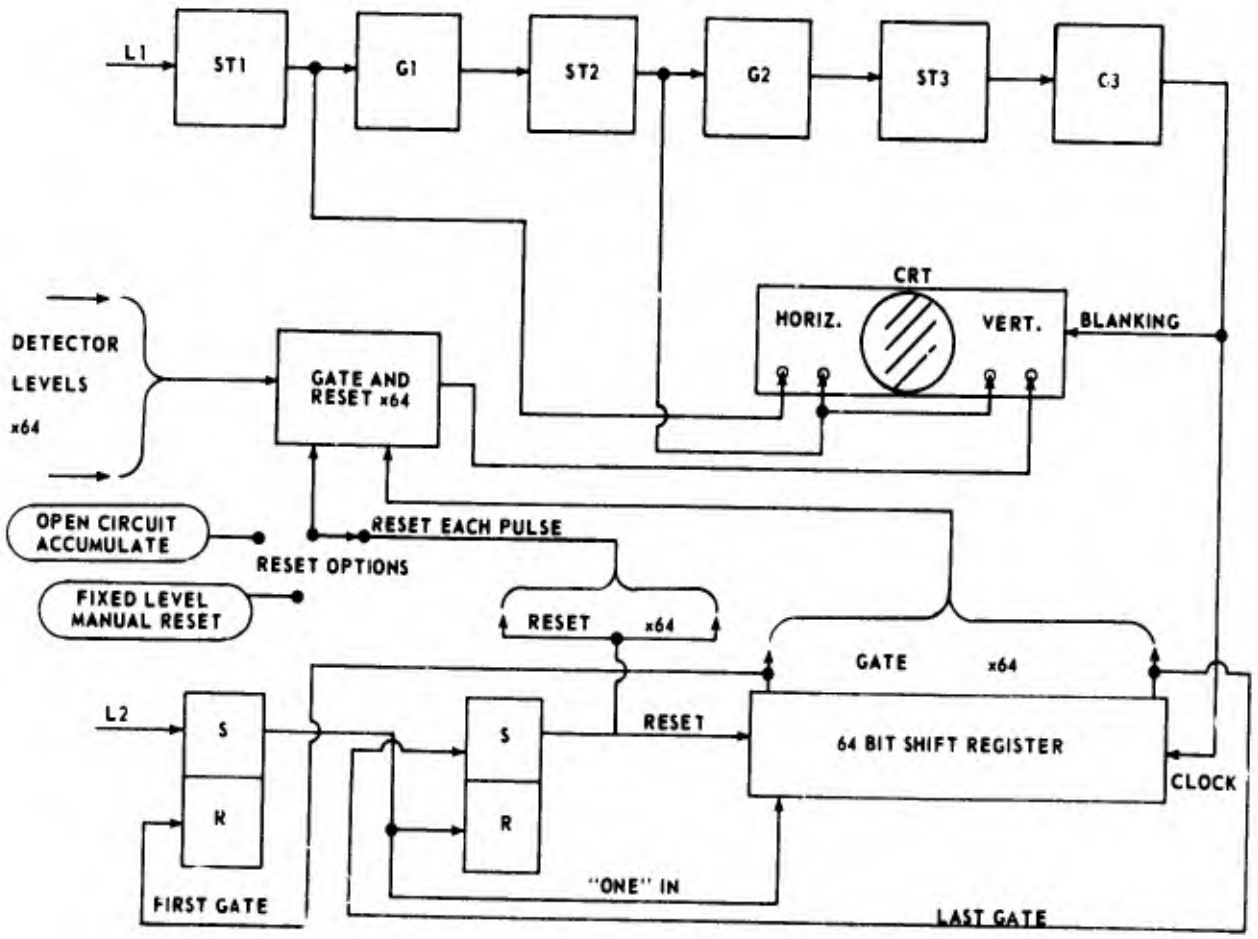

Figure 38. Block diagram of AFRRI LINAC real-time field monitor

triggers a ramp generator, ST1, the output of which is used to trigger a pulse generator, G1. The delay (trigger threshold) and the output width of G1 are independently variable. G1 is then used to gate on another ramp generator, ST2. While G1 is present, a variable number of ST2 ramps are obtained, each of which is used to trigger another pulse generator, G2, also with variable delay and width. G2 then gates on a third ramp generator, ST3, just as G1 gates on ST2. Each ST3 pulse triggers another pulse generator, G3. The system is adjusted so that for each L1 pulse, the number of G2 and G3 pulses per G1 pulse corresponds to the respective number of rows and columns in the detector grid.

To create the background CRT display, a Tektronix RM503 oscilloscope is used. The ST1 and ST2 outputs are added for the vertical input and ST2 is also used for horizontal input. Thus for each L1 pulse, lines with 45^{o} slope, one above the other, re displayed, as shown in Figure 39.

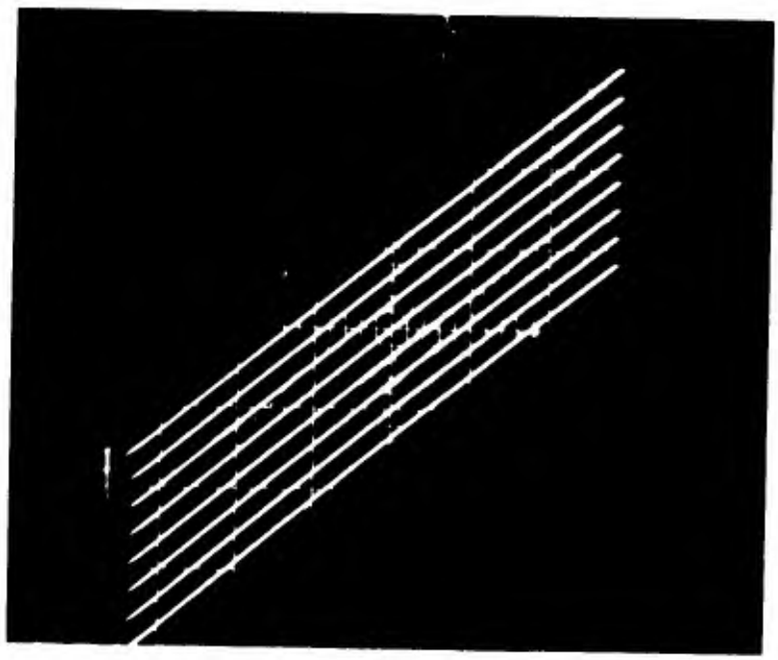

Figure 39. CRT background display for detector grid of eight rows

The G3 pulses are input to a shift register to generate gates for the individual detector level outputs. These levels are added to the CRT horizontal display. Thus, each detector level appears as a horizontal displacement with a zero level lying on the base display. The G3 pulses can also be used to enhance the CRT intensity (blanking), so that by adjustment of the oscilloscope intensity the base lines can be made invisible leaving only the peaks of the detector levels. This is shown in Figure 40, for a uniform field. Finally, the width of the G3 gates can be increased until a histogram effect is created for each row, as shown in Figure 41 for a uniform field.

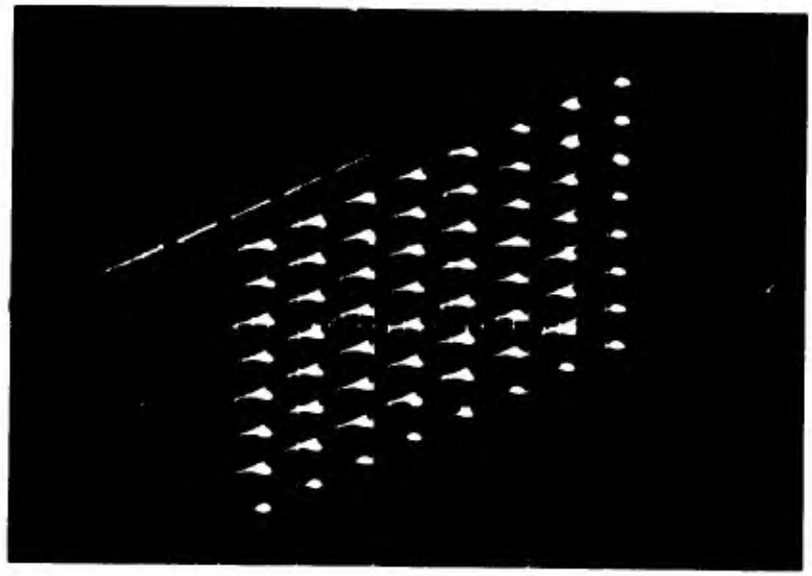

Figure 40. Three-dimensional image of 64 detector levels (8 x 8 grid) for uniform field (point mode)

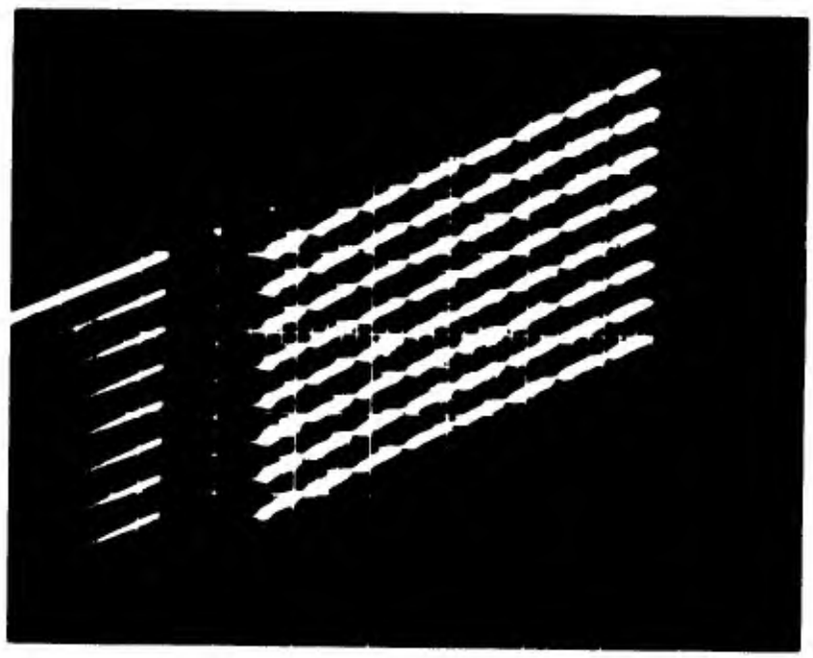

Figure 41. Three-dimensional image of 64 detector levels (8 x 8 grid) for uniform field (histogram mode)

Operation. The 45^{O} slopes, with each detector level visible in its own relative position, create a three-dimensional image. The greater the number of detectors, the greater this impression becomes. It is noted that the horizontal displacement of a level from its base line is quantitatively exact. Only a few detectors are actually needed to determine the beam shape and intensity.

There are two ways in which the perspective can be altered. The easiest is with the horizontal and vertical controls of the oscilloscope itself. The second is by varying the relative amplitudes of the ST1 and ST2 CRT inputs. This has the added advantage that the detector levels are not changed and the oscilloscope controls can be used to expand the horizontal scale to obtain easier and more accurate determinations of the detector levels.

To obtain a sequence of profiles, it is only necessary to use ST1 as the horizontal input and the detector levels as the vertical input. Then the profile for each row of detectors is obtained and the profiles, from top to bottom, appear from left to right and clearly separated for easy inspection (Figure 42). Again, the image is quantitatively exact.

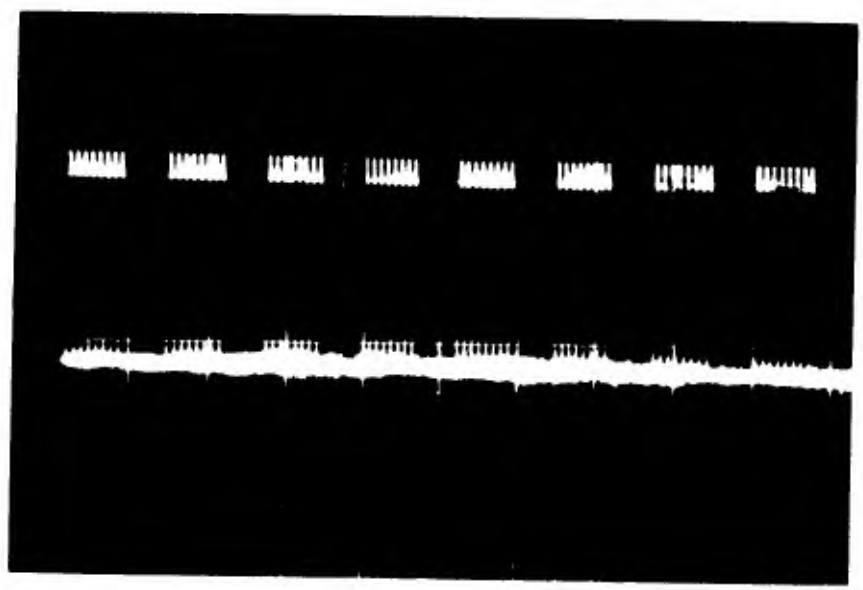

Figure 42. Two-dimensional image of 64 detector levels (8 x 8 grid) for uniform field (profile mode). Each group of eight is the profile for a given row.

Another means of using the system is to have a large grid, but only a few detectors. The detectors are connected to the desired points in the grid and the other points may be left unconnected (yielding essentially a zero level). Since each point of the grid is sampled, only those with detectors will have levels shown in the display, the others lying in the base lines.

The system gives a complete display for each LINAC clock pulse, L1. The levels are only present if the LINAC actually produces a beam pulse (L2, Figure 38). The levels may be reset or not after each L1 pulse and display. If reset after each display, then continuous tuning of the field is possible with immediate visual indication of the results. If not reset, then a given number of pulses are accumulated and the display is continuously present before, during, and after the accumulation. Resetting of the detectors is then done manually.

Usually, field uniformity is the objective. This is achieved when all the detector levels are the same, i.e., when the levels all show as straight lines. This is an easy criterion to manually tune for. If more exotic field shapes are desired, a photograph of the CRT display with Polaroid positive-negative film can be taken when the image is satisfactory. The negative can be fastened over the CRT at any later time. The tuning objective is to simply have the CRT image masked by the film negative.

Fabrication and testing of the system is presently proceeding.

ELECTRON LINEAR ACCELERATOR DOSIMETRY

Principal Investigators: *W. E. Kiker, P. A. Berardo and T. W. Hinz*
Technical Assistance: *C. L. Bransford*

Transmission ion chamber for narrow beam monitoring. One of the potentially most useful properties of an electron linear accelerator (LINAC) as a radiation source is the capability of producing a very narrow beam of radiation. In monitoring such a beam it is necessary that the instrument be nonintercepting or produce a minimum of beam scatter.

To monitor the AFRRI LINAC in narrow beam operation when the dose rate is below about 300 rads per pulse, a transmission ion chamber has been developed that intercepts the beam with 0.06" of polystyrene and 0.002" of aluminum. Plate spacing is 0.0762 cm and a bias voltage of 350 volts is recommended.

A series of measurements was carried out to determine the charge collection characteristics of the chamber and to test a newly developed phenomenological interpretation of Boag's theories of charge collection.[1-4] Data were obtained at plate spacings of 0.0762, 0.406, and 0.737 cm. However, only the results at 0.0762 cm are given here. The full results and comparison with theory will be reported separately.

Figure 43 shows charge collection efficiency as a function of initial charge density in esu/cm^3, produced in the chamber, at bias voltages of 60 and 360 volts, E/p = 1 and 6 V/cm • mm Hg. From an operational point of view the most interesting feature of the data is that at the recommended operating voltage more than 50 percent of the charge is collected at a dose of 500 rads/pulse.

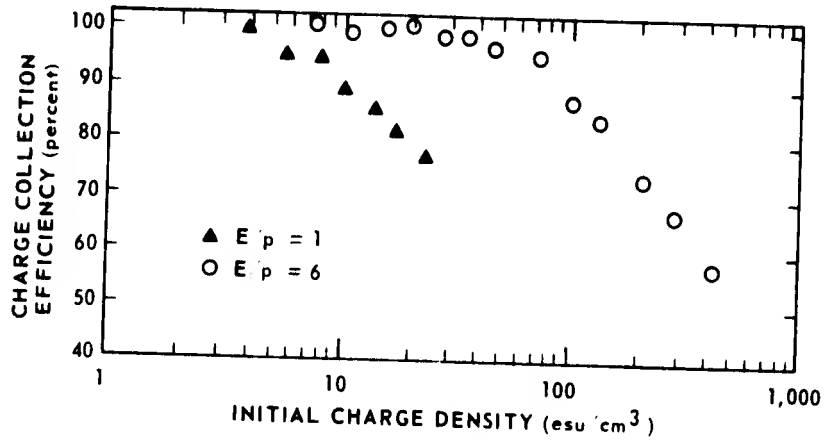

Figure 43 Charge collection efficiency at 60 and 360 volts plate bias

Induction coil for narrow beam, high dose rate monitoring. For narrow beam LINAC operation with a dose rate greater than about 300 rads per pulse the transmission ion chamber described above becomes unreliable and the most convenient means of monitoring is to measure the electrical current in the beam. This is accomplished by means of a coil through which the LINAC beam passes, inducing a 0.1-volt signal for each ampere of beam current. Thus a 300-rad pulse delivered in 1 μsec produces a signal of about 1 mV.

The output of the current monitor is fed directly into a gain-of-100 Hewlett-Packard operational amplifier, no cable being in between. The signal is then brought out of the exposure room where it is further amplified and double-delay-line shaped by a Model 410 ORTEC linear amplifier. A linear gate, opened for 1 μsec by a trigger signal from the LINAC pulse, passes the positive portion of the bipolar signal, which is recorded by a storage oscilloscope.

A series of measurements was made comparing beam current as measured by the induction coil and with a Faraday cup. Agreement was to within ± 5 percent.

A scintillation detector for LINAC beam monitoring. The silicon diodes currently in use for LINAC beam monitoring begin to respond nonlinearly at about 200 rads per pulse. In addition silicon is a nontissue-like material. For these reasons a study is underway to determine the feasibility of developing a scintillation type beam monitor, preferably with a plastic scintillator. Such a device should be linear up to several thousand rads per pulse.

A prototype device has been designed and preliminary tests carried out. An NE102 plastic scintillator, 1/2" in diameter by 1/2" thick, was fixed to the end of a 1/2" diameter by 43" long polished aluminum tube. A silicon photodiode was fixed to the other end of the tube and was well shielded with lead bricks. The output of the photodiode was measured with a current integrator.

These initial measurements were carried out primarily for two purposes, to measure signal to noise ratios and to determine the radiation damage characteristics of the plastic scintillator. With no water scatterer so that dose per pulse was high and bremsstrahlung production low, the signal to noise ratio varied from 18:1 at 5 m to more than 10^3:1 at 2 m. With the water scatterer up the variation was from .3:1 at 4 m to 8.3:1 at 2 m.

Figure 44 shows the relative response of the scintillator as a function of total radiation dose absorbed. Light output did not begin to decrease until a total dose of about 600 kilorads had been received.

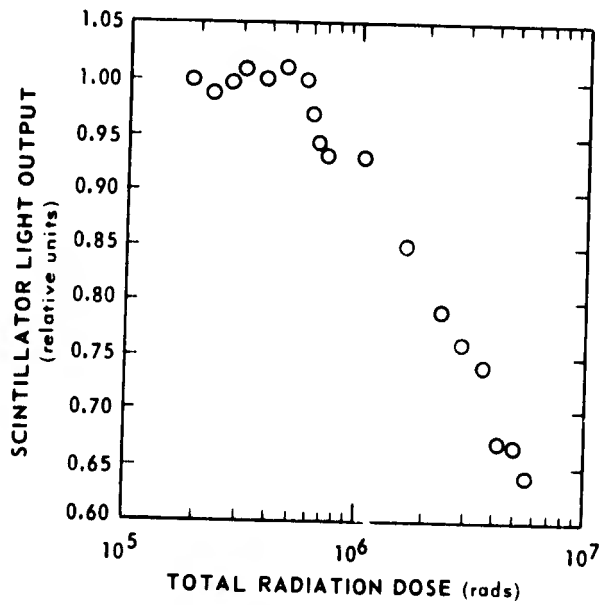

Figure 44. Relative response of scintillator as a function of total radiation dose absorbed

REFERENCES

1. Boag, J. W. Ionization measurements at very h intensities. I. Pulsed radiation beams. Brit. J. Radiol. 23:601-611, 1950.

2. Boag, J. W. The saturation curve for ionization measurements in pulsed radiation beams. Brit. J. Radiol. 25:649-650, 1952.

3. Boag, J. W. Ionization chambers. In: Radiation Dosimetry, 2nd ed., Vol. II, Attix, F. H., Roesch, W. C. and Tochilin, E., editors. New York and London, Academic Press, 1966.

4. Boag, J. W. and Wilson, T. The saturation curve at high ionization intensity. Brit. J. Appl. Phys. 3:222-229, 1952.

MINIATURE IONIZATION CHAMBERS

Principal Investigator: *D. W. Shosa*
Collaborators: *P. A. Berardo and T. W. Hinz*
Technical Assistance: *C. Carter and J. T. Istock*

Investigation of the behavior of miniature ionization chambers in intense pulsed electron beams. For a parallel plate ionization chamber, Boag[1] finds a critical applied voltage, below which positive ion space charge buildup precludes collection of all the charge liberated by a pulse of an electron beam. This voltage is

$$V_o \quad 2\pi\rho d^2 \tag{1}$$

provided that there is no attachment of electrons by neutral molecules or atoms during the collection of the charge and provided that the duration of the beam pulse is short compared to the transit time of positive ions across the gap, i.e.,

$$t \ll \frac{d^2}{2kV} \tag{2}$$

where

- V is the applied voltage (volts)
- V_o is the voltage below which not all charge liberated by the pulse can be collected (volts)
- ρ is the charge density liberated by the beam pulse (esu/cm^3)
- d is the gap width (cm)
- k is the positive ion mobility (cm^2/volt-sec)
- t is the electron beam pulse width (sec).

A solution of Poisson's equation in cylindrical and spherical geometry yields the requisite effective values of d to be used in place of the d in equations (1) and (2). For an inner cavity radius of a and an outer cavity radius of b, one obtains for cylindrical geometry

$$d^+ \quad \left[b^2 \ln \frac{b}{a} - \frac{1}{2}(b^2 - a^2)\right]^{\frac{1}{2}} \tag{3}$$

$$d^- \quad \left[\frac{1}{2}(b^2 - a^2) - a^2 \ln \frac{b}{a}\right]^{\frac{1}{2}} \tag{4}$$

and for spherical geometry

$$d^{+} \quad \left[\frac{1}{3a}(a^3 - 3ab^2 + 2b^3)\right]^{\frac{1}{2}} \tag{5}$$

$$d^{-} \quad \left[\frac{1}{3b}(b^3 - 3a^2b + 2a^3)\right]^{\frac{1}{2}} \tag{6}$$

where the superscript + or − indicates whether positive or negative high voltage is applied to the outer wall of the chamber.

To test the accuracy of the model, a 0.5 cm^3 magnesium ionization chamber was chosen. A schematic diagram is shown in Figure 45. With a maximum applied high voltage of 1000 volts, the minimum positive ion transport time across the gap is ~ 30 μsec. To assure that the pulse width was small, compared to this time, a beam pulse width of 100 nsec was chosen. A point in the beam was selected, for which the water dose (determined with Fricke chemical dosimetry) was 4.1 rads/pulse, from which the esu cm^3-pulse in several gases used could be calculated for a 35-MeV electron beam. In order to satisfy the condition that no attachment occurs during collection, four gases, argon, carbon dioxide, nitrogen, and tissue-equivalent (TE) gas (CH_4, N_2, CO_2), were flowed through the chamber during exposure. These gases have a negligible electron attachment coefficient. The results of experiments in which the quantity ρ/V was varied by varying V are shown in Figures 46 and 47. The agreement of the model with the experimental results is evident. When operated at −1000 V, a pulse of 10 esu/pulse can be completely collected.

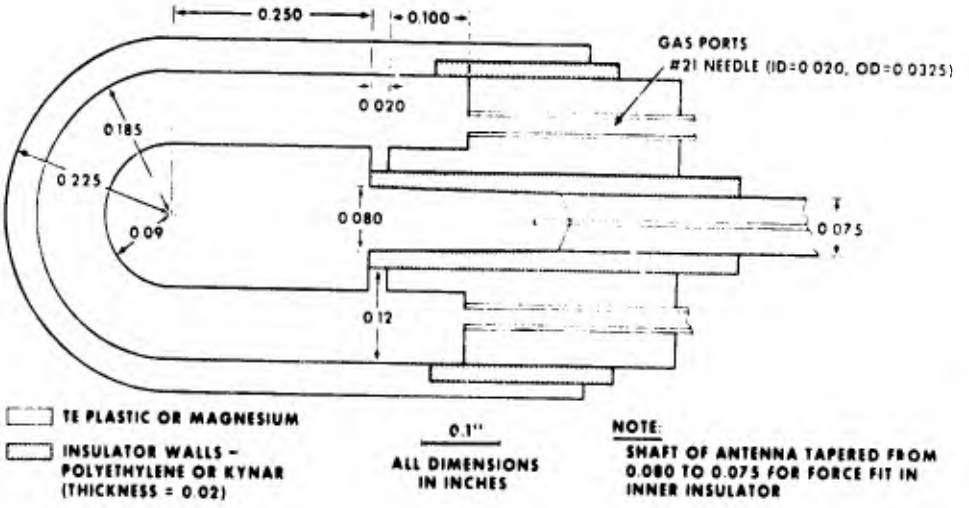

Figure 45. Section of 0.5 cm^3 ionization chamber

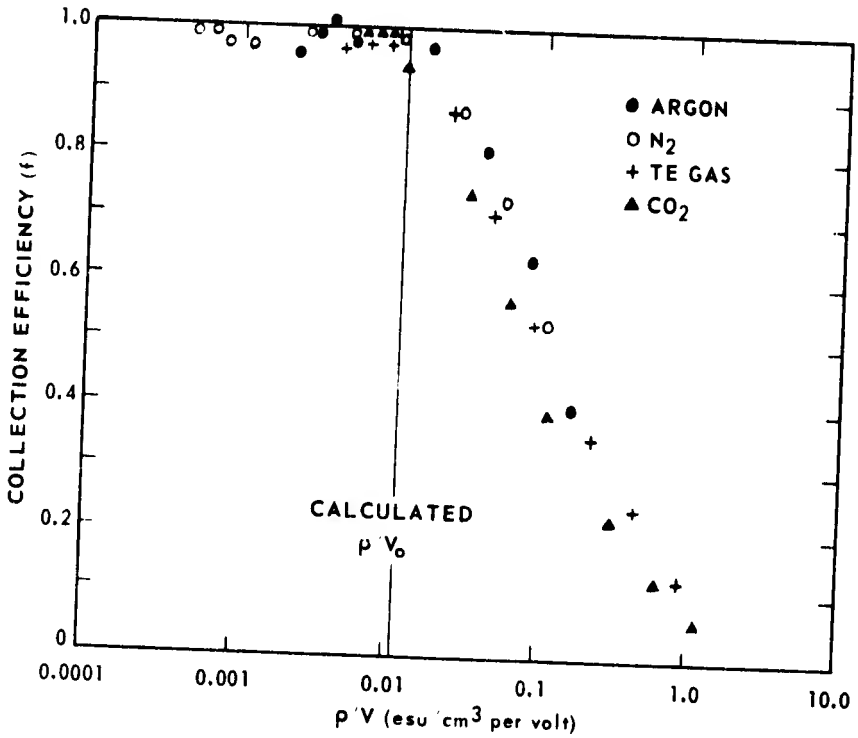

Figure 46. Collection efficiency of 0.5 cm^3 chamber (central anode)

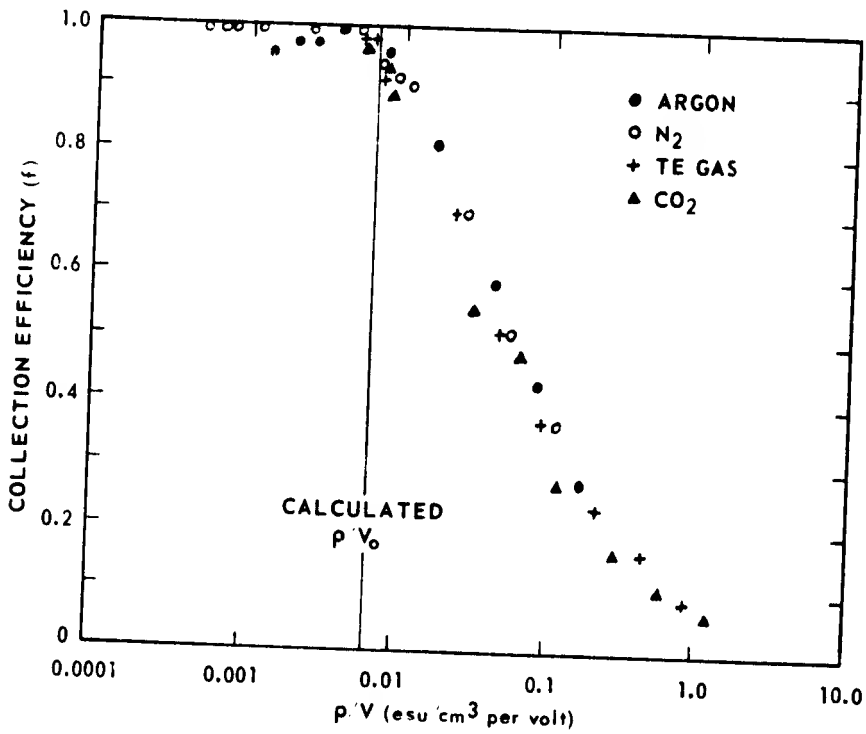

Figure 47. Collection efficiency of 0.5 cm^3 chamber (outer wall anode)

A second, smaller (0.05 cm^3) chamber is shown in Figure 48. With an applied high voltage of 500 volts on an air-filled chamber, it is found that electron attachment occurs with only a 5 percent efficiency for formation of O_2^- so that under these conditions the assumption of negligible attachment is still good even with air in the chamber cavity. The positive ion transport time is 6 - 10 μsec depending on the polarity of the applied voltage. With -500 V applied, a pulse of ~48 esu/cm^3 can be collected. With +500 V applied, a pulse of ~28 esu/cm^3 can be collected.

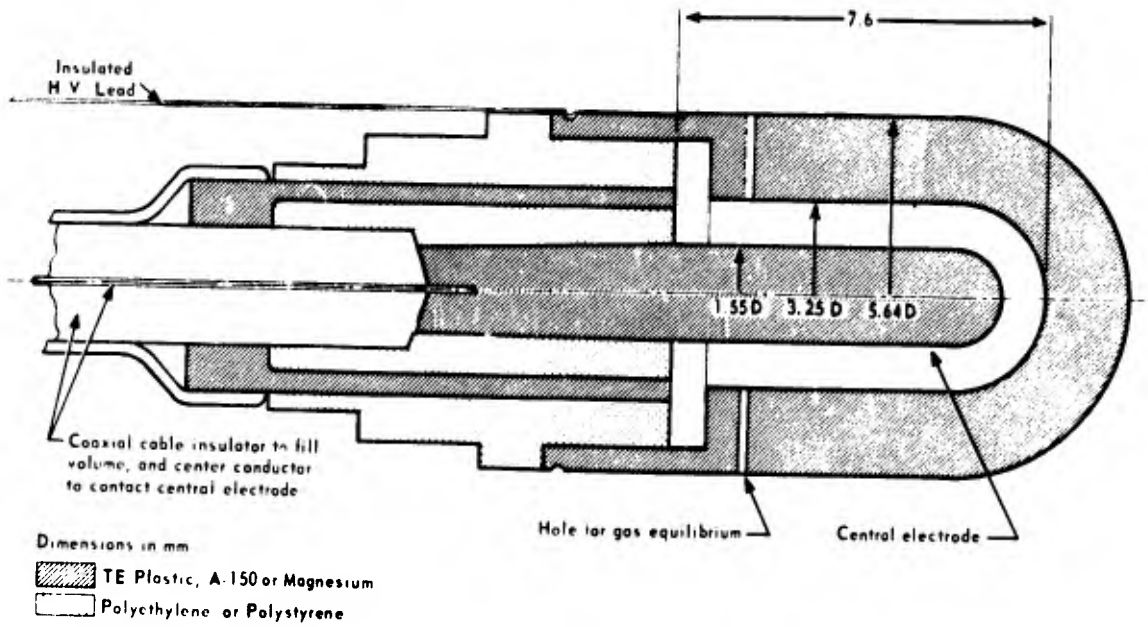

Figure 48. Section of 0.05 cm^3 ionization chamber

Several months of experience during which 0.05 cm^3 air-filled chambers have been operated with -500 V applied to the outer wall indicate that complete collection occurs for doses up to ~50 esu/pulse. These results are based on comparison with Fricke and thermoluminescent dosimetry. The miniature chambers are now used routinely for dosimetry and monitoring in high energy LINAC beams. Even when the pulse width becomes comparable to the positive ion transport time (i.e., 4 μsec compared to ~6 μsec), the agreement between the ion chamber and other dosimeters is maintained.

Paired miniature ionization chambers for reactor dosimetry. Preliminary work on paired magnesium and tissue-equivalent chambers for mixed neutron-gamma fields was presented and a comprehensive report was completed.[2,3]

Two problems associated with the use of 0.05 cm^3 paired chambers have been solved within the past year by designing a 0.5 cm^3 pair. First, with the larger sensitive volume, Compton currents, generated in the signal leads, are minimized relative

to chamber currents. Second, gas flow through the chambers does not result in an uncertain pressure buildup in the cavity. No appreciable sacrifice has been made in terms of reduced field resolution in the mapping of free fields or the measurement of depth-dose distributions. Figure 45 shows a cross section of the 0.5 cm^3 chamber.

The magnesium chambers were the first delivered and initial tests were so promising that they were put in use immediately. They are now used routinely in reactor, LINAC, ^{60}Co, and x-ray fields at the AFRRI; they have become the primary dosimetry system for reactor gamma exposures of dogs at Walter Reed General Hospital; and they monitor the gamma component at the Aberdeen pulsed reactor facility. Tissue-equivalent 0.5 cm^3 chambers have been received from Dr. Spokas at Illinois Benedictine College. These paired chambers now give the AFRRI three sets (0.05 cm^3, 0.5 cm^3 and 50 cm^3) which should provide the versatility necessary for mixed field dosimetry at the AFRRI-TRIGA reactor. AFRRI has been invited to participate in an international intercomparison of neutron dosimetry techniques at the Brookhaven National Laboratory in the coming year. The 0.5 cm^3 chambers were recently tested at dose rates that will be available at that facility, and performance was satisfactory.

REFERENCES

1. Boag, J. W. Ionization chambers. In: Radiation Dosimetry, 2nd ed., Vol. II, Attix, F. H., Roesch, W. C. and Tochilin, E., editors. New York and London, Academic Press, 1966.

2. Shosa, D. W. Reactor dosimetry with paired miniature ionization chambers. Bethesda, Maryland, Armed Forces Radiobiology Research Institute Technical Note TN71-7, 1971.

3. Shosa, D. W. and Verrelli, D. M. Paired miniature ionization chambers for reactor dosimetry. Bethesda, Maryland, Armed Forces Radiobiology Research Institute Annual Research Report ARR-5, pp. 55-57, 1 July 1970 - 30 June 1971.

DESIGN AND UTILIZATION OF A LEVEL DETECTOR FOR DOSIMETRY SUPPORT

Principal Investigators: *T. W. Hinz and J. A. Willis*

Dosimetry support provided for biological experiments on the AFRRI LINAC consists of the following procedure: (1) specification of energy, current, and pulse width parameters of the LINAC; (2) determination of beam scatters needed, position and shielding of subject; (3) measurement of the absorbed dose per pulse in phantom or cadaver, using various dosimeters, and calculation of the number of pulses necessary to deliver the prescribed dose to subject; and (4) monitoring of beam during irradiation of subject.

To reproduce the dose delivered in separate irradiations by the method of step (3), it is necessary that the source be reproducible. Experience has shown that there can be 10 percent variation between irradiations on a given day. Therefore a device was needed which could monitor the beam and stop the LINAC pulser upon reaching the prescribed dose. This report describes the design and use of such a device.

The beam monitor is a live readout device which outputs a current proportional to the dose per pulse being delivered. The current is then integrated by an operational amplifier, and a voltage signal proportional to the dose is obtained. This voltage signal is input to the level detector (LD) where a comparison is made between a preset reference voltage in the LD and the output voltage of the amplifier. If the output voltage equals or exceeds the reference voltage, a signal is sent to the LINAC which stops the pulser.

The monitors presently used are either ion chambers or diodes. During the dosimetry run, the voltage output of the monitor is noted. From the dose determined by the dosimeters in the phantom, the voltage is scaled accordingly. For example, assume the dosimeter in the phantom reads 2,000 rads and the monitor reads 1.0 volt, if the required dose is 6,000 rads, then a reference voltage of 3.0 volts is dialed into the LD. During the irradiation the LD would shut off the LINAC pulser when the output voltage of the monitor equaled 3.0 volts. The following discussion and circuit diagram provide more detailed information.

This circuit is designed to output a standard pulse whenever an input signal exceeds a preset reference voltage. The circuit will accept inputs from -10 to +10 volts dc, and outputs a 12-volt, 5-microsecond positive pulse. The reference voltage is preset via a 10-turn potentiometer. The polarity of the input signal can be selected for either positive or negative inputs, and either a positive or negative trigger slope.

Reference voltage for the circuit is provided by a Zener diode isolated from the circuit by operational amplifier IC-1 (Figure 49). This amplifier provides voltage and current gain. The reference voltage may be set to any value desired between 3.3 V and 10 V. In practice, the output of the reference amplifier is set at 5 V dc via the 5K Trimpot in its feedback loop. The output of the reference amplifier is applied across a 10-turn potentiometer which allows the operator to select any reference voltage between zero and 5 volts with great precision.

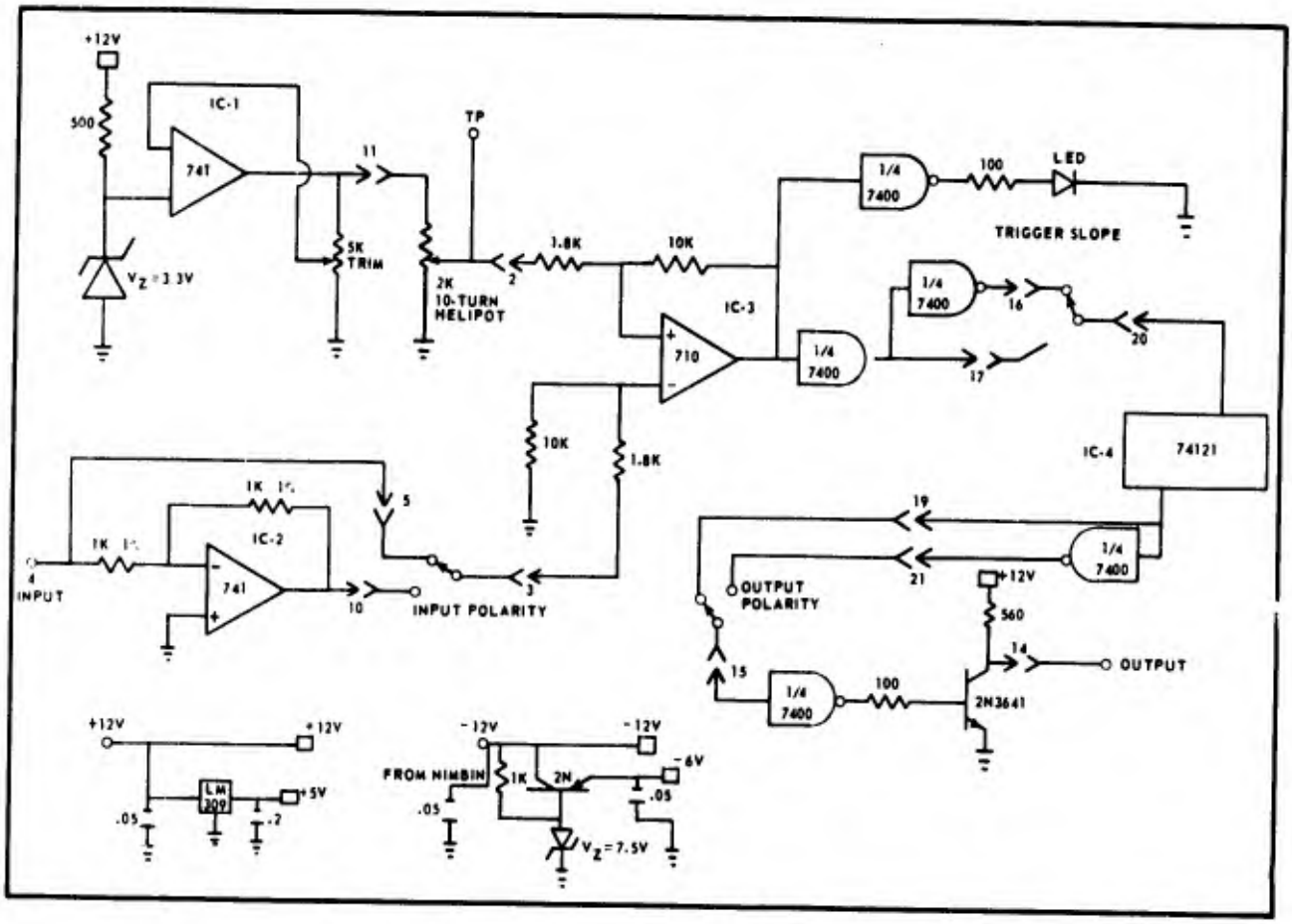

Figure 49. LINAC level detector

The reference voltage from the 10-turn potentiometer, and the input signal from the input polarity switch are compared by a high speed comparator, IC-3. The comparator will output a low logic level if the magnitude of the reference voltage exceeds that of the input voltage. If the input voltage exceeds the reference voltage, the comparator will output a high logic level. The logic state of the comparator is displayed at all times by a front panel light emitting diode (LED). The LED is on when the comparator's output is low, and off when the comparator's output is high. The light-on condition is used to signal that the circuit is ready.

The output of the comparator and its logical complement are coupled to the input of a one-shot, IC-4. The one-shot will trigger on a negative transition from a high to a low logic level at its input. By selecting either the output of the comparator or its logical complement as input to the one-shot, it is possible to select either a positive or negative trigger slope. The pulse duration of the one-shot is fixed by external timing components at 5 microseconds. The pulse and its complement are switched by the output polarity switch to a transistor amplifier which boosts the level of the pulse from the standard 5-volt TTL logic level to a 12-volt logic level.

Power supply regulation is accomplished by utilizing power directly from the NIMBIN power supplies and by dropping these voltages wherever necessary with integrated and discrete voltage regulators.

The level detector has been used routinely for several months in LINAC dosimetry support. The ease of operation and improvement in precision have made it a valuable asset.

ELECTRON IRRADIATION FIELDS FROM THE AFRRI LINAC

Principal Investigators: *T. W. Hinz and P. A. Berardo*

The pulsed electron beam from the AFRRI LINAC is used in a variety of biological and physical experiments. A primary concern is that the electron beam field be large enough to insure uniform irradiation of the subject. This report presents the capabilities of the LINAC to produce Class A electron beam field geometries.

At the exit port, the electron beam passes through a thin aluminum window. The scatter induced by this window and any intervening scattering material causes the electron beam to broaden. The scattering of the beam is less with a higher incident electron energy. Experiments are routinely conducted using either the air between source and subject as the scattering medium or a 1-cm water scatterer placed at the exit port, in addition to the air scatterer. As a result of the beam broadening, the dose per pulse decreases for a given set of LINAC parameters. This is due to the reduction in flux density (electrons/cm^2-sec). The beam size is thus determined by electron beam energy and scattering materials between source and subject. The dose per pulse for a given beam size is dependent upon the electron beam current (electrons/sec) and the pulse width.

The dose per pulse and beam profiles were measured at 10, 20, 30 and 40 MeV at distances of 1, 2, 3, 4 and 5 meters from the exit port, with and without the water scatterer in position. The dose per pulse was measured with Fricke dosimeters, free-in-air, while the profiles were measured by the relative response of a diode which traversed the beam.

The results of this study are presented in Figures 50 and 51. The vertical axes on the graphs are in units of rads/μsec per ampere. This allows the scaling of dose per pulse to any pulse width and electron beam current as measured at beam toroid monitor #6. The field sizes, as given in Figures 50 and 51, are for Class A fields which are defined such that the maximum dose in the field is not more than 1.15 times the minimum dose.

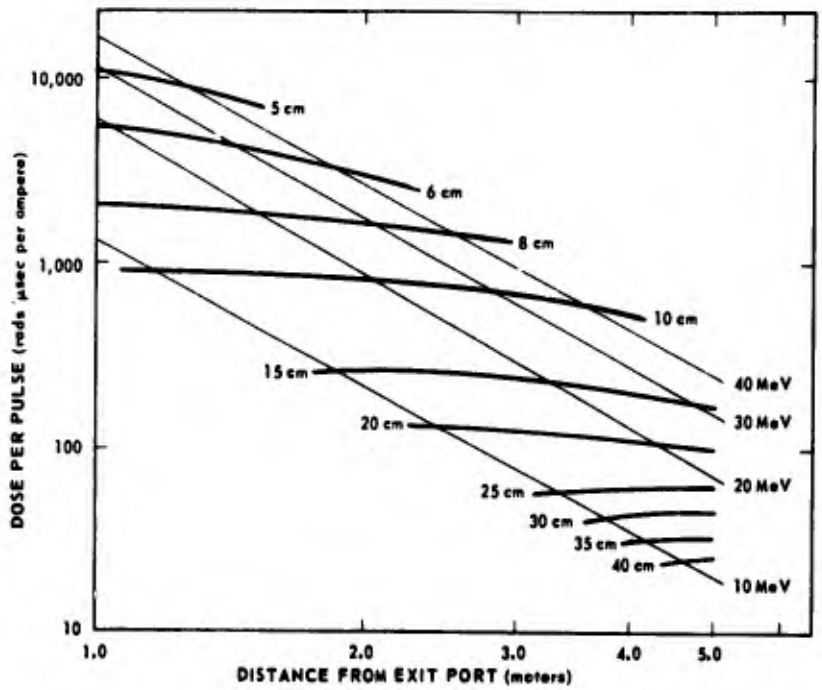

Figure 50. Dose per pulse versus distance (air scatter only)

The data presented in this report are subject to certain restrictions in precision. The electron beam may be focused differently from day to day as it exits from the beam port. This results in different field size and dose per pulse data. It has been found, however, that these are generally not significant differences and that Figures 50 and 51 may be used as guidelines for designing subject irradiations.

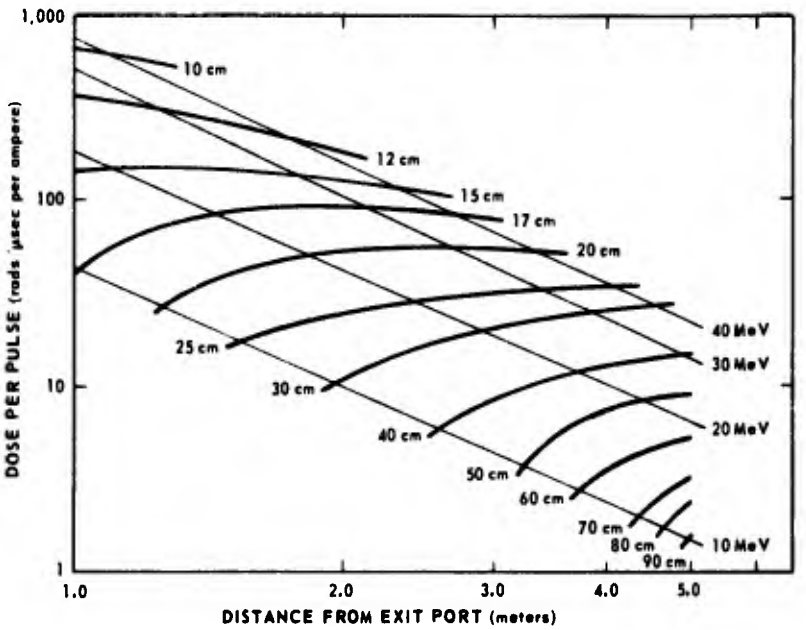

Figure 51. Dose per pulse versus distance (1 cm water scatter)

INDEX TO PRINCIPAL INVESTIGATORS